Lakehead University

Quadrotor altitude and attitude control with neural network

by

Xiao Cui

Under the Supervision of Dr. Xiaoping Liu

For Fulfilling the Partial Requirements of the Master of Science in the Electrical and Computer Engineering

Lakehead University, Thunder Bay, Ontario, Canada

Nov. 2016

Acknowledgments

I would like to take a moment to send my sincere thanks to my supervisor Dr.Xiaoping Liu. During the course of my research, he continuously offered his suggestions and insights on the theoretical development, as well as sharing his experiences on practical implementation and experiments. Without his countless assistantship, this thesis work would be impossible to finish. I was deeply affected by his strong passion and his determined working ethics towards control engineering field. Not only I was trained in a good manner while doing my research, but Dr. Liu opens up numerous research possibilities for me in the future. I would also like to thank to Dr. Krishnamoorthy Natarajan and Dr. Abdelhamid Tayebi for their insights and comments during my thesis seminar. The enrichment of my thesis work would not be possible without their enlightenments and advices.

I would also like to thank to one of my close friend, Mr. Wang Miaomiao. He and I share the very same interests for the quadrotor and UAVs in general. At the early stage of my research, he generously helped with my theoretical understanding, as well as provided numerous valuable suggestions. We continuously maintain a close contact, discussing and exchanging the current research progress and ideas. Hereby, I thank to his generosity, encouragement, assistantship, and most importantly, his friendship.

From the lab, I would like to thank to my dear colleagues, Mr.Joshua Abela, Miss Kaiyu Zhao, Mr. Peter Luong. They have supported me in many different ways. I wish you all a great journey in your future endeavours.

Lastly, I would like to delicate this short paragraph to my family, my mother and my father. During the time facing obstacles, they have been emotionally supporting and encouraging me to not only meet the requirements, but also push beyond the envelop. I thank you for your understanding and love.

Sincerely

Xiao Cui

Abstract

Over the years, the controller design for an unmanned aerial vehicle has been attracting considerable amount of attentions and interests. In this thesis, a quadcopter has been studied intensively, and an adaptive backstepping nonlinear controller, along with altitude control using sonar sensor, has been proposed to ensure the stable flight of a quadcopter.

A quadcopter consists of four motors acting as its control means. The proper thrust and air drags produced by the propellers completes the tasks to stabilize the quadcopter in the pitch, roll and yaw directions. An attitude estimation technique, the Mahony filter, was firstly implemented to yield the accurate Euler angles for the quadrotor. To understand such a complex system, the Euler-Lagrangian equations has been introduced to develop a dynamic model. Following such a mathematical model, using backstepping design technique, an adaptive nonlinear controller is designed for and implemented onto a real quadcopter. The derived mathematical model has its own uncertainties, such as changes in mass and the location of the center of the mass. Due to such a nature, an adaptive controller based on the neural network has been proposed to estimate certain nonlinear terms in the mathematical model. Successfully design and implementation of such a controller can improve the accuracy of the dynamic model.

The unit quaternion representations was also used to eliminate the Gimbal Lock of the Eular angles. A different mathematical model based on Newton equations was also used to further consider the air drag effect of a quadrotor while flying in the air.

Proceeding to the attitude controller design, an altitude controller is also designed to lock the flying height of the quadcopter. The design concepts are based on a traditional nonlinear backstepping method.

Matlab simulation results suggest a possible implementation of the proposed controller for the quadcopter's altitude and attitude control. A couple of real time experiments have been conducted. The results was recorded and analysed.

Contents

1 Introduction **1**

1.1 Brief Discussion on UAVs 1

1.2 Attitude Estimation 2

1.3 Attitude Control 3

1.4 Neural Network 4

1.5 Research Motivation 5

1.6 Thesis Contribution 5

1.7 Thesis Outline 6

2 Experimental Platform **7**

2.1 Platform Overview and Electronics 7

2.1.1 APM 2.6 Pilot Module 7

2.1.2 Digital Compass and GPS Unit 10

2.1.3 MB1240 XL-MaxSonar Sensor 10

2.1.4 RC Control and Wireless Data Transfer 11

2.1.5 The Actuation System 12

2.2 Moment of Inertia 16

2.3 Quadrotor Aerodynamics and Preliminary Calculations 22

3 Attitude Estimation **25**

3.1 The Attitude Representations 25
3.1.1 Rotational Matrix 26
3.1.2 Euler Angle 26
3.1.3 Unit Quaternion 27
3.2 Sensor Calibration 28
3.3 Sensor Fusion Technique 31

4 Quadrotor Dynamics **34**
4.1 Euler Lagrangian Dynamic Model 34
4.2 Dynamic Model Using Newton Equations 36

5 Controller Design and Experiments **38**
5.1 Backstepping Design with Euler Angle Representation 38
5.1.1 Controller Design 38
5.1.2 Experimental Results 41
5.2 Integral Backstepping Design with Euler Angle Representation 41
5.2.1 Controller Design 41
5.2.2 Experimental Results 48
5.3 Backstepping Controller with Unit Quaternion Representation 49
5.3.1 Controller Design 49
5.3.2 Experimental Results 53
5.4 Integral Backstepping with Neural Network 54
5.4.1 Controller Design 54
5.4.2 Experimental Results 61
5.5 Altitude Control 61
5.5.1 Controller Design 61
5.5.2 Experimental Results 65

6 Conclusion **66**

A C Language Flow Chart **68**

B Digital Compass Calibration **69**

List of Figures

1.1 RQ-4 Global Hawk 1

1.2 DJI Phantom 2

2.1 Quadrotor Expiremental Platform 8

2.2 Quadrotor Major Components Layout 8

2.3 (a) APM 2.6 External Physical Structure; (b) APM 2.6 Circuit Board . . . 9

2.4 (a) MS5611-01BA Pressure Sensor; (b) MPU-6050 9

2.5 (a) HMC5883L Digital Compass; (b) U-blox GPS Unit with Compass;(c) 3DR GPS and Compass Module 10

2.6 MB1240 XL-MaxSonar Sensor 11

2.7 (a) JR XGB Remote Control; (b) RG831B with DMSS RA01T Receiver . . . 11

2.8 2.4 Ghz Wireless Data Transfer Radio 12

2.9 (a)The Core of a TPM; (b)The Concept of a TPM 12

2.10 880KV TPM 13

2.11 10x4.7 Propeller both CCW and CW 13

2.12 Afro ESC 14

2.13 Turnigy Nano-tech 2.65 LiPo Battery 15

2.14 Illustration on Assembled Quadcopter 15

2.15 Moment of Inertia Experiment Setup for Roll or Pitch Direction 18

2.16 Moment of Inertia Experiment Setup for Yaw Direction 19

2.17 Oscillation around x Axis . . . 19
2.18 Oscillation around y Axis . . . 20
2.19 Oscillation around z Axis . . . 20
2.20 Natural Frequency with Respect to x Axis . . . 20
2.21 Natural Frequency with Respect to y Axis . . . 20
2.22 Natural Frequency with Respect to z Axis . . . 21
2.23 Operating Principle of a Quadrotor . . . 22

3.1 Unit Quaternion Graphical Representation . . . 28
3.2 HMC-5883 Digital Compass Calibration Results . . . 31
3.3 Filter Testing Results . . . 33

5.1 Block Diagram for Backstepping Control . . . 41
5.2 Backstepping Control with Euler Representation in ϕ Direction . . . 42
5.3 Backstepping Control with Euler Representation in θ Direction . . . 42
5.4 Backstepping Control with Euler Representation in ψ Direction . . . 42
5.5 Block Diagram for Integral Backstepping Control . . . 47
5.6 Integral Backstepping with Euler Representation in ϕ Direction . . . 48
5.7 Integral Backstepping with Euler Representation in θ Direction . . . 48
5.8 Integral Backstepping with Euler Representation in ψ Direction . . . 49
5.9 Block Diagram for Quaternion Backstepping Control . . . 52
5.10 Quaternion Tracking Error . . . 53
5.11 Euler Angle of the Quadrotor . . . 53
5.12 Angular Velocity of the Quadrotor . . . 54
5.13 Neural Network in ϕ Direction . . . 55
5.14 Neural Network in θ Direction . . . 55
5.15 Neural Network in ψ Direction . . . 56

5.16 Block Diagram for Integral Backstepping with Neural Network Control 61

5.17 Neural Cells Outputs for $\dot{\phi}$ input and $\dot{\psi}$ input 62

5.18 Integral Backstepping with Neural Network in ϕ Direction 62

5.19 Integral Backstepping with Neural Network in θ Direction 63

5.20 Integral Backstepping with Neural Network in ψ Direction 63

5.21 Block Diagram for Altitude Control with Integral Backstepping Controller . 65

5.22 Altitude Tracking 65

List of Tables

2.1 880KV Motor Electrical and Mechanical Parameters 13

2.2 Propeller Characteristics 14

2.3 Afro ESC Electrical and Physical Specs. 14

2.4 The Turnigy Nano-Tech 2650 mAh LiPo Battery. 15

2.5 Model Parameters 21

2.6 Propeller Specifications 23

3.1 Rotational Sequence 27

3.2 HMC 5883 Digital Compass Calibration Results 31

List of Abbreviations

UAV – Unmanned Aerial Vehicle.
PID – Proportional Integral Derivative.
PD – Proportional Derivative.
KF – Kalman Filter.
EKF – Extended Kalman Filter.
AEKF – Additive Extended Kalman Filter.
PWM – Pulse Width Modulation.
LQR – Linear Quadratic Regulator.
SMC – Sliding Mode Control.
GPS – Global Positioning System.
FIR – Finite Impulse Response.
APM – Arduino Pilot Module.
ESC – Electronics Speed Control.
DMP – Digital Motion Processing.
I2C – Inter-Integrated Circuit.
SPI – Serial Peripheral Interface.
IMU – Inertial Measurement Unit.
UART – Universal Asynchronous Receive and Transmit.
CPU – Central Processing Unit.
DMSS – Dual Modulation Spectrum System.
DSSS – Direct Sequence Spread Spectrum.
FHSS – Frequency Hopping Spread Spectrum.
PPM – Pulse Position Modulation.
TPM – Three Phase Motor.
LiPo – Lithium Polymer.
SPI – Serial Peripheral Interface.
LBT – Listen Before Talk.
TDM – Time Division Multiplexing.
FFT – Fast Fourier Transform.

Chapter 1

Introduction

1.1 Brief Discussion on UAVs

The definition of the Unmanned Aerial Vehicle (UAV) is a rigid body flying in the air without any onboard human interference. They can be built in many different format. It could be a helicopter, or a fixed-wing aircraft, and of course a quadrotor.

Fig. 1.1 shows a fixed wing type drone designed by U.S. military. It is called RQ-4 Global Hawk, which has a wingspan of 39.9 meters and is 14 meters in length. It has a cruising speed of 575km/h and can reach up to a top speed of 629km/h. The service ceiling altitude is at 60,000 ft. It can fly up to 32 hours without any re-adjustment. It successfully accomplished many surveillance and reconnaissance mission for the U.S. military [1].

Figure 1.1: RQ-4 Global Hawk

This thesis research, however, is based on a quadrotor, which is shown in Fig. 1.2. It is a DJI phantom quadrotor designed and manufactured by a Chinese company located in southern China. It weighs about 1200 grams and has a diagonal size of 350mm. It can reach

a vertical take off speed of 5m/s and maximum horizontal translational speed of 16m/s.

Figure 1.2: DJI Phantom

A quadrotor has many different advantages in terms of the high maneuverability, hovering capability, vertical take off and landing. Comparing with standard helicopters, or a fixed wing aircraft, the quadrotors are more agile, efficient, safe and of course can be designed in a fairly small dimension [2, 3].

Due to all these unique characteristics of the quadrotors, they have been used in many different applications, such as military services, surveillance, rescue, remote inspection, photography, aviation enthusiastic, and research projects conducted by different companies and universities.

1.2 Attitude Estimation

To be able to successfully control the attitude of a quadrotor, an accurate attitude estimation is vital to ensure the proper function of any possible control strategy. Before jumping onto different methods of yielding the attitude of a quadrotor, we need to gain considerable amount of understanding about three different types of attitude representation, which are the rotational matrix, the Euler angle, and the quaternion, respectively [4]. These three different types of attitude representation techniques will be discussed in details later on. For now, we will be using Euler angles for a simpler and more intuitive illustration purposes.

Three different types of sensors, gyroscope, accelerometer, and magnetometer, are commonly used to measure the Euler angles. There are quite a few algorithms have been studies intensively to estimate the attitude of a quadrotor. The basic trigonometry may be used to produce the pitch, roll, and yaw angles directly from the accelerometer readings. However, the accelerometer is extremely prone to the vibration, so the jitters and the noises will have a huge negative impact on the results. To perform an integration on the angular velocity from the gyroscope reading is another alternative to produce the pitch, roll, and yaw angles. However, the error accumulation from the integration will cause a drift on the final results, hence this method is not appropriate for our applications.

Along with the advancement of the mathematics, a couple more complex attitude estimation

algorithms have entered the horizon. Dr. Robert Mahony, along with his research team, has made a great contribution in attitude estimation [5]. The filter is quite powerful by employing the nonlinear observer. The proposed estimation scheme is able to be implemented onto a low cost and compact micro-controller, such as the ATMAGE 2560. In [5], the filter with the unit quaternion representation was being experimented. On the other hand, in [6], the filter went under the similar experiments with rotational matrix representation. The paper [5] proposed a strategy to decouple the roll and pitch from the yaw. Through the anti-windup nonlinear integrator, the designed filter was able to produce accurate estimations with fast responses by adding the gyro-bias compensation.

The Kalman Filter(KF) is another efficient method for attitude estimation, Instead of having a nonlinear observer stated in [5, 6], the KF is firstly predicting the current state variables from the previous, and then update the estimated state variables with the scaled predicted state and measurement noises. The KF is originally designed for linear systems, however, in order to predict a nonlinear attitude dynamics, the Extended Kalman Filter (EKF) is then introduced [7, 8]. The EKF is quite computational complex and its linerization may lead to the divergence. A more advanced filter, such as Additive Extended Kalman Filter(AEKF) [9], should be implemented to correct such an issue. However, considering the computational power of the microprocessor ATMEGA 2560 used in this thesis work, to ensure a reliable performance, the Mahony filter is applied to estimate the attitude of the quadcopter.

1.3 Attitude Control

Many different types of control schemes have been proposed over the years [10–15]. In [10], the author was using the mathematical model derived by Euler Lagrangian method. Based on such a dynamic model, a backstepping control algorithm is developed to ensure the asymptotically stability in the pitch, roll, and yaw directions, as well as the translational movement along the x, y and z directions. Under the goal of achieving a better practical engineering implementation, a nonlinear relationship between the input Pulse Width Modulation (PWM) signal and the motor rotational speed was studied, a polynomial function was constructed and implemented as part of the final design.

A backstepping method similar to [13] is used to ensure the attitude stabilization of the quadrotor, as well as the trajectory tracking. The designed control scheme is based on a dynamic model, which is viewed under three different sub-categories: under-actuated system, actuated system, and fully propelled system.

The widely used Proportional Integral Derivative (PID) controller was studied and implemented in [11, 14, 15]. Linear Quadratic Regulator (LQR) controller [11, 14] and PID controller [15] all exhibit few disadvantages in the response to the aggressive maneuver, since the linear controller can only perform well in a constrained domain. Such a problem is especially escalated in [11], where the PID and LQR controllers were firstly being used. It was then discovered that the strong disturbances were poorly rejected as in the presence of the wind. Therefore, a nonlinear backstepping controller is used and implemented onto the quadrotor.

Various other controllers are proposed, such as robust control, H_∞ and Sliding Mode Control (SMC) stated in literature [16–19]. The theory development and computer simulation are suggesting the good control outcomes, though there are no signs of real experimental results. In [19], a nonlinear control law is considered using the unit quaternion and measured angular velocities to provide the asymptotic stability. The proposed control scheme does not require the values of the system parameters, hence it is robust to the modeling errors. The controller is taking the full advantage of a nonlinear design, where a large angle maneuverability is achievable.

Further more in [18], an SMC is presented to provide a high maneuverability and robustness to the surrounding disturbances. The position controller is yielding the desired tracking of the pitch and roll attitude. The designed controller, based on a robust compensation technique, is capable of automatic taking off, hovering, and the position tracking. Another controller design approch [17] is using a high order sliding mode observer design to model the external disturbances, such as wind and noises. The numerical simulation results prove the proposed functionality of the designed controller. Another control law, based on total energy of a rigid body and Lyapunov design technique, is constructed [20]. In the comparison to the PD controller, the proposed control scheme has a PD like structure with a feedforward compensation.

In [12], a PD^2 structured quaternion-based feedback controller is designed to achieve exponential attitude stabilization. The dynamical model is improved by using Newton equations and taking the aerodynamics effects into the consideration. In [21], a passive control scheme without the angular velocity measurements was announced. To create a passivity property, an auxiliary system is introduced to estimate the angular velocities. The controller is designed by using the output of the auxiliary system and the unit quaternion attitude tracking error. Such a control scheme ensures the almost global asymptotic stability.

1.4 Neural Network

The majority control scheme design and development are heavily based on the dynamic model. The errors in the model parameter measurements, the external disturbances, and the proper assumptions on neglecting certain model parameters can all be the factors to deteriorate the performance of the designed controller. A robust control scheme mentioned in [22, 23] earlier can be used to solve the problems caused by certain external disturbances and model uncertainties. However, a possible better approach has always being studied. Because neural networks can be used to estimate unknown parameters, nonlinearities, and dynamics, etc. It has then been applied to control nonlinear systems with unknown parameters, nonlinearities, and dynamics [24]. In [24], the neural network is applied to estimate an unknown system. The neural model for the unknown nonlinear system is learnt by the backpropagation training algorithm. A predictive controller is designed by minimizing the errors between the reference signal and the predicted output from the neural model. The proposed controller guarantees that the output of the real system can be made close to the reference signal. Such a design method has been applied to the flow rate control and temperature control systems.

In [25–28], different controller design approaches are used with neural network to control quadrotors. In [25], the controller network works in conjunction with the sensory and motor network. The classical concepts of the neural network are used, where the information is being passed through the linkages among the neural cells. The sensory and the navigation networks are utilized to generate the signal for the motor network. The design is capable with the proof of computer simulations.

Another insight is reported in [27], where the outside control loop is used to generate the desired angular velocity for the faster inner loop which regulates the velocity. Along with Lyapunov function, the neural network acts as the estimator for all the uncertainties, which may caused by the inaccuracy of model parameters, unwanted surrounding noises, and the external disturbances. A Finite Impulse Response (FIR) assisted with neural network control strategy [28] ensures a promising result on the control output. A fractional order $PI^{\lambda}D^{\mu}$ is deployed in this article.

1.5 Research Motivation

Under the influential theory development in [10,12,14,23], along with the close observation on the aerodynamics reaction of the quadrotor, a clear and well plotted backstepping technique will be utilized to develop a controller design scheme. Different from [10], an integrator will be added to eliminate the steady state error. To ensure the robustness of the quadrotor, two different dynamic modeling methods, Euler Lagragian and Newton, will be adopted.

The control scheme will firstly be based on the Euler angle representation, though as mentioned earlier, the Euler angle singularity problem also known as gimbal lock will cause the problem of the controller's performance. A more sophisticated quaternion representation will be adopted later on.

With more enlightening ideas coming from [25,26] and [24], a neural network will be included into this thesis research. Implementing the neural networks may enhance the tolerance of the error in the model parameters measurements. The system may also handle the disturbances in a better fashion, which may increase the robustness of the system. Because the added complex calculation for the neural network will be lengthening the sampling period for the practical implementation, triangular activation functions and fairly simple network are chosen for the initial set up for the neural network.

1.6 Thesis Contribution

- By collecting the oscillation data, and applying the Fast Fourier Transformation, the natural frequency of the quadrotor is found in Chapter 2. Hence, the moment of inertia is computed.
- A sensor fusion technique in Chapter 3 is implemented to estimate the attitude of the quadrotor in the three dimensional space. The algorithm is based on the published

work in [5]. The experimental results will be posted in Chapter 3. To cope with the different types of the sensory noise, an average filter is applied onto the sensor readings to seek out the noise bias. A necessary digital compass is also performed to ensure the proper heading of the quadrotor.

- The actual flight experiments of attitude control using the various different control schemes discussed in Chapter 5 will be conducted. The nonlinear controllers are derived based on the backstepping technique. A neural network is also added to the controller design.
- An altitude control will be implemented by using a sonar sensor in Section 5.5. A second order butterworth filter is applied to eliminate the noise of the feedback signal.

1.7 Thesis Outline

In this thesis work, Chapter 1 provides the background information of the quadrotor and literature reviewed during the research. Chapter 2 elaborates the details on the hardware selection, aerodynamics of the quadrotor system as well as the method of measuring the moment of inertia. Chapter 3 briefly discusses the sensor usage, which includes the sensor fusion technique, calibration issues for the different sensory unit. Chapter 4 introduces different type of dynamic models. Chapter 5 devotes to controller design with the experiments and simulation results. Chapter 6 gives a summary of this thesis work and suggests the possible future work.

Chapter 2

Experimental Platform

The design of the physical frames for quadrotor is a vital step prior in selecting the appropriate actuation systems and other electronics systems onboard. Many companies and individuals are delicate in the research and development of the quadrotor frames suitable for various applications. Many different types of the quadrotor UAVs are being publicly displayed in [29–32]. A fairly large scale of quadrotor UAV has been designed and tested in [33]. Without a suitable electronics brain, a well developed quadrotor frame is not nearly good enough for a complete quadrotor design. Paparazzi, Pixhawk, Mikrokopter, Arduino Pilot Module(APM) etc. are all the famous brand names of micro-controllers. The control algorithm is coded into these micro-controllers.

2.1 Platform Overview and Electronics

Fig.2.1 is the complete physical build for the experimental quadrotor. The frame was directly purchased from [34], so were majority of other components. The quadrotor consists 4 three phase motors with properly pitched propellers installed on each motor and one APM 2.6 arduino pilot module, which is responsible for running the flight control algorithm. The Electronics Speed Control (ESC) module will eventually convert PWM signals into three phase voltage signals which rotate the motors. Fig.2.2 is showing the general layout for the major components of the quadrotor.

2.1.1 APM 2.6 Pilot Module

The APM 2.6 pilot module is responsible for implementing the nonlinear control algorithm while the quadrotor flying in the air. A 16 MHz ATMEGA 2560 micro-controller is used in this device. There are various different electronics and sensing units onboard. An Inertial Measurement Unit (IMU) MPU 6050 is used to provide the motion tracking. A MS5611-01BA baro metric pressure sensor offers the air pressure readings within different altitude. It is compatible with 3DR Ublox GPS and the embedded digital compass. The 8 channels digital

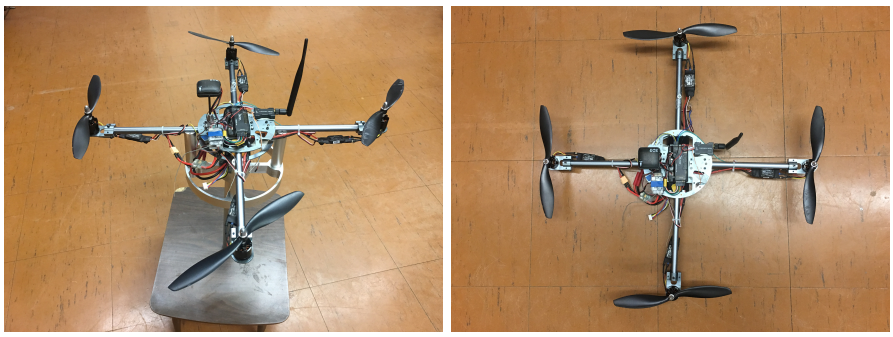

Figure 2.1: Quadrotor Expiremental Platform

input and output is versatile and convenient for possible do-it-yourself (DIY) projects, and expanding more functionalities on the quadrotor. 12 analogue inputs allow communications with various sensors, such as sonar, laser, radar, etc. For transferring data back and forth with a ground computer, a telemetry port is utilized for the Universal Asynchronous Receive and Transmit (UART) communications.

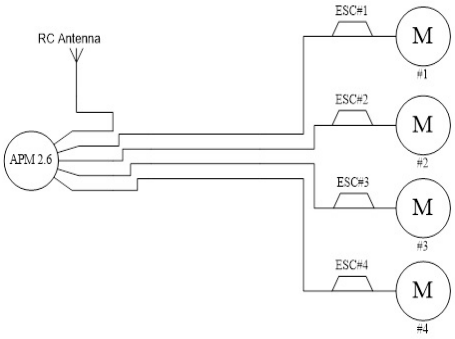

Figure 2.2: Quadrotor Major Components Layout

* *ATMEGA 2560 Micro-Controller*

  The ATMEGA 2560 in Fig.2.3 is designed and manufactured by Atmel Limited which is one of the technological companies interested in researching and developing compact and low cost micro-controllers. It has a 8-bit AVR Central Processing Unit (CPU) and operates at 16 MHz maximum operating frequency. It has 86 General Purpose Input and Output (GPIO) pins. The flash memory is 256 kilo bytes. The controller also has the capability of power-on reset and programmable brown-out detection, which ensures the safe operations of the system when the possible damage may occur due to the power surges. The ATMEGA 2560 is not as powerful as many other micro-controllers available on the market, such as TI controller C2000 32 bits micro-processors [35]. However, it is cheaper, smaller, and simpler in term of programming, so it was chosen by many university research projects and hobbyists.

* *MPU6050 Inertial Measurement Unit*

  The MPU-6050 in Fig.2.4(b) is an IMU, which is used to constantly measure the

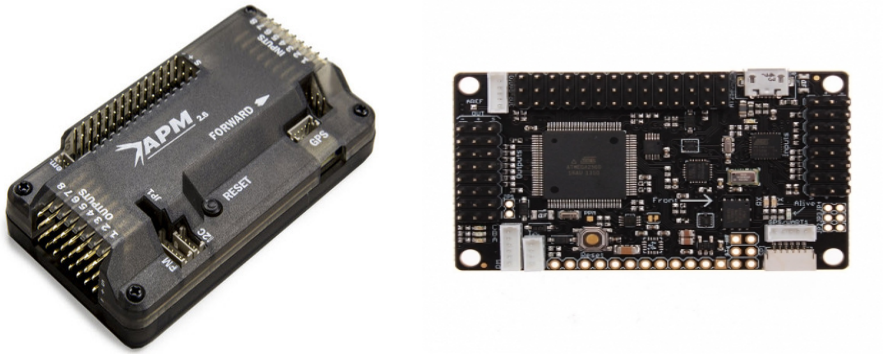

(a) (b)

Figure 2.3: (a) APM 2.6 External Physical Structure; (b) APM 2.6 Circuit Board

acceleration and angular velocity of a rigid body. It is the world's first 6 axis motion tracking devices, which have a 3 axis accelerometer and gyroscope, as well as a Digital Motion Processing (DMP) unit. For the measurement capability, a 3 axis accelerometer has a full scale of $\pm 2g, \pm 4g, \pm 8g, \pm 16g$, on the other hand, a 3 axis gyroscope can measure a full scale of $\pm 250°/s, \pm 500°/s, \pm 1000°/s, \pm 2000°/s$. The data transfer is done with a 400KHz Inter-Integrated Circuit (I^2C) or a 1 MHz Serial Peripheral Interface (SPI).

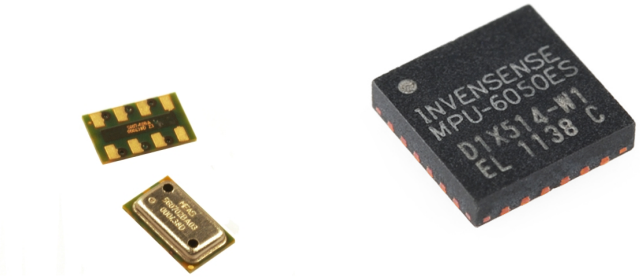

(a) (b)

Figure 2.4: (a) MS5611-01BA Pressure Sensor; (b) MPU-6050

∗ *MS5611-01BA Pressure Sensor*

The APM 2.6 system is also equipped with a barometric pressure sensing unit MS5611-01BA, shown in Fig. 2.4(a). It works under an operating pressure of 0.15 PSI - 17.4 Psi, which is equivalent to 1 kPa to 120 kPa. It can measure up to 10 cm in distance with the high resolution module. For the altitude control of the UAVs, a barometric pressure sensor is extremely important to provide the altitude feedback signals. However, the sensor may not function properly in the closed ground proximity, since the ambient pressure is roughly the same within 100 meters range above the

sea level. Hence, around the lower altitude, a sonar sensor is used to achieve a better result.

2.1.2 Digital Compass and GPS Unit

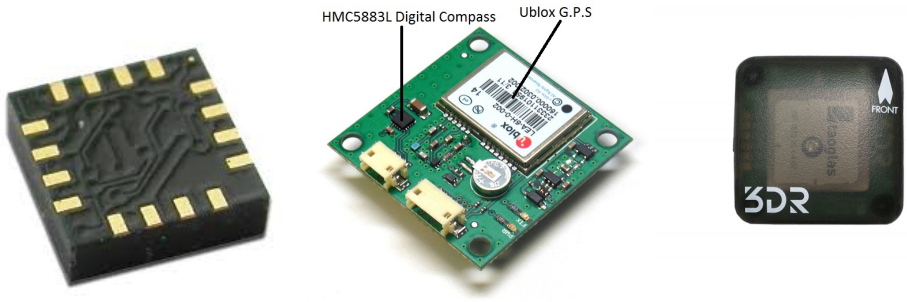

(a) (b) (c)

Figure 2.5: (a) HMC5883L Digital Compass; (b) U-blox GPS Unit with Compass;(c) 3DR GPS and Compass Module

A digital compass, known as a magnetometer, measures the earth magnetic field, which provides the important correctional information for the filter fusion techniques mentioned in [5,6]. A 3 axis digital compass HMC5883L, as shown in the Fig.2.5(a), has a typical supply voltage of 2.5V and an average current draw of $100\mu A$. It can measure a magnetic field ranging from ± 0.88 to ± 8.1 Gauss. It is a low cost surface-mount, multi-chip module with the options of I^2C and SPI digital interfaces. A GPS ublox LEA-6H module is responsible for updating the latitude and longitude information at 5 Hz sampling rate. As shown in Fig.2.5(c), the digital compass and the GPS unit are integrated into the same printed circuit board. In order to eliminate the electrical and mechanical noises coming from the quadrotor, both sensors are being installed couple inches above the platform. Fig.2.5(b) shows the internal structure for the 3DR GPS and compass module.

2.1.3 MB1240 XL-MaxSonar Sensor

The MB1240 XL-MaxSonar Sensor in Fig.2.6 is a reliable sensing unit with a real-time calibration for the changing conditions, which include temperature, electrical and acoustic noises. The power requirements can be as low as 3.3V, which is suitable for the APM 2.6 flight control module. The detection range is from 20 cm to 1068 cm (0.65 to 35 feet). The sensor has a high resistance against the electrical and acoustic noises. It operates with digital as well as analogue output. Hence, it is ideal to use for the quadrotor and other robotics projects, where the rejection of the noise is vital for the successful testing and implementation.

Figure 2.6: MB1240 XL-MaxSonar Sensor

2.1.4 RC Control and Wireless Data Transfer

* *RC Control*

  The JR XBG remote control, shown in Fig.2.7(a), generates the Pulse Position Modulation (PPM) signals, which have a Dual Modulation Spectrum System (DMSS) with 2.4Ghz bandwidth. Prior to the development of the DMSS, JR was widely known for its high response Direct Sequence Spread Spectrum (DSSS) and great ability of interference avoidance Frequency Hopping Spread Spectrum (FHSS). The DMSS antenna in Fig.2.7(b) is simply the combination of the Frequency Hopping (FH) and Spread Spectrum (SS), which provides significantly improved remote control user's experience. The XBG controller has 8 different channels and is user friendly for programming the function of the switches. Different alarm system is equipped, hence any abnormal flying activities will be notified and warned instantaneously without looking at the LCD display on the remote.

(a) (b)

Figure 2.7: (a) JR XGB Remote Control; (b) RG831B with DMSS RA01T Receiver

* *Wireless Data Transfer*

  A 3DR 915Mhz radio telemetry in Fig.2.8 is used for data transmitting and receiving. The maximum power consumption is up to the 100mW with a data transfer rate of 250 kbps. It supports the Listen Before Talk (LBT) with a fairly small physical dimensions. Without the antenna installed, the electronics components only weigh 4 grams. The

Figure 2.8: 2.4 Ghz Wireless Data Transfer Radio

antenna weighs only 1.5g. The FHSS as well as the Time Division Multiplexing (TDM) are also supported in this device. The communications are effective within 3 to 4 Km range, depending on the surrounding interferences and obstacles.

2.1.5 The Actuation System

A proper selection of the motors and propellers is based on the knowledge of the physical characteristics of a quadrotor, such as the total mass of the drone, the diagonal length, the moment of inertia, etc. The propulsion system of a quadcopter is basically composed of 3 major components, the motors, the propellers and the ESC. In [36–39], an introductive guidance on how to form the body of the quadrotor was discussed, which includes the topic on how to pick the right size of motors and propeller blades. In [37, 39], the working principles of many quadcopter related electronics are being explained. In this short section, the functionality and the fundamental working principles of the electronics and mechanical propel system will be elaborated.

* *Three Phase Brushless Motors (TPM)*

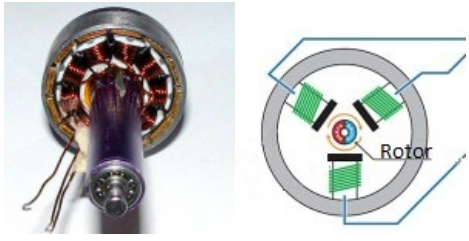

(a) (b)

Figure 2.9: (a)The Core of a TPM; (b)The Concept of a TPM

The three phase brushless motors are the popular choices for the quadrotor applications.

The motor works in a very similar fashion in compare with a simple DC motor, where the brush is intermittently making contacts with the commutator at a fairly high frequency, the induced magnetic field from the current flowing in the coil will generate a torque. However, neither a brush nor the commutator will be seen in a three phase motor.

Figure 2.10: 880KV TPM

As shown in Fig.2.9(b), with the constant magnetic field, the three different coils are being charged with three phase currents which are 120 electrical degrees lagging from one another. This causes a constant shifting of a magnetic field on the coil, hence the rotor will spin in order to catch up with the changing in the magnetic field. In this thesis work, a 880KV motor, shown in Fig.2.10, is chosen. Table 2.1 illustrates some basic electrical and mechanical specifications chosen for the quadrotor.

KV(RPM/V)	Voltage	Max Power	Weight	Dimensions
880KV	7.4-14.8V	302.4W	55.3g	27.8x40.5mm

Table 2.1: 880KV Motor Electrical and Mechanical Parameters

* *Propeller*

By considering the total mass of the quadrotor, the motor and the battery, four 10x4.7 propeller blades, as shown in Fig.2.11, are used for the experimental platform.

Figure 2.11: 10x4.7 Propeller both CCW and CW

The different pitch angles determine the direction of spinning (i.e. the Counter Clock Wise (CCW) and Clock Wise (CW) spinning). The thrust and power coefficient can be found in [40]. The propeller aerodynamics effect and thrust calculations will be introduced later on in this thesis. Table 2.2 gives some basic parameters for the propellers.

	Symbols	Value	Units
Radius	r	0.124	m
Thurst coefficient	C_T	0.1225	n/a
Power coefficient	C_P	0.051	n/a

Table 2.2: Propeller Characteristics

* *Electronic Speed Control*

Figure 2.12: Afro ESC

The ESC module is responsible for converting the PWM signals into a three phase current signal for driving the brushless motors. For the quadrotor applications, the ESC should support high enough PWM signal frequency, i.e., around 300Hz with at least 10 amps current handling capability, since the each selected motor draws 18 Amps. An Afro ESC, shown in Fig.2.12, is selected for the experimental quadrotor, which is able to handle 1 KHz PWM input frequency and outputs 30 Amps maximum. A 2-4S lipo battery is required for the proper function of the device. A couple important parameters of the chosen ESC is given in Table 2.3.

Current Draw	Voltage Range	Input Freq.	Weight	Dimensions
30A Continous	2-4s LiPo	1Khz	26.5g	50x25x11mm

Table 2.3: Afro ESC Electrical and Physical Specs.

* *Power Module*

A Turnigy nano-tech 2650 mAh high discharge Lithium Polymer (LiPo) battery, shown in Fig.2.13, is used for the quadrotor to provide the necessary power on board.

The LiPo battery can provide compelling advantages in comparison to the traditional batteries. The LiPo battery cell can be easily formed into different shapes, which can

Figure 2.13: Turnigy Nano-tech 2.65 LiPo Battery

be used in many mobile devices, laptops, cellular phones, etc. Most of the quadrotors use the LiPo batteries due to its light weight, high charge capacities, and fairly high discharge rates. Table 2.4 describes the related parameters for the battery used.

Capacity	Voltage	Discharge	Weight	Dimensions
2650mAh	4 cell 14.8V	35C constant	291g	145x45x22mm

Table 2.4: The Turnigy Nano-Tech 2650 mAh LiPo Battery.

* *The Assembled System Overview*

An assembled quadrotor is shown in Fig. 2.14. All the components are being positioned and installed under the rule of thumb of maintaining the center of the gravity around the center point of the quadrotor. Since the noises are introduced by the motors and other electrical modules on board the quadrotor, such as the power converter, the battery, ESC, etc, and since these components will distort the magnetic field, a digital compass post is installed to elevate the compass mounting position to reduce the noise interferences. To counter the weight of the GPS module, a wireless data transmit and receive antenna is positioned roughly in the opposite direction from the GPS module. For more details of the assembled quadrotor, one can refer to Fig. 2.14.

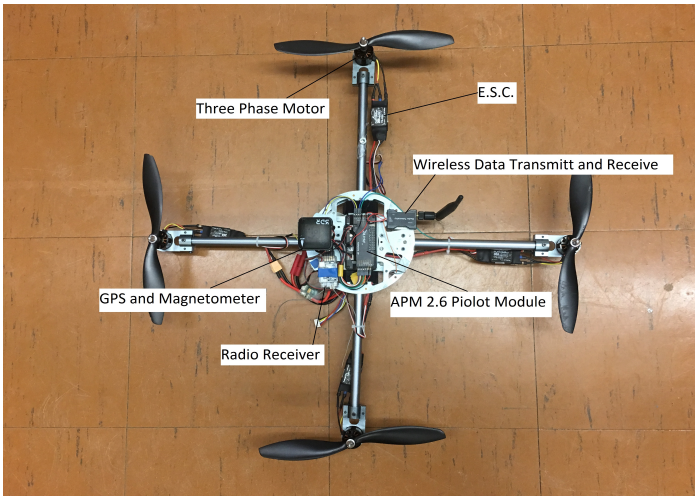

Figure 2.14: Illustration on Assembled Quadcopter

2.2 Moment of Inertia

The moment of inertia is an extremely important parameter for the accuracy of the dynamic model. Before designing the mathematical model, the value of the moment of inertia needs to be identified. There are several methods to complete such a task. The quadrotor can be disassembled and the moment of inertia can be measured for each individual component. The moment of inertia for the system can be calculated by the summation of the all. However, it is quite a complex task to disassembling the quadrotor, as well as measuring them individually may have a considerable amount of inaccuracy due to the human error and the instrumentation mis-calibration. Hence, the moment of inertia is measured for the whole quadrotor system using the Euler Lagrangian model.

With the inspiration of [41, 42], an Euler Lagrangian method is deployed for calculating the moment of inertia respecting to the x, y and z axis. The total kinetic energy on a rigid body is the rotational kinetic energy neglecting the small amount of energy on the suspension wire. It can then be expressed by the following equation

$$K_{total} = \frac{1}{2} I_\beta \dot{\Theta}^2 + \frac{1}{2} m(\dot{\Theta} l)^2 \tag{2.1}$$

where I_β represents the moment of inertia, β is the x, y or z excitation axis. Θ represents angle with respected to the roll, pitch or the yaw direction. m describes the total mass of the quadrotor. Notice here the mass of the suspension wire has been neglected. $\dot{\Theta}$ is the angular velocity respected to the roll, pitch or the yaw direction. l denotes the length from the suspending point to the center of the quadrotor. The potential energy is given in (2.2)

$$V = mg(l - l\cos(\Theta)) \tag{2.2}$$

where g is the gravitational constant, V is the potential energy. Under the theoretical guidance from Euler Lagrangian equation, the Lagrangian can then be found by subtracting the total potential energy V from the total kinetic energy K. Substituting (2.1) and (2.2) into (2.3) produces the following

$$L = K - V = \frac{1}{2} I_\beta \dot{\Theta}^2 + \frac{1}{2} m(\dot{\Theta} l)^2 - mg(l - l\cos(\Theta)) \tag{2.3}$$

which satisfies the following equation

$$\frac{d}{dt}\left(\frac{\partial L}{\partial \dot{\Theta}}\right) - \frac{\partial L}{\partial \Theta} = 0 \tag{2.4}$$

Substituting (2.3) into (2.4) yields the conclusion in (2.5)

$$(I_\beta + ml^2)\ddot{\Theta} + mgl\sin\Theta = 0 \tag{2.5}$$

Since Θ is a very small angle, which is less than $\pm 10°$, $\sin(\Theta) \approx \Theta$. Then, (2.6) can be easily verified

$$(I_\beta + ml^2)\ddot{\Theta} + mgl\Theta = 0 \tag{2.6}$$

By applying the Laplace transform to (2.6) with zero initial conditions, we then get

$$(I_\beta + ml^2)s^2 + mgl = 0 \tag{2.7}$$

Writing (2.7) into the standard form gives (2.8).

$$s^2 + \frac{mgl}{I_\beta + ml^2} = 0 \tag{2.8}$$

Comparing (2.8) with the characteristic polynomial of a standard 2^{nd} order system $s^2 + 2\zeta\omega_{n,\beta} + \omega_{n,\beta}^2$, it follows that $\omega_{n,\beta}$ can be calculated by (2.9)

$$\omega_{n,\beta} = \sqrt{\frac{mgl}{I_\beta + ml^2}} \tag{2.9}$$

which implies that the moment of inertia can be determined by (2.10)

$$I_\beta = \frac{mgl}{\omega_{n,\beta}^2} - ml^2 \tag{2.10}$$

The natural frequency can be calculated based on the date collected from the swing experiments, which is done by hanging the quadrotor system with thin wires, releasing it on a small initial angle, and recording the oscillation of the quadrotor. When taking the measurements for the pitch and roll direction, a thin fish wire is used to tie on the quadrotor's ends onto a hanging post (tie the different ends depending on wether the roll or pitch is measured). When taking the measurements in the yaw direction, the diagonal two ends of the quadrotor are tied to the hanging post, so the system can rotate back and forth around its center. The experimental setup can be seen in Fig. 2.15 and Fig. 2.16 By reading the oscillations of the pitch, roll, and yaw angles, the oscillation graphs, as shown in Fig. 2.17, 2.18 and 2.19, were recorded

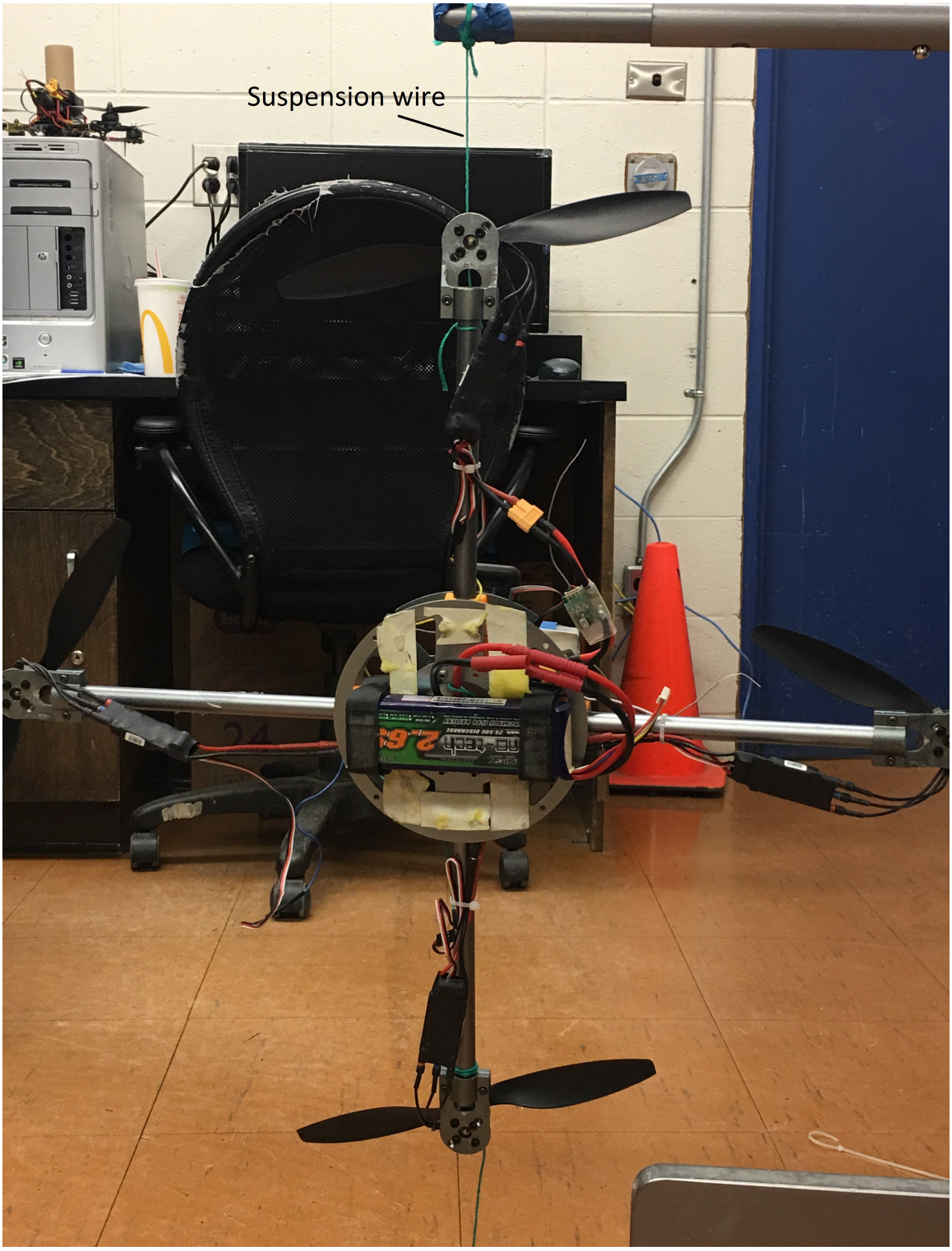

Figure 2.15: Moment of Inertia Experiment Setup for Roll or Pitch Direction

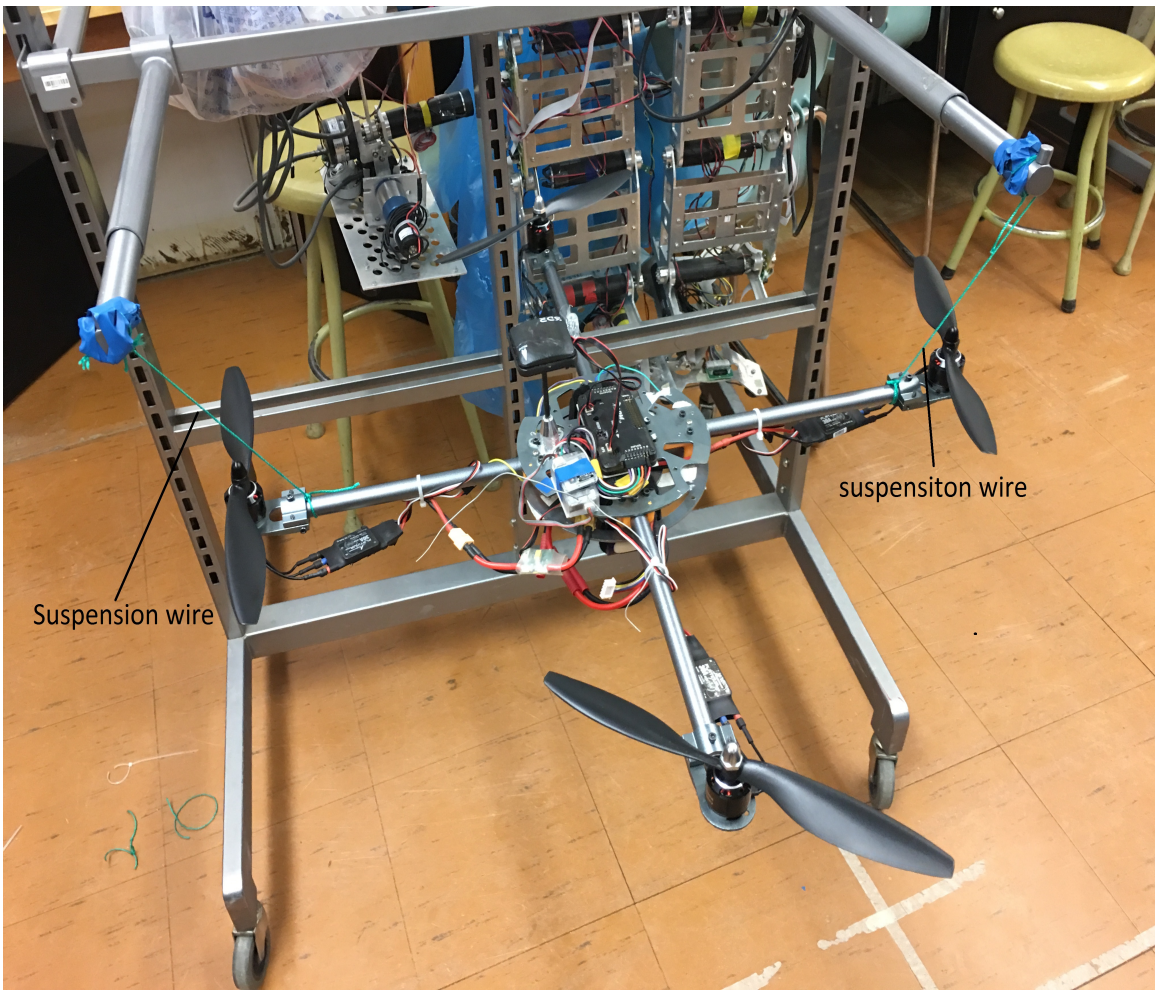

Figure 2.16: Moment of Inertia Experiment Setup for Yaw Direction

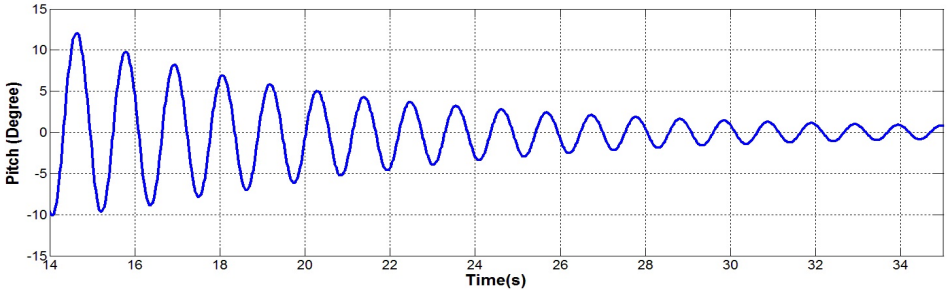

Figure 2.17: Oscillation around x Axis

By using MATLAB Fast Fourier Transform (FFT), we can then obtain the natural frequency in hertz. The results can be seen in Figs. 2.20-2.22, for the roll, pitch and yaw direction, respectively.

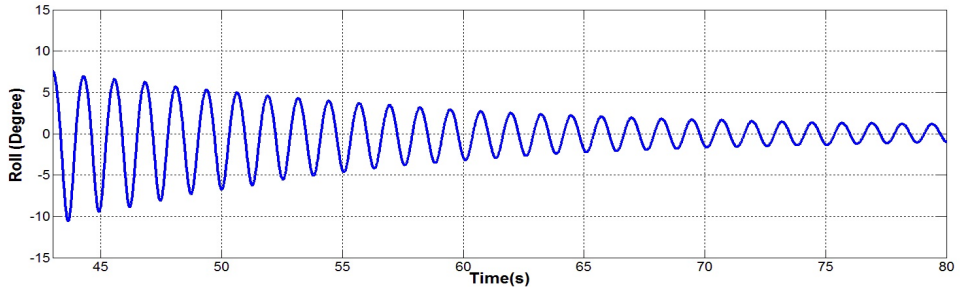

Figure 2.18: Oscillation around y Axis

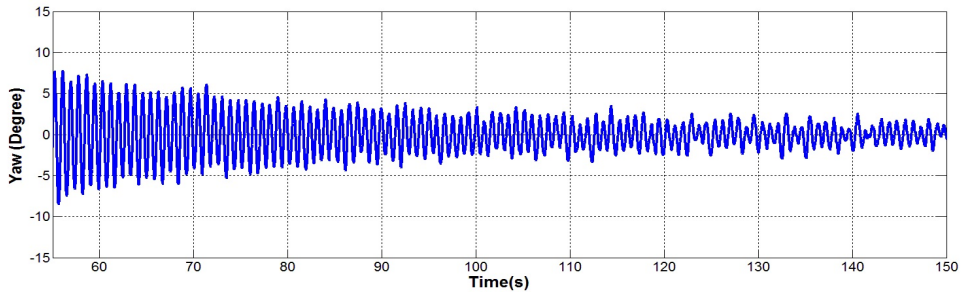

Figure 2.19: Oscillation around z Axis

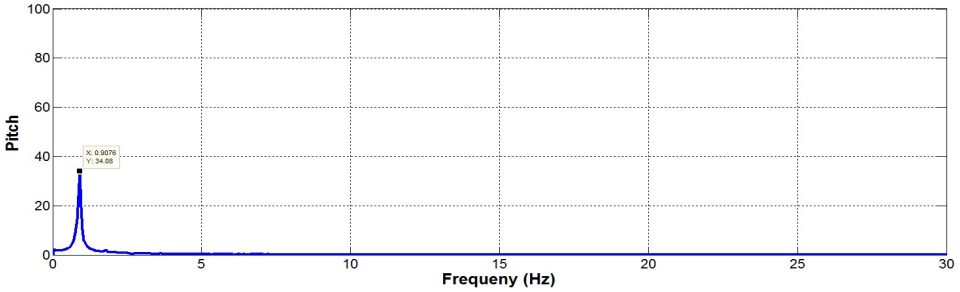

Figure 2.20: Natural Frequency with Respect to x Axis

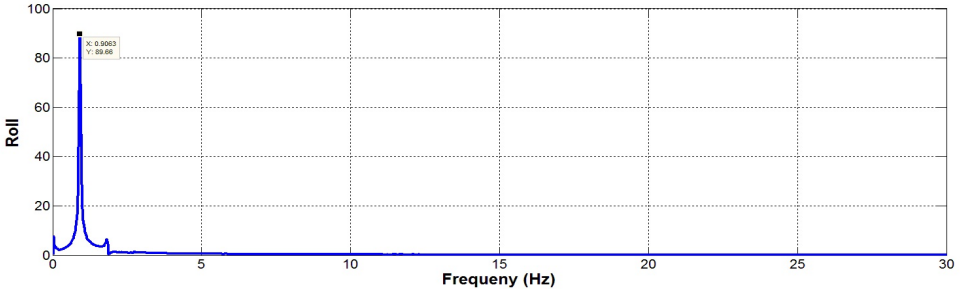

Figure 2.21: Natural Frequency with Respect to y Axis

Once the natural frequencies are calculated, one can simply substitute them into (2.10), along with other known constants, to calculate the moment of inertia. Table 2.5 shows the

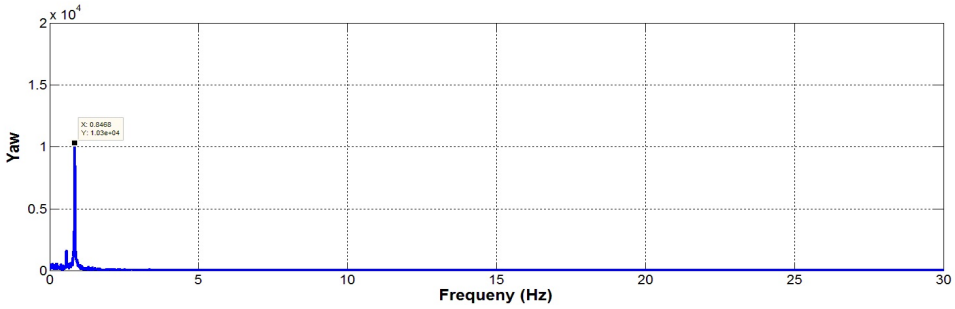

Figure 2.22: Natural Frequency with Respect to z Axis

results and certain important system parameters. While conducting the experiments, a great effort has been made to reduce the oscillation coupling among the x, y and z axes to the minimum, though completely diminishing such a phenomenon is quite impossible. The oscillation coupling among the x, y and z axes are neglected when the moments of inertia are calculated.

Parameter	Description	Value
$\omega_{n,x}$	Natural Frequency in x direction	5.6944 rad/s
$\omega_{n,y}$	Natural Frequency in y direction	5.7027rad/s
$\omega_{n,z}$	Natural Frequency in z direction	5.3208 rad/s
I_x	x direction moment of interia	0.0124 $kg \cdot m^2$
I_y	y direction moment of interia	0.01204 $kg \cdot m^2$
I_z	z direction moment of interia	0.02982 $kg \cdot m^2$
m	Total mass of the quadrotor	1.279 kg
g	Gravitational Contstant	$9.81m/s^2$
l	Distance from the center to the suspension point	$0.29m$

Table 2.5: Model Parameters

2.3 Quadrotor Aerodynamics and Preliminary Calculations

* *Quadrotor Aerodynamics*

  As showing in Fig.2.23, the motors m1, m2, m3 and m4 are spinning simultaneously to generate the total trust in the summation of T1, T2, T3 and T4. The motors m1 and m4 are rotating in the CCW direction, where the air drag creates a CW torque on the center body of the drone. In the complete opposite side, the motors m2 and m4 are rotating in the CW direction, hence the air drag generates a CCW torque on the center body of the drone. At the equilibrium point, the torque, generated by these opposite rotating pair of the propellers, is cancelled out. Therefore, the quadrotor is able to maintain a fixed heading.

  In the pitch direction, if motor m1 is rotating faster than motor m2, then the difference in the vertical thrust forces between T2 and T3 will induce a tilting angle, which will change the attitude of the quadrotor in the pitch direction. Similar behaviour applies to the roll direction, where a roll tilting angle will appear if the difference in the thrust forces is generated between m2 and m3.

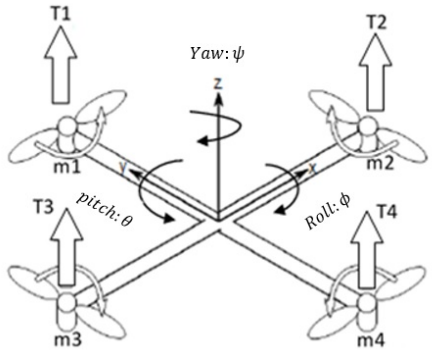

Figure 2.23: Operating Principle of a Quadrotor

* *The Propeller Aerodynamics*

  The aerodynamics of the propeller has been researched and tested intensively over the years, and many authors have advocated their results in [43, 44]. In this thesis work, the thrust moment is considered for the propeller aerodynamics effect, where

$$T_i = b\bar{\omega}_i^2 \tag{2.11}$$

  where b is the thrust factor, $\bar{\omega}_i$ expresses the motor speed, $i \in (1, 2, 3, 4)$. By the momentum theory in [44], (2.11) can then be expressed as:

$$b = \frac{4C_T \rho r^4}{\pi^2} \tag{2.12}$$

  where C_T is the thrust coefficient, which can be found from [45] or [46], r is the radius of the circular area while the propeller is spinning, and ρ is the air density. C_T heavily

Parameters	Description	Units
C_T	0.1225	-
C_p	0.051	-
ρ	1.225	kg/m^3
A	0.04676	m^2
r	0.122	m
b	1.347323e-5	-
d	2.1783e-7	-

Table 2.6: Propeller Specifications

depends on the shape of the propeller blades. The momentum and blade theory can be used to calculate such a coefficient, for more details, please see [44]. With (2.11) and (2.12), one can rewrite the thrust moment by

$$T_i = \frac{4C_T\rho A^2\bar{\omega}_i^2}{\pi^4} \tag{2.13}$$

where A is the circular area while the propeller is spinning.

The rotating of the propeller not only creates the thrust, but also introduces a drag moment on the quadrotor, which, in turns, controls the stability of the yaw direction. This quantity can be defined as:

$$d = \frac{4C_p\rho r^5}{\pi^3} \tag{2.14}$$

C_p is the power factor of the propeller, the same as for the thrust coefficient. C_p can be found in the manufacture's website in [45], or in [46] where many different characteristic parameters of the various types of the propellers manufactured by different companies can be found. Table 2.6 is a quick summarization on the coefficients used for the propeller as well as the calculated drag factor d and the thrust factor b. Recalling (2.11), along with the observation we made in Fig. 2.23, the torque can be rewritten as

$$\begin{bmatrix} \tau_\phi \\ \tau_\theta \\ \tau_\psi \end{bmatrix} = \begin{bmatrix} bl(\bar{\omega}_1^2 - \bar{\omega}_4^2) \\ bl(\bar{\omega}_2^2 - \bar{\omega}_3^2) \\ d(\bar{\omega}_1^2 + \bar{\omega}_4^2 - \bar{\omega}_2^2 - \bar{\omega}_3^2) \end{bmatrix} \tag{2.15}$$

The total vertical thrust can be written as

$$T_{total} = U_1 = b(\bar{\omega}_1^2 + \bar{\omega}_2^2 + \bar{\omega}_3^2 + \bar{\omega}_4^2) \tag{2.16}$$

Combining both (2.15) and (2.16), one can derive the following:

$$\begin{bmatrix} U_1 \\ \tau_\phi \\ \tau_\theta \\ \tau_\psi \end{bmatrix} = \begin{bmatrix} b & b & b & b \\ 0 & -bl & 0 & bl \\ -bl & 0 & bl & 0 \\ d & -d & d & -d \end{bmatrix} \begin{bmatrix} \bar{\omega}_1^2 \\ \bar{\omega}_2^2 \\ \bar{\omega}_3^2 \\ \bar{\omega}_4^2 \end{bmatrix} \tag{2.17}$$

Now, we have the relationship between the torque and the angular speeds of the propellers. We can then easily convert the desired torque to the rotational speeds for the propellers.

* *Thrust Calculation*

The total possible thrust is directly related to (2.11), where the maximum rotational speed of the propeller will be substituted into (2.11). During the prior discussion in Section 2.1.5, a 880KV TPM motor and a 2650 mAh 14.8V LiPo battery are used for the quadrotor actuation system. The rotor maximum rotational speed is directly related to the battery used and the motor performance specifications. Therefore, $\bar{\omega}_{\max}$ can be calculated with the following equation:

$$\bar{\omega}_{\max} = 14.8V \times 880KV \times \frac{2\pi}{60s} = 1363.81rad/s \tag{2.18}$$

By using (2.11) once more, the maximum total thrust can be determined by

$$T_{total} = 4b\bar{\omega}_{\max}^2 = 4 \times 1.09986 \times 10^{-5} \times (1363.81)^2 = 81.83N = 8.341kg \tag{2.19}$$

which means that the maximum thrust is able to pull a total weight of $8.341kg$ up in the air. The total weight of the drone is $1.279kg$, hence the drone will lift off the ground when the throttle reaches approximately 15%.

Chapter 3

Attitude Estimation

Due to the lack of the attitude measurements from the sensory technology, a robust and reliable attitude estimation is a vital step in order to achieve optimal control results on a system. This area of research can be traced all the way back to the 60s. Since then, different contributions have been made in [47–50]. Due to the sensor noise and gyroscope bias, to retrieve an attitude of a rigid body becomes uncertain by using the basic trigonometry on the acceleration measurements and performing the integration on the angular velocity measurements. A fairly reliable and well established EFK was extensively discussed in [7, 8], where the current state variables are predicted based on the previous quantities with additive noise.

In this thesis work, a very same filtering concept coming from [5] is implemented. A nonlinear attitude estimator is introduced, which allows the decoupling of the pitch and roll from the yaw estimation. On the other hand, in order to improve the integrator wind-up issue, the dynamics of the gyroscope bias estimation has been modified. Before embarking onto the discussion of such a sensor fusion technique, a brief attitude representation of a rigid body need to be discussed in the following sections.

3.1 The Attitude Representations

A well established and designed rigid body representation is extremely important for the control scheme design and implementation. The attitude representation is describing how a rigid body is placed in the three dimensional space. There are quite a few different methods developed to represent the attitude of a rigid body over the years, such as Euler angles, Tait-Bryan angles, orientation vector, rotational matrix, and quaternion representations. A very detailed illustrations can be found in [4]. The Euler angle, rotational matrix and the unit quaternion representation will be elaborated in this thesis work. Later on, the Euler angle and the unit quaternion representations are used for the controller design.

When describing the attitude representation, two different coordinate systems are used,

which are the inertial frame denoted as I and the body frame denoted as B. The inertial frame I is usually attached to the earth, while the z_B of the body frame is perpendicular to the surface of the ground, x_B is defined as the front of the quadrotor, and y_B is perpendicular to the vertical cross section of the quadrotor.

3.1.1 Rotational Matrix

The rotational matrix is also known as the direct cosine matrix, which is able to exchange the coordinate systems between the inertial frame I and the body frame B. It is one of the most popular representation methods being used, due to its intuitive understanding and straight forward calculation. However, such an algorithm is quite cumbersome to calculate, hence it may not be suitable for the practical implementations. Since the body frame attitude need to be projected onto the inertial frame, we can then perform a dot product which is defined as follow:

$$\hat{a} \cdot \hat{b} = ||a||\ ||b|| \cos\theta \tag{3.1}$$

where the two unit vectors $\hat{a} \in (\hat{x}_B, \hat{y}_B, \hat{z}_B)$ and $\hat{b} \in (\hat{x}_I, \hat{y}_I, \hat{z}_I)$ are used. A full rotation of a rigid body can be dissected into three different rotations respect to the x, y,and z axis. Representing them in the three dimensional space by using the right hand rules, one can consider the following matrices:

$$R_x = \begin{bmatrix} 1 & 0 & 0 \\ 0 & \cos\phi & -\sin\phi \\ 0 & \cos\phi & \cos\phi \end{bmatrix} \quad R_y = \begin{bmatrix} \cos\theta & 0 & \sin\theta \\ 0 & 1 & 0 \\ -\sin\theta & 0 & \cos\theta \end{bmatrix} \quad R_z = \begin{bmatrix} \cos\psi & -\sin\psi & 0 \\ \sin\psi & \cos\psi & 0 \\ 0 & 0 & 1 \end{bmatrix} \tag{3.2}$$

The rotational matrix from the body to the inertial frame can be obtained from the multiplication of the three rotational matrices defined in (3.2), as shown below.

$$\begin{aligned} R &= R_z\ R_y\ R_x \\ &= \begin{bmatrix} \cos\theta\cos\psi & \cos\phi\cos\psi\sin\theta - \cos\phi\sin\psi & \sin\phi\sin\psi + \cos\phi\cos\psi\sin\theta \\ \cos\theta\sin\psi & \cos\phi\cos\psi + \cos\phi\sin\theta\sin\psi & \cos\phi\sin\theta\sin\psi - \cos\psi\sin\phi \\ -\sin\theta & \cos\theta\cos\phi & \cos\theta\cos\phi \end{bmatrix} \end{aligned} \tag{3.3}$$

The direct cosine matrix is a convenient tool to use when transferring between the inertial and body frames. A couple important characteristics of the rotational matrix need to be mentioned:

$$R^T R = R R^T = I_3, \det(R) = 1 \tag{3.4}$$

where I_3 is the identity matrix.

3.1.2 Euler Angle

The Euler angle representation is discovered and developed by Leonhard Euler, which is to describe the attitude of a rigid body respect to the inertial frame. The Euler angle has a very clear physical understanding, one can easily picture the attitude of the rigid body in the three dimensional space by using the Euler angle system. In most of the cases, the

Euler angles are defined as ϕ, θ,and ψ which are named as the roll, pitch and yaw. They are the rotations respect to the x, y and z axis. The singularity problem or the gimbal lock is the major disadvantages for the Euler angle representation, where one degree of the freedom is lost from such phenomenon. For example, if the pitch gimbal and the yaw gimbal overlaps, then changes in the roll and the yaw is describing the same rotation of a rigid body. The problem can be resolved by adding one extra gimbal, or using a different attitude representation, such as the unit quaternion representation. From the rotational matrix (3.3), a rotational sequence of the yaw-pitch-roll performed is shown in Table 3.1.

1.rotation respect to the z axis with angle $\psi, x\ y\ z \Rightarrow x'\ y'\ z'$
2.rotation respect to the y axis with angle $\theta, x'\ y'\ z' \Rightarrow x''\ y''\ z''$
3.rotation respect to the z axis with angle $\phi, x''\ y''\ z'' \Rightarrow x'''\ y'''\ z'''$

Table 3.1: Rotational Sequence

Another 12 possible rotational sequences including the above example are as following:

$$\begin{aligned} &x-y-z, \quad z-y-x \\ &y-z-x, \quad x-z-y \\ &z-x-y, \quad y-x-z \\ &z-x-z, \quad x-z-x \\ &x-y-x, \quad y-x-y \\ &y-z-y, \quad z-y-z \end{aligned}$$

3.1.3 Unit Quaternion

With the inspiration of the Euler's rotation theorem, where it was stated that any rotations of a rigid body respect to a fixed point is equivalent to the rotation around a axis which is through that fixed point by a given angle θ. It can be seen in Fig. 3.1. The unit quaternion is represented by four different components, which are expressed as follow:

$$Q = \begin{bmatrix} q_0 \\ q \end{bmatrix} = \begin{bmatrix} q_0 \\ q_1 \\ q_2 \\ q_3 \end{bmatrix} = \begin{bmatrix} \cos\frac{\theta}{2} \\ \hat{k}_x \sin\frac{\theta}{2} \\ \hat{k}_y \sin\frac{\theta}{2} \\ \hat{k}_z \sin\frac{\theta}{2} \end{bmatrix} \tag{3.5}$$

As shown in (3.5), the unit quaternion only has four parameters. In the comparison with the rotational matrix, where nine different parameters are involved in calculating the attitude of the quadrotor, the unit quaternion representation dramatically reduces the computational complexity without singularity problem.

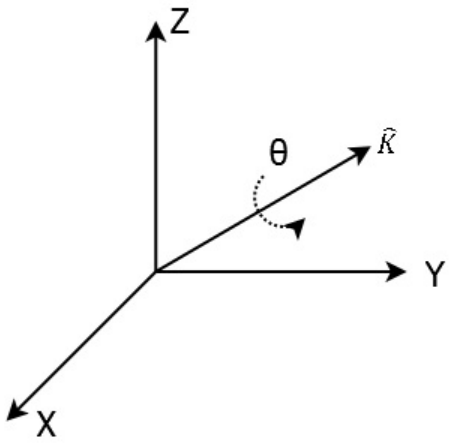

Figure 3.1: Unit Quaternion Graphical Representation

The mathematical properties of the quaternion representation are introduced below, which will be used as part of the controller design. The length of the unit quaternion is one, that is

$$q_0^2 + q^T q = 1 \tag{3.6}$$

The multiplication of the two quaternion are given by:

$$Q \odot P = \begin{bmatrix} q_0 p_0 - q^T p \\ q_0 p + p_0 q + q \times p \end{bmatrix} \tag{3.7}$$

where $\odot$ denotes the quaternion multiplication. The inverse of a quaternion is defined by:

$$Q^{-1} = \begin{bmatrix} q_0 \\ -q \end{bmatrix} \tag{3.8}$$

To calculate the discrepancies between the two different quaternion, one can have the following expressions:

$$E = Q^{-1} \odot P = \begin{bmatrix} q_0 p_0 + q^T p \\ q_0 p - p_0 q - q \times p \end{bmatrix} = \begin{bmatrix} q_0 p_0 + q^T p \\ p_1 q_0 - p_0 q_1 + p_2 q_3 - p_3 q_2 \\ p_2 q_0 - p_0 q_2 - p_1 q_3 + p_3 q_1 \\ p_1 q_2 - p_0 q_3 - p_2 q_1 + q_0 p_3 \end{bmatrix} \tag{3.9}$$

3.2 Sensor Calibration

The onboard sensors, such as accelerometer, gyroscope and magnetometer, are all affected by the different biases. These noise should be modeled mathematically before the implementation of the proposed controller for the quadrotor. A detailed calibration method is discussed in this subsection.

* *Gyroscope and Accelerometer Calibration*

The gyroscope readings are modeled as follows:

$$\omega_B = \omega_{B-actual} + b_{gyro} \tag{3.10}$$

where $\omega_{B-actual}$ denotes the angular velocity without the noise interferences with respect to the actual body frame and b_{gyro} describes the bias of the gyroscope. A straightforward averaging method is applied to calculate the bias. It can then be expressed by

$$b_{gyro} = \frac{1}{samples} \sum_{k=1}^{samples} b_{gyro}(k) \tag{3.11}$$

Before the quadrotor taking off, 1500 samples are summed and averaged. The gyro bias is then calculated. The accelerometer calibration is quite necessary due to its high sensitivity to the vibration noises. The noise model can be described by

$$a_B = R^T a_{accl} + b_{accl} \tag{3.12}$$

where a_{accl} is the measured linear acceleration in the inertial frame, R^T is the rotational matrix transferring from the inertial frame to the body frame, and b_{accl} denotes the measurement bias which can be defined by

$$b_{accl} = \frac{1}{samples} \sum_{k=1}^{samples} a_B(k) \tag{3.13}$$

Again, 1500 samples are recorded and processed with equation (3.13) before taking off.

* *Magnetometer Calibration*

There are five different sources of errors involved in the magnetometer measurements. At the physical level, these errors can be broken into two categories, those inherent by the sensors and those from the measurements of the magnetic fields. The scale factor errors denoted by E_{scale} and null shift errors denoted by E_{shift} are a trait of each individual sensing element, where the null shift error is a DC offset coming from the sensor itself. The physical misalignment errors denoted by E_{mis} are caused by manufacturing tolerances in the construction of the sensor sets. The hard iron and the soft iron errors denoted by E_{iron}, on the other hand, are side effects when measuring a magnetic field. As a result, if there is a strong magnetic material or a couple spinning motors around the sensors, the magnetic field will then be distorted, hence the accuracy of the readings will be negatively impacted.

The errors can be expressed mathematically in (3.14)

$$\hat{B} = E_{mis}E_{iron}E_{scale}(1+\delta)B^{earth} + E_{shift} \tag{3.14}$$

where the $\hat{B}$ is the measured value from the sensor. To calibrate the digital compass, [41,51,52] provides the in-depth theory and precise procedure to follow. The calibration procedure is completely based on the published work [51]. Many references are taken

from [41]. A well calibrated magnetic field can be represented by a sphere geometrically. The whole calibration procedure can be started by defining the x axis as the reference, hence this axis does not have any misaligned error. Then, the magnetic measurements $\hat{B}_{x-b}$ along the x axis, including errors, can be modeled by

$$\hat{B}_{x-b} = aB_{x-b} + x_o \tag{3.15}$$

where x_0 is the total offset error, a is the total scale error on the x direction of the sensor, and B_{x-b} is the ideal measurements without any errors. Since the x direction is chosen as the reference for the misalignment error, the magnetic measurements in the y direction can be described by

$$\hat{B}_{y-b} = b(B_{y-b}\cos(\rho) + B_{x-b}\sin(\rho)) + y_0 \tag{3.16}$$

In (3.16), $\hat{B}_{y-b}$ is the actual measurements from the sensor, b is the total scale error in the y direction, B_{y-b} is the ideal measurements without errors, ρ is the total angular misalignment error between the y direction and the y sensor, and y_0 is then the total offest error in the y direction. By the similar concepts, one can derive the math model for the digital compass z axis measurement $\hat{B}_{z-b}$ as

$$\hat{B}_{z-b} = c(B_{z-b}\cos(\phi)\cos(\theta) + B_{b-x}\sin(\phi)\cos(\theta) + B_{b-y}\sin(\theta)) + z_0 \tag{3.17}$$

where $\hat{B}_{z-b}$ is the actual measurements from the sensor, c is the total scale error in the z direction, B_{z-b} is the ideal measurements without errors, θ is the total angular misalignment error between the z direction and the z sensor, and z_0 is then the total offest error in the z direction.

Without any error interferences, an ideal magnetic field takes a shape of sphere with a radius of B, which can be described in the following equation.

$$B^2 = B_{x-b}^2 + B_{y-b}^2 + B_{z-b}^2 \tag{3.18}$$

The procedure for solving the B_{x-b}, B_{y-b}, and B_{z-b} from (3.15), (3.16), and (3.17) can be found in Appendix B. By substituting the results B_{x-b}, B_{y-b}, and B_{z-b} from (3.15), (3.16), and (3.17) into (3.18), the following equation is obtained.

$$\begin{aligned} &A\hat{B}_{x-b}^2 + B\hat{B}_{x-b}\hat{B}_{y-b} + C\hat{B}_{x-b}\hat{B}_{z-b} + D\hat{B}_{y-b}^2 + E\hat{B}_{y-b}\hat{B}_{z-b} \\ &+ F\hat{B}_{z-b}^2 + G\hat{B}_{x-b} + H\hat{B}_{y-b} + I\hat{B}_{z-b} + J = 0 \end{aligned} \tag{3.19}$$

where the A, B, C, D, E, F, G, H, I, and J are the function of a, b, c, x_0, y_0, z_0, ρ, θ, and ϕ. The sphere equation (3.18) turns into an off centered and distorted ellipsoid (3.19).

The strength of earth magnetic field varies on the different geographic locations at the mean sea level. The decomposition of the earth magnetic field is found to be $m_{earth} = (0.15578, -0.001027, 0.54279)$ [53, 54]. More details on these calibration algorithm will be introduced later on in Appendix B. For the sakes of demonstrations, the results are posted into Table 3.2.

Fig. 3.2 shows the graphical results before and after the calibration of the magnetometer.

Parameter Name	Description	value
x_0	offset error x	0.0165
y_0	offset error y	-0.0803
z_0	offset error z	-0.1482
ρ	misalignment x	0.04363
θ	misalignment y	-0.0237
ϕ	misalignment z	0.05445
a	scale error x	0.4532
b	scale error y	0.5781
c	scale error z	0.5845

Table 3.2: HMC 5883 Digital Compass Calibration Results

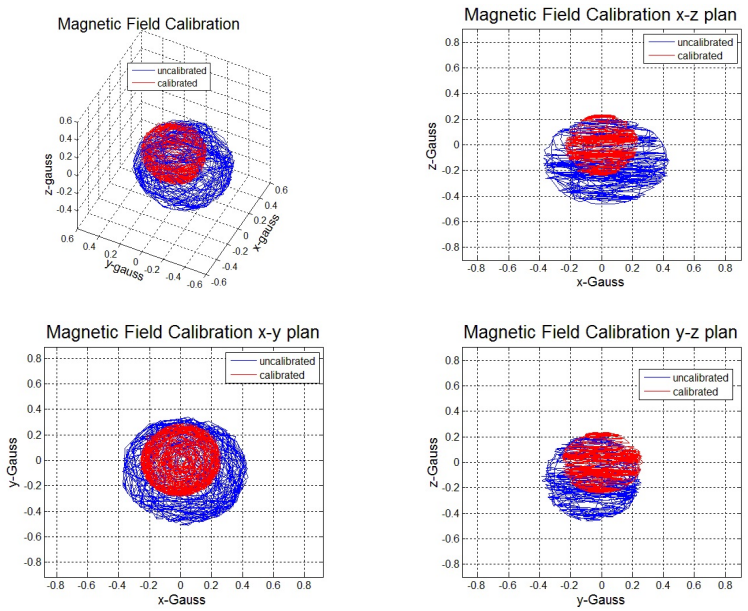

Figure 3.2: HMC-5883 Digital Compass Calibration Results

3.3 Sensor Fusion Technique

The development of a reliable and robust attitude estimation technique is quite important for controller design and implementations. The sensor fusion technique used in this thesis work is taken from [5,6]. The theoretical derivation and proof will not be discussed in details, however the more practical implementations will be elaborated in this thesis.

Some definitions are explained in the following equations.

$$\begin{aligned} u_B &= -\frac{a_B}{g} \\ u_I &= [\ 0 \quad 0 \quad 1\ ]^T \\ v_B &= \frac{\pi_{u_B} m_B}{||\pi_{u_I} m_I||} \\ v_I &= \frac{\pi_{\pi_I} m_B}{||\pi_{u_I} m_I||} \end{aligned} \tag{3.20}$$

where u_B is the real measurements from the accelerometer, m_B is the real measurements from the magnetometer, m_I is the magnetic field of the earth, and $\pi_x = ||x||^2 I_3 - xx^T$. The observer is composed of the estimation $\hat{R}$ of the rotational matrix R from the body frame to the inertial frame, and the estimation of the bias $\hat{b}$. Define $\hat{u}_B = \hat{R}^T u_I$ and $\hat{v}_B = \hat{R}^T v_I$. Then, the complete observer with the bias estimation can be written by

$$\begin{aligned} \dot{\hat{R}} &= \hat{R}(\Omega_y - \hat{b} + \sigma_R) \\ \dot{\hat{b}} &= -k_b \hat{b} + k_b sat_\Delta(\hat{b}) + \sigma_b \end{aligned} \tag{3.21}$$

where the estimations of the unknown bias σ_b and the innovation term σ_R are given by.

$$\begin{aligned} \sigma_R &= k_1 u_B \times \hat{u}_B + k_2 \hat{u}_B \hat{u}_B^T (v_B \times \hat{v}_B) \\ \sigma_b &= -k_3 u_B \times \hat{u}_B - k_4 v_B \times \hat{v}_B \end{aligned} \tag{3.22}$$

with Ω_y being the measured angular velocity with the bias error and the saturation function $sat_\Delta(\hat{b})$ being defined by $sat_\Delta(\hat{b}) = \hat{b}\min(1, \Delta/||\hat{b}||)$. All the coefficients from k_1 to k_4, k_b, and Δ are the positive real numbers. By using the quaternion representation, (3.21) can be written as

$$\dot{\hat{q}} = \frac{1}{2} A(\hat{\Omega}) \hat{q} \tag{3.23}$$

$$\dot{\hat{b}} = -k_b + k_b sat_\Delta(\hat{b}) + \sigma_b \tag{3.24}$$

where $\hat{\Omega}$ is given by

$$\hat{\Omega} = \Omega_y - \hat{b} + \sigma_R \tag{3.25}$$

and the $A(\hat{\Omega})$ is defined by

$$A(\hat{\Omega}) := \begin{bmatrix} 0 & -\hat{\Omega}^T \\ \hat{\Omega} & -\hat{\Omega}_\times \end{bmatrix} \tag{3.26}$$

with

$$\hat{\Omega}_\times = \begin{bmatrix} 0 & -\hat{\Omega}_3 & \hat{\Omega}_2 \\ \hat{\Omega}_3 & 0 & -\hat{\Omega}_1 \\ -\hat{\Omega}_2 & \hat{\Omega}_1 & 0 \end{bmatrix} \tag{3.27}$$

where $\hat{\Omega} = [\hat{\Omega}_1, \hat{\Omega}_2, \hat{\Omega}_3]^T$. Considering the limited computational power of the microcontroller, a discrete version of the attitude estimation is applied. Hence, integrating (3.23) and (3.24) yields

$$\hat{q}_{k+1} = \exp\left(\frac{T}{2} A(\hat{\Omega})\right) \hat{q}_k \tag{3.28}$$

and

$$\hat{b}_{k+1} = T(-k_b\hat{b}_k + k_b sat_\Delta(\hat{b}_k) + \sigma_b) + \hat{b}_k \tag{3.29}$$

Applying the Taylor series expansion to (3.28) gives

$$\hat{q}_{k+1} = \left(cos\left(\frac{T}{2}|\hat{\Omega}_k|\right) I_4 + \frac{T}{2} sinc\left(\frac{T}{2}|\hat{\Omega}_k|\right) A(\hat{\Omega}_k) \right) \hat{q}_k \tag{3.30}$$

The sampling time T is set to be 0.01s, and the values of the k are chosen as follows:

$$k_1 = 1.2,\ k_2 = 0.5,\ k_3 = \frac{k_1}{32}, k_4 = \frac{k_2}{32}$$

Fig. 3.3 shows the actual experimental results, which suggest a successful implementation of the filtering technique. During the experiment, the initial conditions for the filter are given by ± 45 degrees for both pitch and roll angles, respectively, and -80 degrees for the yaw angle. The experimental results are obtained by placing the quadrotor on a flat surface (i.e. the pitch and roll angles are both zero) and pointing to the north which implies that the yaw is zero degrees.

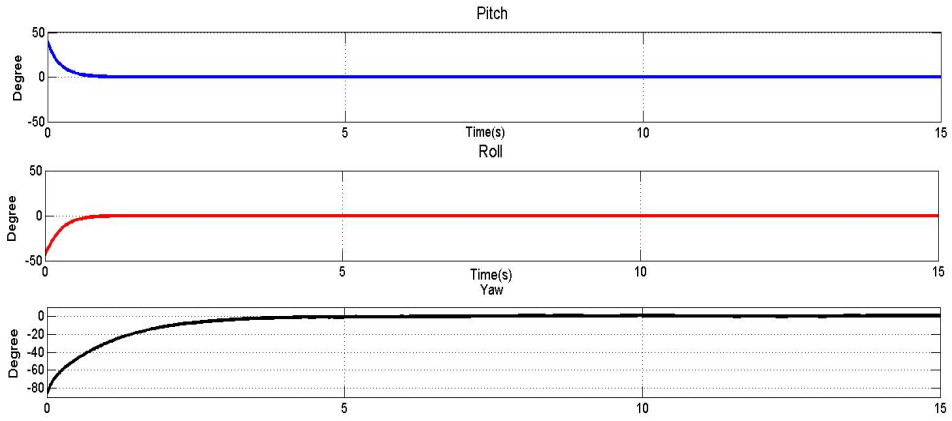

Figure 3.3: Filter Testing Results

Chapter 4

Quadrotor Dynamics

The controller design in this thesis work is inspired by the work done in [10] [11], as well as [21]. Since an integrator has the effect of eliminating the steady state error, an integration term is also added to the backstepping technique to further enhance the performance of the nonlinear controller. It is well known that the uncertainties of the model parameters will affect the performance of the system. In order to reduce the impact of the uncertainties, an intelligent controller using the neural network is applied to estimate the nonlinear terms of the dynamic model.

The backstepping technique is heavily based on the math model, hence a fairly well developed dynamic model need to be addressed first before any kind of elaboration on the controller design. In this thesis, an Euler Lagrangian equation is used to establish the dynamic model of the quadrotor first, and then in order to avoid the singularity of the Euler angles, the quaternion based dynamics is utilized based on the Newton equations.

4.1 Euler Lagrangian Dynamic Model

The quadrotor has six degrees of the freedom, which can be represented as pitch ϕ, roll θ and yaw ψ rotational movements respect to the x, y and z axes of the inertial frame, and the translational movements along the x, y and z directions of the inertial frame. Define $\mu = (\phi, \theta, \psi) \in \mathbb{R}^3$ and $\zeta = (x, y, z) \in \mathbb{R}^3$. It is assumed that $(\phi, \theta) \in [-\frac{\pi}{2}, \frac{\pi}{2}]$ and $\psi \in [-\pi, \pi)$. The translational and rotational kinetic energy can be described by the following equations

$$\begin{aligned} T_{trans} &= \frac{1}{2} m \dot{\zeta}^T \dot{\zeta} \\ T_{rot} &= \frac{1}{2} \dot{\mu}^T I \dot{\mu} \end{aligned} \tag{4.1}$$

where m is the mass of the quadrotor, $I = RI_B$ is the inertia matrix in the inertial frame with $I_B = \begin{bmatrix} I_x & 0 & 0 \\ 0 & I_y & 0 \\ 0 & 0 & I_z \end{bmatrix}$ being the inertia matrix in the body frame which was measured

by the experiments discussed in Chapter 2. The total potential energy is calculated by $U = mgz$ with g being the gravitational constant. By the Lagrangian modelling method, the following function is defined first.

$$L(q, \dot{q}) = T_{trans} + T_{rot} - U = \frac{1}{2} m \dot{\zeta}^T \dot{\zeta} + \frac{1}{2} \dot{\mu}^T I \dot{\mu} - mgz \tag{4.2}$$

Then, applying the Euler Lagrangian equation to (4.2) yields

$$\frac{d}{dt} \frac{\partial L}{\partial \dot{q}} - \frac{\partial L}{\partial q} = (F_\zeta, \tau) \tag{4.3}$$

where τ represents the torque applied on the center of the quadrotor and F_ζ is the translational force defined as $F_\zeta = RF_B$ with $F_B = \begin{bmatrix} 0 & 0 & U_1 \end{bmatrix}^T$ and R being the rotational matrix from the body frame to the inertial frame. U_1 is the total thrust moment generated by four motors, which can be determined by

$$U_1 = T_1 + T_2 + T_3 + T_4 \tag{4.4}$$

The Euler Lagrangian dynamic model is derived as follows:

$$\begin{bmatrix} \ddot{x} \\ \ddot{y} \\ \ddot{z} \end{bmatrix} = \begin{bmatrix} \cos\phi \sin\theta \cos\psi + \sin\phi \sin\psi \\ \cos\phi \sin\theta \sin\psi - \sin\phi \cos\psi \\ \cos\phi \cos\theta \end{bmatrix} \frac{U_1}{m} + \begin{bmatrix} 0 \\ 0 \\ -g \end{bmatrix} \tag{4.5}$$

$$\begin{bmatrix} \ddot{\phi} \\ \ddot{\theta} \\ \ddot{\psi} \end{bmatrix} = \begin{bmatrix} \dot{\theta}\dot{\psi} \left(\frac{I_y - I_z}{I_x} \right) - \frac{J_r}{I_x} \dot{\theta} \bar{\omega} \\ \dot{\phi}\dot{\psi} \left(\frac{I_z - I_x}{I_y} \right) + \frac{J_r}{I_y} \dot{\phi} \bar{\omega} \\ \dot{\phi}\dot{\theta} \left(\frac{I_x - I_y}{I_z} \right) \end{bmatrix} + \begin{bmatrix} \frac{l}{I_x} & 0 & 0 \\ 0 & \frac{l}{I_y} & 0 \\ 0 & 0 & \frac{1}{I_z} \end{bmatrix} \begin{bmatrix} \tau_\phi \\ \tau_\theta \\ \tau_\psi \end{bmatrix} \tag{4.6}$$

where g is the gravitational constant, m is the mass of the quadrotor, J_r is the moment of inertia of the motor, I_x is the moment of inertia of the quadrotor respect to x axis in the body frame, I_y is the moment of inertia of the quadrotor respect to y axis in the body frame, I_z is the moment of inertia of the quadrotor respect to z axis in the body frame, τ_ϕ is the rotational torque around the body center in ϕ direction with respect to body frame, τ_θ is the rotational torque around the body center in θ direction with respect to body frame, τ_ψ is the rotational torque around the body center in ψ direction with respect to body frame, ϖ denotes the rotor speed difference, which can be determined by

$$\bar{\omega} = \sum_{k=1}^{4} (-1)^{\kappa+1} (\omega \times e_3) \bar{\omega}_k \tag{4.7}$$

with $\omega \in \mathbb{R}^3$ being the angular velocity of the quadrotor with respect to the body frame. $\bar{\omega}_k$ represents the rotational speed of motor $k \in (1, 2, 3, 4)$

All the other related constants can be found in Chapter 2, where many different parameters are measured and discussed. A quick observation from the mathematical model confirms that the quadrotor is an under-actuated system, which contains six outputs with only four inputs.

4.2 Dynamic Model Using Newton Equations

As mentioned in Chapter 3, a singularity problem can demolish the performance of the controller, since one degree of freedom is lost when the gimbal lock occurs. In order to solve such a problem, another dynamic model using Newton equations of motion [41] [55] with unit quaternion representation is also used in this thesis work, which can be mathematically modeled by:

$$\dot{\zeta} = v \tag{4.8}$$

$$\dot{v} = ge_3 - \frac{1}{m}U_1 R e_3 \tag{4.9}$$

$$\dot{R} = RS(\omega) \tag{4.10}$$

$$I_B\dot{\omega} = -\omega \times I_B\omega - G_a + \tau \tag{4.11}$$

$$J_r\dot{\bar{\omega}}_i = \tau_i - Q_i \tag{4.12}$$

where $\zeta \in \mathbb{R}^3$ is the displacement of the center of mass of the body frame with respect to the inertial frame, $v \in \mathbb{R}^3$ is the translational velocity of the quadrotor with respect to the inertial frame, $g \in \mathbb{R}$ is the gravitational constant, $e_3 = [0, 0, 1]^T \in \mathbb{R}^3$ is the unit vector representing the z axis of the inertial frame, $m \in \mathbb{R}$ is the mass of the quadrotor, $U_1 \in \mathbb{R}$ is the total thrust generated by the motors, $I_B \in \mathbb{R}^3$ is the inertia matrix of the quadrotor with respect to the body frame, $\omega \in \mathbb{R}^3$ is the angular velocity of the quadrotor with respect to the body frame, $G_a \in \mathbb{R}$ is the gyroscopic torque, $\tau \in \mathbb{R}^3$ is the input torque on the x, y and z directions, $J_r \in \mathbb{R}$ is the moment of inertia of the motor i, $i = 1, 2, 3, 4$, $\bar{\omega}_i \in \mathbb{R}$ is the angular velocity of the motor i, $i = 1, 2, 3, 4$, $\tau_i \in \mathbb{R}$ is the torque generated by the motor i, $i = 1, 2, 3, 4$, $S(\cdot)$ is the skew symmetric matrix defined by

$$S(x) = \begin{bmatrix} 0 & -x_3 & x_2 \\ x_3 & 0 & -x_1 \\ -x_2 & x_1 & 0 \end{bmatrix} \tag{4.13}$$

In (4.12), Q_i is the reactive torque influenced by air drag, which is defined by

$$Q_i = d\bar{\omega}_i^2, i \in (1, 2, 3, 4) \tag{4.14}$$

with d being the rotor air drag factor, which is explained in more details in Section 2.3. In (4.11), the gyroscopic torque G_a is closely related to the rate of the rotation of the motors as well as the angular velocities respect to the x and y axes, which can be determined by

$$G_a = \begin{bmatrix} \omega_y J_r \left(\bar{\omega}_1 - \bar{\omega}_2 - \bar{\omega}_3 + \bar{\omega}_4\right) \\ -\omega_x J_r \left(\bar{\omega}_1 - \bar{\omega}_2 - \bar{\omega}_3 + \bar{\omega}_4\right) \\ 0 \end{bmatrix} \tag{4.15}$$

The principle for the equation (4.15) can be seen in an intuitive way from Fig. 2.23. $\bar{\omega}_1 + \bar{\omega}_4 - \bar{\omega}_2 - \bar{\omega}_3$ is the difference in the speeds of the motors. Along with the body rotational effect as well as the moment of inertia from the motors, one can then yield the gyroscopic torque G_a.

If the unit quaternion representation is used, (4.9) and (4.10) should be replaced with

$$\dot{v} = ge_3 - \frac{1}{m}U_1 \Re(Q)\, e_3 \tag{4.16}$$

$$\dot{Q} = \frac{1}{2} Q \odot Q_\omega = \frac{1}{2} \begin{bmatrix} -q^T \\ q_0 I_3 + S(q) \end{bmatrix} \omega \tag{4.17}$$

where $Q = [q_0, q_1, q_2, q_3]^T$ and

$$\Re(Q) = \begin{bmatrix} 1 - 2\left(q_2^2 + q_3^2\right) & 2\left(-q_0 q_3 + q_1 q_2\right) & 2\left(q_0 q_2 + q_1 q_3\right) \\ 2\left(q_0 q_3 + q_1 q_2\right) & 1 - 2\left(q_1^2 + q_3^2\right) & 2\left(-q_0 q_1 + q_2 q_3\right) \\ 2\left(-q_0 q_2 + q_1 q_3\right) & 2\left(q_0 q_1 + q_2 q_3\right) & 1 - 2\left(q_1^2 + q_2^2\right) \end{bmatrix} \tag{4.18}$$

By taking (4.15) into consideration, the above mentioned dynamics (4.10) and (4.11) can also be rewritten in the following Euler angles representations:

$$\dot{\phi} = \omega_x + \omega_y \sin\phi \tan\theta + \omega_z \cos\phi \tan\theta \tag{4.19}$$

$$\dot{\theta} = \omega_y \cos\phi - \omega_z \sin\phi \tag{4.20}$$

$$\dot{\psi} = \omega_y \sin\phi \sec\theta + \omega_z \cos\phi \sec\theta \tag{4.21}$$

$$\dot{\omega}_x = \frac{I_y - I_z}{I_x}\omega_y\omega_z + \omega_y J_r\left(\bar{\omega}_1 - \bar{\omega}_2 - \bar{\omega}_3 + \bar{\omega}_4\right) + \frac{1}{I_x}\tau_\phi \tag{4.22}$$

$$\dot{\omega}_y = \frac{I_z - I_x}{I_y}\omega_x\omega_z - \omega_x J_r\left(\bar{\omega}_1 - \bar{\omega}_2 - \bar{\omega}_3 + \bar{\omega}_4\right) + \frac{1}{I_y}\tau_\theta \tag{4.23}$$

$$\dot{\omega}_z = \frac{I_x - I_y}{I_z}\omega_x\omega_y + \frac{1}{I_z}\tau_\psi \tag{4.24}$$

Chapter 5

Controller Design and Experiments

This chapter is devoted to the nonlinear controller theoretical development, and its experimental outcomes. Various control schemes are discussed using the backstepping method. Under the inspiration of the [10]- [12], [20], the controller is mathematically derived, and then it is put into a real quadcopter for the actual flight test. Later on, a neural network is added to the control scheme as the estimation techniques for imitating certain nonlinear terms in the mathematical model. The results are being reviewed at end of the each section and a brief observation and discussion on the results are provided.

5.1 Backstepping Design with Euler Angle Representation

5.1.1 Controller Design

This section aims to design an attitude controller by using Euler angle representation. The backstepping design method is used to construct an attitude stabilization controller. Let ϕ_d, θ_d, ψ_d denote the desired Euler angles and $\dot{\phi}_d$, $\dot{\theta}_d$, $\dot{\psi}_d$ represent their derivatives. Define the errors as follows:

$$e_1 = \phi - \phi_d \tag{5.1}$$
$$e_2 = \dot{\phi} - \dot{\phi}_d \tag{5.2}$$
$$e_3 = \theta - \theta_d \tag{5.3}$$
$$e_4 = \dot{\theta} - \dot{\theta}_d \tag{5.4}$$
$$e_5 = \psi - \psi_d \tag{5.5}$$
$$e_6 = \dot{\psi} - \dot{\psi}_d \tag{5.6}$$

The following positive definite function is introduced:

$$V_1 = \frac{1}{2}e_1^2 + \frac{1}{2}e_3^2 + \frac{1}{2}e_5^2 \tag{5.7}$$

Differentiating it with respect to time gives

$$\begin{aligned}
\dot{V}_1 &= e_1\dot{e}_1 + e_3\dot{e}_3 + e_5\dot{e}_5 \\
&= e_1e_2 + e_3e_4 + e_5e_6 \\
&= -k_1e_1^2 + k_1e_1^2 + e_1e_2 - k_3e_3^2 + k_3e_3^2 + e_3e_4 - k_5e_5^2 + k_5e_5^2 + e_5e_6 \\
&= -k_1e_1^2 - k_3e_3^2 - k_5e_5^2 + e_1(e_2 + k_1e_1) + e_3(e_4 + k_3e_3) + e_5(e_6 + k_5e_5) \\
&= -k_1e_1^2 - k_3e_3^2 - k_5e_5^2 + e_1\bar{e}_2 + e_3\bar{e}_4 + e_5\bar{e}_6
\end{aligned} \tag{5.8}$$

where k_1, k_3, and k_5 are the positive gains and

$$\begin{aligned}
\bar{e}_2 &= e_2 + k_1e_1 \\
\bar{e}_4 &= e_4 + k_3e_3 \\
\bar{e}_6 &= e_6 + k_5e_5
\end{aligned} \tag{5.9}$$

with $-k_1e_1$, $-k_3e_3$, and $-k_5e_5$ are known as virtual control. It can be seen that $\dot{V}_1$ is negative definite when e_2, e_4, and e_6 are equal to their virtual control. The derivative of $\bar{e}_2$, $\bar{e}_4$, and $\bar{e}_6$ will be used later, which by using (4.6), can be determined by

$$\begin{aligned}
\dot{\bar{e}}_2 &= \dot{e}_2 + k_1\dot{e}_1 \\
&= \ddot{\phi} - \ddot{\phi}_d + k_1e_2 \\
&= \dot{\theta}\dot{\psi}\left(\frac{I_y - I_z}{I_x}\right) - \frac{J_r}{I_x}\dot{\theta}\bar{\omega} + \frac{l}{I_x}\tau_\phi - \ddot{\phi}_d + k_1e_2
\end{aligned} \tag{5.10}$$

$$\begin{aligned}
\dot{\bar{e}}_4 &= \dot{e}_4 + k_3\dot{e}_3 \\
&= \ddot{\theta} - \ddot{\theta}_d + k_3e_4 \\
&= \dot{\phi}\dot{\psi}\left(\frac{I_z - I_x}{I_y}\right) + \frac{J_r}{I_y}\dot{\phi}\bar{\omega} + \frac{l}{I_y}\tau_\theta - \ddot{\theta}_d + k_3e_4
\end{aligned} \tag{5.11}$$

$$\begin{aligned}
\dot{\bar{e}}_6 &= \dot{e}_6 + k_5\dot{e}_5 \\
&= \ddot{\psi} - \ddot{\psi}_d + k_5e_6 \\
&= \dot{\phi}\dot{\theta}\left(\frac{I_x - I_y}{I_z}\right) + \frac{1}{I_z}\tau_\psi - \ddot{\psi}_d + k_5e_6
\end{aligned} \tag{5.12}$$

Now, the positive definite function V_2 is defined by

$$V_2 = V_1 + \frac{1}{2}\bar{e}_2^2 + \frac{1}{2}\bar{e}_4^2 + \frac{1}{2}\bar{e}_6^2 \tag{5.13}$$

By using (5.8), the derivative of V_2 can be derived as follows:

$$\begin{aligned}
\dot{V}_2 &= \dot{V}_1 + \bar{e}_2\dot{\bar{e}}_2 + \bar{e}_4\dot{\bar{e}}_4 + \bar{e}_6\dot{\bar{e}}_6 \\
&= -k_1e_1^2 - k_3e_3^2 - k_5e_5^2 + e_1\bar{e}_2 + e_3\bar{e}_4 + e_5\bar{e}_6 \\
&\quad -k_2\bar{e}_2^2 - k_4\bar{e}_4^2 - k_6\bar{e}_6^2 + \bar{e}_2\left(\dot{\bar{e}}_2 + k_2\bar{e}_2\right) + \bar{e}_4\left(\dot{\bar{e}}_4 + k_4\bar{e}_4\right) + \bar{e}_6\left(\dot{\bar{e}}_6 + k_6\bar{e}_6\right) \\
&= -k_1e_1^2 - k_3e_3^2 - k_5e_5^2 - k_2\bar{e}_2^2 - k_4\bar{e}_4^2 - k_6\bar{e}_6^2 \\
&\quad +\bar{e}_2\left(\dot{\bar{e}}_2 + k_2\bar{e}_2 + e_1\right) + \bar{e}_4\left(\dot{\bar{e}}_4 + k_4\bar{e}_4 + e_3\right) + \bar{e}_6\left(\dot{\bar{e}}_6 + k_6\bar{e}_6 + e_5\right)
\end{aligned} \tag{5.14}$$

where k_2, k_4, and k_6 are the positive gains. Substituting (5.10)-(5.12) into (5.14) yields:

$$\begin{aligned}\dot{V}_2 = &-k_1e_1^2 - k_3e_3^2 - k_5e_5^2 - k_2\bar{e}_2^2 - k_4\bar{e}_4^2 - k_6\bar{e}_6^2 \\ &+\bar{e}_2\left[\dot{\theta}\dot{\psi}\left(\frac{I_y - I_z}{I_x}\right) - \frac{J_r}{I_x}\dot{\theta}\bar{\omega} + \frac{l}{I_x}\tau_\phi - \ddot{\phi}_d + k_1e_2 + k_2\bar{e}_2 + e_1\right] \\ &+\bar{e}_4\left[\dot{\phi}\dot{\psi}\left(\frac{I_z - I_x}{I_y}\right) + \frac{J_r}{I_y}\dot{\phi}\bar{\omega} + \frac{l}{I_y}\tau_\theta - \ddot{\theta}_d + k_3e_4 + k_4\bar{e}_4 + e_3\right] \\ &+\bar{e}_6\left[\dot{\phi}\dot{\theta}\left(\frac{I_x - I_y}{I_z}\right) + \frac{1}{I_z}\tau_\psi - \ddot{\psi}_d + k_5e_6 + k_6\bar{e}_6 + e_5\right] \end{aligned} \tag{5.15}$$

Setting the last three terms in (5.15) to zero gives:

$$\begin{aligned}\tau_\phi &= \frac{I_x}{l}\left[-\dot{\theta}\dot{\psi}\left(\frac{I_y - I_z}{I_x}\right) + \frac{J_r}{I_x}\dot{\theta}\bar{\omega} + \ddot{\phi}_d - k_1e_2 - k_2\bar{e}_2 - e_1\right] \\ \tau_\theta &= \frac{I_y}{l}\left[-\dot{\phi}\dot{\psi}\left(\frac{I_z - I_x}{I_y}\right) - \frac{J_r}{I_y}\dot{\phi}\bar{\omega} + \ddot{\theta}_d - k_3e_4 - k_4\bar{e}_4 - e_3\right] \\ \tau_\psi &= I_z\left[-\dot{\phi}\dot{\theta}\left(\frac{I_x - I_y}{I_z}\right) + \ddot{\psi}_d - k_5e_6 - k_6\bar{e}_6 - e_5\right] \end{aligned} \tag{5.16}$$

which makes $\dot{V}_2$ negative definite. By substituting (5.9) into (5.16), (5.16) can be rewritten as:

$$\tau_\phi = \frac{I_x}{l}\left[-\dot{\theta}\dot{\psi}\left(\frac{I_y - I_z}{I_x}\right) + \frac{J_r}{I_x}\dot{\theta}\bar{\omega} - (k_1k_2 + 1)e_1 - (k_1 + k_2)e_2\right] \tag{5.17}$$

$$\tau_\theta = \frac{I_y}{l}\left[-\dot{\phi}\dot{\psi}\left(\frac{I_z - I_x}{I_y}\right) - \frac{J_r}{I_y}\dot{\phi}\bar{\omega} - (k_3k_4 + 1)e_3 - (k_3 + k_4)e_4\right] \tag{5.18}$$

$$\tau_\psi = I_z\left[-\dot{\phi}\dot{\theta}\left(\frac{I_x - I_y}{I_z}\right) - (k_5k_6 + 1)e_5 - (k_5 + k_6)e_6\right] \tag{5.19}$$

Using the aerodynamic equation in (2.15), (5.17), (5.18), and (5.19) can be changed to the following:

$$bl(\bar{\omega}_1^2 - \bar{\omega}_4^2) - \frac{J_r}{l}\dot{\theta}\bar{\omega} = \frac{I_x}{l}\left[-\dot{\theta}\dot{\psi}\left(\frac{I_y - I_z}{I_x}\right) - (k_1k_2 + 1)e_1 - (k_1 + k_2)e_2\right] \tag{5.20}$$

$$bl(\bar{\omega}_2^2 - \bar{\omega}_3^2) + \frac{J_r}{l}\dot{\phi}\bar{\omega} = \frac{I_y}{l}\left[-\dot{\phi}\dot{\psi}\left(\frac{I_z - I_x}{I_y}\right) - (k_3k_4 + 1)e_3 - (k_3 + k_4)e_4\right] \tag{5.21}$$

$$d(\bar{\omega}_1^2 + \bar{\omega}_4^2 - \bar{\omega}_2^2 - \bar{\omega}_3^2) = I_z\left[-\dot{\phi}\dot{\theta}\left(\frac{I_x - I_y}{I_z}\right) - (k_5k_6 + 1)e_5 - (k_5 + k_6)e_6\right] \tag{5.22}$$

where $\bar{\omega} = \bar{\omega}_1 - \bar{\omega}_2 - \bar{\omega}_3 + \bar{\omega}_4$. The motor speeds $\bar{\omega}_1$, $\bar{\omega}_2$, $\bar{\omega}_3$, $\bar{\omega}_4$ can be determined from (5.20), (5.21), (5.22) and (2.16), that is,

$$b(\bar{\omega}_1^2 + \bar{\omega}_4^2 + \bar{\omega}_2^2 + \bar{\omega}_3^2) \quad = \quad U_1 \tag{5.23}$$

where U_1 is the vertical lifting power given by the RC controller, later on, this lifting force will be generated by the backstepping altitude controller. By applying the gradient descent method, the motor angular velocities can be solved from (5.20)-(5.23), which are able to stabilize the quadrotor at the desired attitude. The block diagram of the closed-loop system for the attitude control is shown in Fig. 5.1.

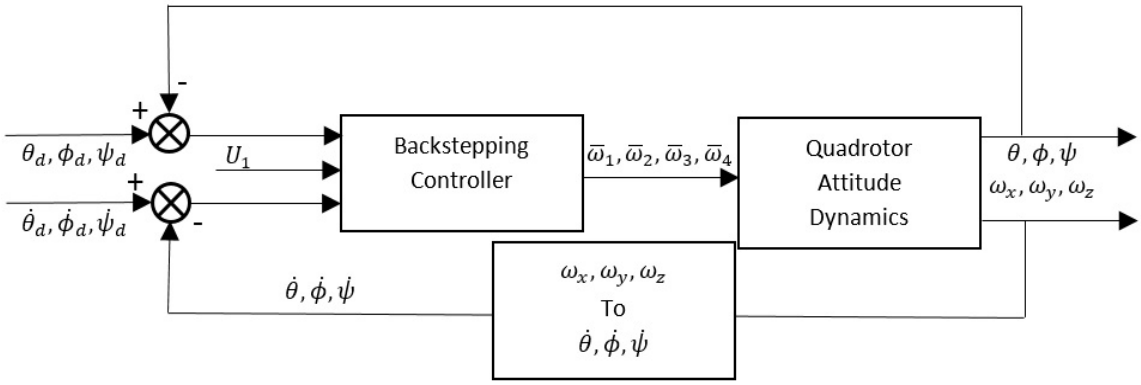

Figure 5.1: Block Diagram for Backstepping Control

5.1.2 Experimental Results

The experimental data are recorded while the quadrotor is flying in the air. The drone was first vertically taken off by a human operator, and it was then maintained in a stable flight. The gain coefficients are $k_1 = 13.5, k_2 = 3, k_3 = 15, k_4 = 4.5, k_5 = 420, k_6 = 0.5$. As shown in Figs. 5.2-5.4, the proposed controller performs well without any strong external disturbances. By observing the graphs, the quadrotor movement are well within $\pm 10^\circ$ with relatively small angular velocity during the flight.

5.2 Integral Backstepping Design with Euler Angle Representation

5.2.1 Controller Design

In order to further eliminate the steady state error for the system, one can introduce an integration term to incorporate with the controller design. Such a methodology is quite similar to the backstepping derivation in Section 5.1.1. Again, let ϕ_d, θ_d, ψ_d denote the

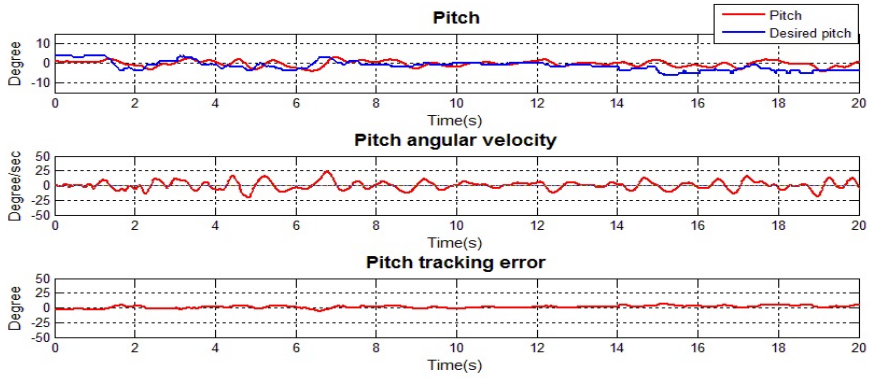

Figure 5.2: Backstepping Control with Euler Representation in ϕ Direction

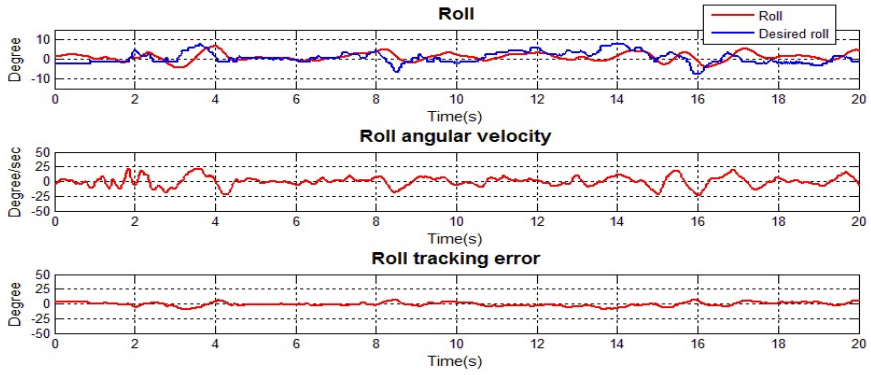

Figure 5.3: Backstepping Control with Euler Representation in θ Direction

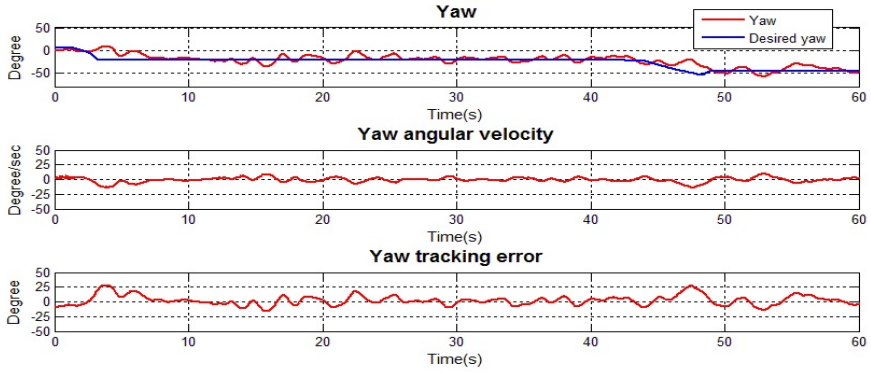

Figure 5.4: Backstepping Control with Euler Representation in ψ Direction

desired Euler angles and $\dot{\phi}_d$, $\dot{\theta}_d$, $\dot{\psi}_d$ represent their derivative. One can define the following

error terms:

$$
\begin{aligned}
e_{i1} &= \int \phi - \phi_d && (5.24)\\
e_1 &= \phi - \phi_d && (5.25)\\
e_2 &= \dot{\phi} - \dot{\phi}_d && (5.26)\\
e_{i2} &= \int \theta - \theta_d && (5.27)\\
e_3 &= \theta - \theta_d && (5.28)\\
e_4 &= \dot{\theta} - \dot{\theta}_d && (5.29)\\
e_{i3} &= \int \psi - \psi_d && (5.30)\\
e_5 &= \psi - \psi_d && (5.31)\\
e_6 &= \dot{\psi} - \dot{\psi}_d && (5.32)
\end{aligned}
$$

Introduce the positive definite Lyapunov function:

$$
V_1 = \frac{1}{2}e_{i1}^2 + \frac{1}{2}e_{i2}^2 + \frac{1}{2}e_{i3}^2 \tag{5.33}
$$

The time derivative of the equation (5.33) can then be expressed as:

$$
\begin{aligned}
\dot{V}_1 &= e_{i1}\dot{e}_{i1} + e_{i2}\dot{e}_{i2} + e_{i3}\dot{e}_{i3}\\
&= e_{i1}e_1 + e_{i2}e_3 + e_{i3}e_5\\
&= -k_{i1}e_{i1}^2 + k_{i1}e_{i1}^2 + e_{i1}e_1 - k_{i2}e_{i2}^2 + k_{i2}e_{i2}^2 + e_{i2}e_3 - k_{i3}e_{i3}^2 + k_{i3}e_{i3}^2 + e_{i3}e_5\\
&= -k_{i1}e_{i1}^2 - k_{i2}e_{i2}^2 - k_{i3}e_{i3}^2 + e_{i1}\left(e_1 + k_{i1}e_{i1}\right) + e_{i2}\left(e_3 + k_{i2}e_{i2}\right) + e_{i3}\left(e_5 + k_{i3}e_{i3}\right)\\
&= -k_{i1}e_{i1}^2 - k_{i2}e_{i2}^2 - k_{i3}e_{i3}^2 + e_{i1}\bar{e}_1 + e_{i2}\bar{e}_3 + e_{i3}\bar{e}_5 \qquad (5.34)
\end{aligned}
$$

where k_{i1}, k_{i2}, and k_{i3} are the positive gains and the following relationships are used:

$$
\begin{aligned}
\bar{e}_1 &= e_1 + k_{i1}e_{i1}\\
\bar{e}_3 &= e_3 + k_{i2}e_{i2}\\
\bar{e}_5 &= e_5 + k_{i3}e_{i3} \qquad (5.35)
\end{aligned}
$$

Differentiating the above respect to time gives the following:

$$
\begin{aligned}
\dot{\bar{e}}_1 &= e_2 + k_{i1}e_1 && (5.36)\\
\dot{\bar{e}}_3 &= e_4 + k_{i2}e_3\\
\dot{\bar{e}}_5 &= e_6 + k_{i3}e_5
\end{aligned}
$$

$\dot{V}_1$ is negative definite when e_1, e_3 and e_5 equals to the virtual controller $-k_{i1}e_{i1}, -k_{i2}e_{i2}$ and $-k_{i3}e_{i3}$. Construct a second Lyapunov function, which includes V_1, as follows:

$$V_2 = V_1 + \frac{1}{2}\bar{e}_1^2 + \frac{1}{2}\bar{e}_3^2 + \frac{1}{2}\bar{e}_5^2 \tag{5.37}$$

Applying the time derivative onto (5.37), we can then get the following:

$$\begin{aligned}
\dot{V}_2 &= \dot{V}_1 + \bar{e}_1\dot{\bar{e}}_1 + \bar{e}_3\dot{\bar{e}}_3 + \bar{e}_5\dot{\bar{e}}_5 \\
&= -k_{i1}e_{i1}^2 - k_{i2}e_{i2}^2 - k_{i3}e_{i3}^2 + e_{i1}\bar{e}_1 + e_{i2}\bar{e}_3 + e_{i3}\bar{e}_5 \\
&\quad +\bar{e}_1\dot{\bar{e}}_1 + \bar{e}_3\dot{\bar{e}}_3 + \bar{e}_5\dot{\bar{e}}_5 \\
&= -k_{i1}e_{i1}^2 - k_{i2}e_{i2}^2 - k_{i3}e_{i3}^2 - k_1\bar{e}_1^2 - k_3\bar{e}_3^2 - k_5\bar{e}_5^2 \\
&\quad +k_1\bar{e}_1^2 + k_3\bar{e}_3^2 + k_5\bar{e}_5^2 + \bar{e}_1\left(\dot{\bar{e}}_1 + e_{i1}\right) + \bar{e}_3\left(\dot{\bar{e}}_3 + e_{i2}\right) + \bar{e}_5\left(\dot{\bar{e}}_5 + e_{i3}\right) \\
&= -k_{i1}e_{i1}^2 - k_{i2}e_{i2}^2 - k_{i3}e_{i3}^2 - k_1\bar{e}_1^2 - k_3\bar{e}_3^2 - k_5\bar{e}_5^2 \\
&\quad +\bar{e}_1\left(k_1\bar{e}_1 + \dot{\bar{e}}_1 + e_{i1}\right) + \bar{e}_3\left(k_3\bar{e}_3 + \dot{\bar{e}}_3 + e_{i2}\right) + \bar{e}_5\left(k_5\bar{e}_5 + \dot{\bar{e}}_5 + e_{i3}\right) \\
&= -k_{i1}e_{i1}^2 - k_{i2}e_{i2}^2 - k_{i3}e_{i3}^2 - k_1\bar{e}_1^2 - k_3\bar{e}_3^2 - k_5\bar{e}_5^2 \\
&\quad +\bar{e}_1\left(k_1\bar{e}_1 + e_2 + k_{i1}e_1 + e_{i1}\right) + \bar{e}_3\left(k_3\bar{e}_3 + e_4 + k_{i2}e_3 + e_{i2}\right) \\
&\quad +\bar{e}_5\left(k_5\bar{e}_5 + e_6 + k_{i3}e_5 + e_{i3}\right) \\
&= -k_{i1}e_{i1}^2 - k_{i2}e_{i2}^2 - k_{i3}e_{i3}^2 - k_1\bar{e}_1^2 - k_3\bar{e}_3^2 - k_5\bar{e}_5^2 + \bar{e}_1\bar{e}_2 + \bar{e}_3\bar{e}_4 + \bar{e}_5\bar{e}_6
\end{aligned} \tag{5.38}$$

$$\bar{e}_2 = k_1\bar{e}_1 + e_2 + k_{i1}e_1 + e_{i1} \tag{5.39}$$

$$\bar{e}_4 = k_3\bar{e}_3 + e_4 + k_{i2}e_3 + e_{i2} \tag{5.40}$$

$$\bar{e}_6 = k_5\bar{e}_5 + e_6 + k_{i3}e_5 + e_{i3} \tag{5.41}$$

Once again, one can construct the third Lyapunov function in the following:

$$V_3 = V_2 + \frac{1}{2}\bar{e}_2^2 + \frac{1}{2}\bar{e}_4^2 + \frac{1}{2}\bar{e}_6^2 \tag{5.42}$$

Differentiating the above respect to the time yields:

$$\dot{V}_3 = \dot{V}_2 + \bar{e}_2\dot{\bar{e}}_2 + \bar{e}_4\dot{\bar{e}}_4 + \bar{e}_6\dot{\bar{e}}_6 \tag{5.43}$$

where $\dot{\bar{e}}_2, \dot{\bar{e}}_4$ and $\dot{\bar{e}}_6$can be found as:

$$\dot{\bar{e}}_2 = k_1\dot{\bar{e}}_1 + \dot{e}_2 + k_{i1}\dot{e}_1 + \dot{e}_{i1} = k_1\dot{\bar{e}}_1 + \ddot{\phi} - \ddot{\phi}_d + k_{i1}\dot{e}_1 + e_1 \tag{5.44}$$

$$\dot{\bar{e}}_4 = k_3\dot{\bar{e}}_3 + \dot{e}_4 + k_{i2}\dot{e}_3 + \dot{e}_{i2} = k_3\dot{\bar{e}}_3 + \ddot{\theta} - \ddot{\theta}_d + k_{i2}\dot{e}_3 + e_3 \tag{5.45}$$

$$\dot{\bar{e}}_6 = k_5\dot{\bar{e}}_5 + \dot{e}_6 + k_{i3}\dot{e}_5 + \dot{e}_{i3} = k_5\dot{\bar{e}}_5 + \ddot{\psi} - \ddot{\psi}_d + k_{i3}\dot{e}_5 + e_5 \tag{5.46}$$

Introducing (4.6), $\dot{\bar{e}}_2, \dot{\bar{e}}_5$and $\dot{\bar{e}}_8$ can then be evaluated as:

$$\dot{\bar{e}}_2 = k_1\dot{\bar{e}}_1 + \dot{\theta}\dot{\psi}\left(\frac{I_y - I_z}{I_x}\right) - \frac{J_r}{I_x}\dot{\theta}\bar{\omega} + \frac{l}{I_x}\tau_\phi - \ddot{\phi}_d + k_{i1}\dot{e}_1 + e_1 \tag{5.47}$$

$$\dot{\bar{e}}_4 = k_3\dot{\bar{e}}_3 + \dot{\phi}\dot{\psi}\left(\frac{I_z - I_x}{I_y}\right) + \frac{J_r}{I_y}\dot{\phi}\bar{\omega} + \frac{l}{I_y}\tau_\theta - \ddot{\theta}_d + k_{i2}\dot{e}_3 + e_3 \tag{5.48}$$

$$\dot{\bar{e}}_6 = k_5\dot{\bar{e}}_5 + \dot{\phi}\dot{\theta}\left(\frac{I_x - I_y}{I_z}\right) + \frac{1}{I_z}\tau_\psi - \ddot{\psi}_d + k_{i3}\dot{e}_5 + e_5 \tag{5.49}$$

Substituting the above three equations and $\dot{V}_2$ into (5.43), we then get the following:

$$\begin{aligned}
\dot{V}_3 &= \dot{V}_2 + \bar{e}_2\left(k_1\dot{\bar{e}}_1 + \dot{\theta}\dot{\psi}\left(\frac{I_y - I_z}{I_x}\right) - \frac{J_r}{I_x}\dot{\theta}\bar{\omega} + \frac{l}{I_x}\tau_\phi - \ddot{\phi}_d + k_{i1}\dot{e}_1 + e_1\right) \\
&\quad + \bar{e}_4\left(k_3\dot{\bar{e}}_3 + \dot{\phi}\dot{\psi}\left(\frac{I_z - I_x}{I_y}\right) + \frac{J_r}{I_y}\dot{\phi}\bar{\omega} + \frac{l}{I_y}\tau_\theta - \ddot{\theta}_d + k_{i2}\dot{e}_3 + e_3\right) \\
&\quad + \bar{e}_6\left(k_5\dot{\bar{e}}_5 + \dot{\phi}\dot{\theta}\left(\frac{I_x - I_y}{I_z}\right) + \frac{1}{I_z}\tau_\psi - \ddot{\psi}_d + k_{i3}\dot{e}_5 + e_5\right) \\
&= -k_{i1}e_{i1}^2 - k_{i2}e_{i2}^2 - k_{i3}e_{i3}^2 - k_1\bar{e}_1^2 - k_3\bar{e}_3^2 - k_5\bar{e}_5^2 \\
&\quad + \bar{e}_2\left(\bar{e}_1 + k_1\dot{\bar{e}}_1 + \dot{\theta}\dot{\psi}\left(\frac{I_y - I_z}{I_x}\right) - \frac{J_r}{I_x}\dot{\theta}\bar{\omega} + \frac{l}{I_x}\tau_\phi - \ddot{\phi}_d + k_{i1}\dot{e}_1 + e_1\right) \\
&\quad + \bar{e}_4\left(\bar{e}_3 + k_3\dot{\bar{e}}_3 + \dot{\phi}\dot{\psi}\left(\frac{I_z - I_x}{I_y}\right) + \frac{J_r}{I_y}\dot{\phi}\bar{\omega} + \frac{l}{I_y}\tau_\theta - \ddot{\theta}_d + k_{i2}\dot{e}_3 + e_3\right) \\
&\quad + \bar{e}_6\left(\bar{e}_5 + k_5\dot{\bar{e}}_5 + \dot{\phi}\dot{\theta}\left(\frac{I_x - I_y}{I_z}\right) + \frac{1}{I_z}\tau_\psi - \ddot{\psi}_d + k_{i3}\dot{e}_5 + e_5\right)
\end{aligned} \tag{5.50}$$

Make the following, so that $\dot{V}_3$ is negative definite:

$$-k_2\bar{e}_2 = \bar{e}_1 + k_1\dot{\bar{e}}_1 + \dot{\theta}\dot{\psi}\left(\frac{I_y - I_z}{I_x}\right) - \frac{J_r}{I_x}\dot{\theta}\bar{\omega} + \frac{l}{I_x}\tau_\phi - \ddot{\phi}_d + k_{i1}\dot{e}_1 + e_1 \tag{5.51}$$

$$-k_4\bar{e}_4 = \bar{e}_3 + k_3\dot{\bar{e}}_3 + \dot{\phi}\dot{\psi}\left(\frac{I_z - I_x}{I_y}\right) + \frac{J_r}{I_y}\dot{\phi}\bar{\omega} + \frac{l}{I_y}\tau_\theta - \ddot{\theta}_d + k_{i2}\dot{e}_3 + e_3 \tag{5.52}$$

$$-k_6\bar{e}_6 = \bar{e}_5 + k_5\dot{\bar{e}}_5 + \dot{\phi}\dot{\theta}\left(\frac{I_x - I_y}{I_z}\right) + \frac{1}{I_z}\tau_\psi - \ddot{\psi}_d + k_{i3}\dot{e}_5 + e_5 \tag{5.53}$$

(5.51),(5.52),(5.53) can then be rewritten as:

$$\begin{aligned}
\tau_\phi &= \frac{I_x}{l}\left(-k_2\bar{e}_2 - \bar{e}_1 - k_1\dot{\bar{e}}_1 - \dot{\theta}\dot{\psi}\left(\frac{I_y - I_z}{I_x}\right) + \frac{J_r}{I_x}\dot{\theta}\bar{\omega} + \ddot{\phi}_d - k_{i1}\dot{e}_1 - e_1\right) \\
&= \frac{I_x}{l}\left(-k_2\left(k_1\left(e_1 + k_{i1}e_{i1}\right) + e_2 + k_{i1}e_1 + e_{i1}\right) - \left(e_1 + k_{i1}e_{i1}\right)\right. \\
&\quad \left. -k_1\left(e_2 + k_{i1}e_1\right) - \dot{\theta}\dot{\psi}\left(\frac{I_y - I_z}{I_x}\right) + \frac{J_r}{I_x}\dot{\theta}\bar{\omega} + \ddot{\phi}_d - k_{i1}e_2 - e_1\right) \\
&= \frac{I_x}{l}\left(-k_1k_2e_1 - k_1k_{i1}k_2e_{i1} - k_2e_2 - k_{i1}k_2e_1 - k_2e_{i1} - e_1 - k_{i1}e_{i1}\right. \\
&\quad \left. -k_1e_2 - k_1k_{i1}e_1 - \dot{\theta}\dot{\psi}\left(\frac{I_y - I_z}{I_x}\right) + \frac{J_r}{I_x}\dot{\theta}\bar{\omega} + \ddot{\phi}_d - k_{i1}e_2 - e_1\right) \\
&= \frac{I_x}{l}\left(-\left(k_1k_2 + k_1k_{i1} + k_{i1}k_2 + 2\right)e_1 - \left(k_1k_{i1}k_2 + k_{i1} + k_2\right)e_{i1}\right. \\
&\quad \left. -\left(k_2 + k_1 + k_{i1}\right)e_2 - \dot{\theta}\dot{\psi}\left(\frac{I_y - I_z}{I_x}\right) + \frac{J_r}{I_x}\dot{\theta}\bar{\omega} + \ddot{\phi}_d\right) \qquad (5.54)
\end{aligned}$$

$$\begin{aligned}
\tau_\theta &= \frac{I_y}{l}\left(-k_4\bar{e}_4 - \bar{e}_3 - k_3\dot{\bar{e}}_3 - \dot{\phi}\dot{\psi}\left(\frac{I_z - I_x}{I_y}\right) - \frac{J_r}{I_y}\dot{\phi}\bar{\omega} + \ddot{\theta}_d - k_{i2}\dot{e}_3 - e_3\right) \\
&= \frac{I_y}{l}\left(-k_4\left(k_3\left(e_3 + k_{i2}e_{i2}\right) + e_4 + k_{i2}e_3 + e_{i2}\right) - \left(e_3 + k_{i2}e_{i2}\right)\right. \\
&\quad \left. -k_3\left(e_4 + k_{i2}e_3\right) - \dot{\phi}\dot{\psi}\left(\frac{I_z - I_x}{I_y}\right) - \frac{J_r}{I_y}\dot{\phi}\bar{\omega} + \ddot{\theta}_d - k_{i2}e_4 - e_3\right) \\
&= \frac{I_y}{l}\left(-\left(k_3k_4 + k_3k_{i2} + k_{i2}k_4 + 2\right)e_3 - \left(k_3k_{i2}k_4 + k_{i2} + k_4\right)e_{i2}\right. \\
&\quad \left. -\left(k_4 + k_3 + k_{i2}\right)e_4 - \dot{\phi}\dot{\psi}\left(\frac{I_z - I_x}{I_y}\right) - \frac{J_r}{I_y}\dot{\phi}\bar{\omega} + \ddot{\theta}_d\right) \qquad (5.55)
\end{aligned}$$

$$\begin{aligned}
\tau_\psi &= I_z\left(-k_6\bar{e}_6 - \bar{e}_5 - k_5\dot{\bar{e}}_5 - \dot{\phi}\dot{\theta}\left(\frac{I_x - I_y}{I_z}\right) - \frac{1}{I_z}\tau_\psi + \ddot{\psi}_d - k_{i3}\dot{e}_5 - e_5\right) \\
&= I_z\left(-k_6\left(k_5\left(e_5 + k_{i3}e_{i3}\right) + e_6 + k_{i3}e_5 + e_{i3}\right) - \left(e_5 + k_{i3}e_{i3}\right)\right. \\
&\quad \left. -k_5\left(e_6 + k_{i3}e_5\right) - \dot{\phi}\dot{\theta}\left(\frac{I_x - I_y}{I_z}\right) - \frac{1}{I_z}\tau_\psi + \ddot{\psi}_d - k_{i3}e_6 - e_5\right) \\
&= I_z\left(-\left(k_5k_6 + k_5k_{i3} + k_{i3}k_6 + 2\right)e_5 - \left(k_5k_{i3}k_6 + k_{i3} + k_6\right)e_{i3}\right. \\
&\quad \left. -\left(k_6 + k_5 + k_{i3}\right)e_6 - \dot{\phi}\dot{\theta}\left(\frac{I_x - I_y}{I_z}\right) - \frac{1}{I_z}\tau_\psi + \ddot{\psi}_d\right) \qquad (5.56)
\end{aligned}$$

Once the above control law is obtained, one can have the following relationships:

$$
\begin{aligned}
bl(\bar{\omega}_1^2 - \bar{\omega}_4^2) - \frac{J_r}{l}\dot{\theta}\bar{\omega} &= \frac{I_x}{l}\left(-\left(k_1k_2 + k_1k_{i1} + k_{i1}k_2 + 2\right)e_1 - \left(k_1k_{i1}k_2 + k_{i1} + k_2\right)e_{i1}\right. \\
&\quad \left. - \left(k_2 + k_1 + k_{i1}\right)e_2 - \dot{\theta}\dot{\psi}\left(\frac{I_y - I_z}{I_x}\right) + \ddot{\phi}_d\right) \qquad (5.57) \\
bl(\bar{\omega}_2^2 - \bar{\omega}_3^2) + \frac{J_r}{l}\dot{\phi}\bar{\omega} &= \frac{I_y}{l}\left(-\left(k_3k_4 + k_3k_{i2} + k_{i2}k_4 + 2\right)e_3 - \left(k_3k_{i2}k_4 + k_{i2} + k_4\right)e_{i2}\right. \\
&\quad \left. - \left(k_4 + k_3 + k_{i2}\right)e_4 - \dot{\phi}\dot{\psi}\left(\frac{I_z - I_x}{I_y}\right) + \ddot{\theta}_d\right) \qquad (5.58) \\
d(\bar{\omega}_1^2 + \bar{\omega}_4^2 - \bar{\omega}_2^2 - \bar{\omega}_3^2) &= I_z\left(-\left(k_5k_6 + k_5k_{i3} + k_{i3}k_6 + 2\right)e_5 - \left(k_5k_{i3}k_6 + k_{i3} + k_6\right)e_{i3}\right. \\
&\quad \left. - \left(k_6 + k_5 + k_{i3}\right)e_6 - \dot{\phi}\dot{\theta}\left(\frac{I_x - I_y}{I_z}\right) + \ddot{\psi}_d\right) \qquad (5.59) \\
b(\bar{\omega}_1^2 + \bar{\omega}_4^2 + \bar{\omega}_2^2 + \bar{\omega}_3^2) &= U_1 \qquad (5.60)
\end{aligned}
$$

where (2.15) is used for τ_ϕ, τ_θ, and τ_ψ, (5.60) comes from (2.16), U_1 is the vertical lifting power given by the RC controller, which will be generated by the backstepping altitude controller in the later sections, and $\bar{\omega} = \bar{\omega}_1 - \bar{\omega}_2 - \bar{\omega}_3 + \bar{\omega}_4$ is the differences in the rotational speeds of the diagonal propeller pair. The desired rotational speeds of the propellers $\bar{\omega}_1, \bar{\omega}_2, \bar{\omega}_3, \bar{\omega}_4$ can then be calculated by applying the gradient decent method to (5.57)-(5.60). Fig. 5.5 shows the block diagram for the closed-loop system with the attitude controller using the integral backstepping method.

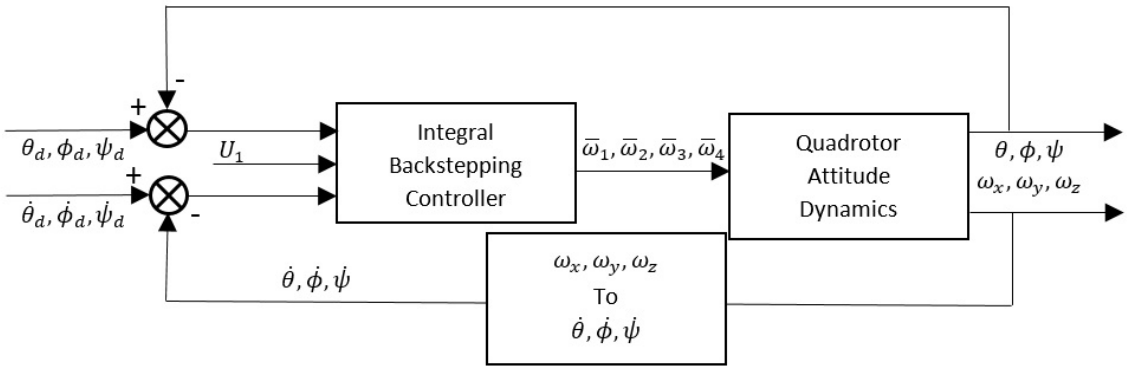

Figure 5.5: Block Diagram for Integral Backstepping Control

5.2.2 Experimental Results

The experimental results shown in Figs. (5.6)-(5.8) prove a functional control scheme for the quadrotor. The added integrator control reduced the steady state error and it also adds robustness during the flight. Comparing with only backstepping controller, the integral backstepping controller is way much less fragile. From the graphs, the pitch, roll and yaw movements are controlled within $\pm 10^{\circ}$ and the angular velocity is fairly small. The gain coefficients are $k_{i1} = 0.6, k_1 = 16, k_2 = 2, k_{i2} = 1, k_3 = 17, k_4 = 2, k_{i3} = 0.7, k_4 = 1.0, k_5 = 350$. The gain coefficients are similar in the roll and pitch direction (i.e. $k_{i1} = 0.6, k_1 = 16, k_2 = 2$ for the ϕ direction, $k_{i2} = 1, k_3 = 17, k_4 = 2$ for the θ direction). The slight difference in the gain coefficients are coming from the slight unsymmetrical shape of the quadrotor. The lower air drag factors cause a slower reaction in the yaw direction, to control the heading of the quadrotor, a much higher gain is needed to provide the quick and more air drag force.

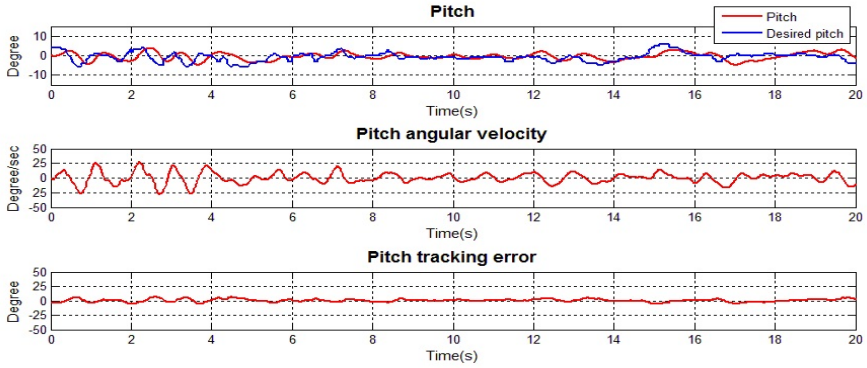

Figure 5.6: Integral Backstepping with Euler Representation in ϕ Direction

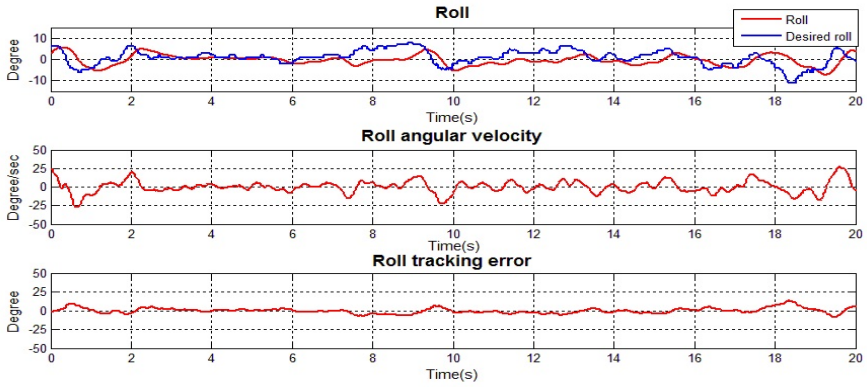

Figure 5.7: Integral Backstepping with Euler Representation in θ Direction

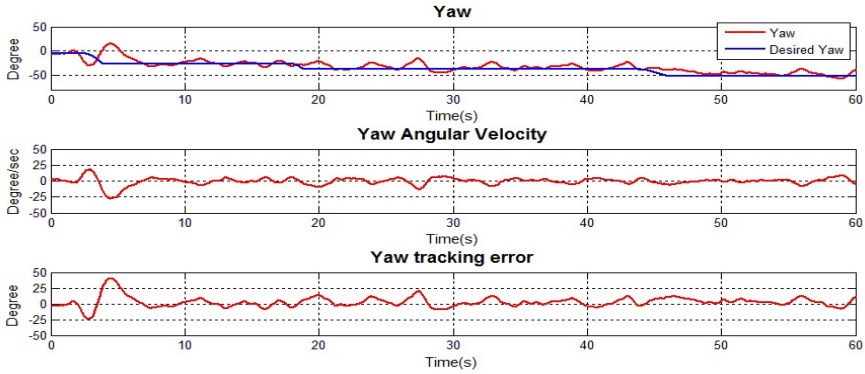

Figure 5.8: Integral Backstepping with Euler Representation in ψ Direction

5.3 Backstepping Controller with Unit Quaternion Representation

5.3.1 Controller Design

The unit quaternion representation is employed for this section to derive the controller of the quadrotor. The main goal is to maintain the stability of the vector part of the quatenrion (i.e. $q = \begin{bmatrix} q_1 & q_2 & q_3 \end{bmatrix}^T$). q_0 will be constrained by the unique characteristics of the unit quaternion in (3.6), which shows that the length of a unit quaternion is always equal to one. The main disadvantages of unit quaternion is the non-uniqueness, where each attitude can be represented by both $\pm$Q. It is worth mentioning that the negligence of such a major drawback may lead to a quaternion unwinding problem [56].

By deploying a very similar method when deriving the backstepping controller using the Euler angle representation, one can approach the controller design problem using the unit quaternion representation.

Let $q_d \in \mathbb{R}^3$ and $\omega_d \in \mathbb{R}^3$ be the desired attitude and angular velocities of the quadrotor with respect to the body frame. Then, the desired quaternion $Q_d = \left[q_{0d}, q_d^T\right]^T$ satisfies the following differential equation:

$$\dot{Q}_d = \frac{1}{2} Q_d \odot Q_{\omega_d} = \frac{1}{2} \begin{bmatrix} -q_d^T \\ q_{0d} I_3 + S\left(q_d\right) \end{bmatrix} \omega_d \tag{5.61}$$

The tracking error, that is, the difference between the desired quaternion Q_d and the actual quaternion denoted as $Q = \left[q_0, q^T\right]^T$, can be calculated by

$$Q_e = \begin{bmatrix} q_{0e} \\ q_e \end{bmatrix} = Q_d^{-1} \odot Q = \begin{bmatrix} q_{0d} q_0 + q^T q_d \\ q_{0d} q - q_0 q_d - q_d \times q \end{bmatrix} \tag{5.62}$$

It follows from [41] that, with $\omega_d = 0$ and $\omega_e = \omega - \omega_d = \omega$, Q_e satisfies the following

differential equation

$$\dot{Q}_e = \begin{bmatrix} \dot{q}_{0e} \\ \dot{q}_e \end{bmatrix} = \frac{1}{2} \begin{bmatrix} -q_e^T \omega \\ q_{0e}\omega + S(q_e)\,\omega \end{bmatrix} \tag{5.63}$$

which is equivalent to

$$\dot{Q}_e = \frac{1}{2} \begin{bmatrix} -q_e^T \omega \\ \omega q_{0e} - S(\omega)\, q_e \end{bmatrix} \tag{5.64}$$

Using the backstepping technique, a Lyapunov function can then be chosen as:

$$V_1 = q_e^T q_e + (q_{0e} - 1)^2 \tag{5.65}$$

The first order derivative of V_1 can be expressed as:

$$\dot{V}_1 = 2q_e^T \dot{q}_e + 2(q_{0e} - 1)\dot{q}_{0e} \tag{5.66}$$

Substituting (5.64) into (5.66) yields:

$$\begin{aligned} \dot{V}_1 &= q_e^T \left[\omega q_{0e} + S(\omega)\, q_e\right] - (q_{0e} - 1) q_e^T \omega \\ &= q_{0e} q_e^T \omega + q_e^T S(\omega)\, q_e - q_{0e} q_e^T \omega + q_e^T \omega \\ &= q_e^T S(\omega)\, q_e + q_e^T \omega \\ &= q_e^T \omega + q_e^T \omega^* - q_e^T \omega^* \\ &= q_e^T \omega^* + (\omega - \omega^*)^T q_e \end{aligned} \tag{5.67}$$

The virtual controller ω^* will be designed first by setting the following:

$$\omega^* = \begin{bmatrix} \omega_x^* \\ \omega_y^* \\ \omega_z^* \end{bmatrix} = \Upsilon_1 q_e = \begin{bmatrix} -k_1 q_{1e} \\ -k_2 q_{2e} \\ -k_3 q_{3e} \end{bmatrix} \tag{5.68}$$

where $\Upsilon_1 = \begin{bmatrix} k_1 & 0 & 0 \\ 0 & k_2 & 0 \\ 0 & 0 & k_3 \end{bmatrix} > 0$ with the positive gains k_1, k_2, and k_3. Hence, it follows from (5.64) that the following is true:

$$\dot{\omega}^* = \begin{bmatrix} \dot{\omega}_x^* \\ \dot{\omega}_y^* \\ \dot{\omega}_z^* \end{bmatrix} = \Upsilon_1 \dot{q}_e = \Upsilon_1 \left(\omega q_{0e} - S(\omega)\, q_e\right) \tag{5.69}$$

Then, (5.67) can be rewritten as

$$\dot{V}_1 = -q_e^T \Upsilon_1 q_e + (\omega - \omega^*)^T q_e \tag{5.70}$$

We can now define the second Lyapunov function as below:

$$V_2 = V_1 + \frac{1}{2} (\omega - \omega^*)^T (\omega - \omega^*) \tag{5.71}$$

The first order derivative of (5.71) is:

$$\begin{aligned}
\dot{V}_2 &= \dot{V}_1 + (\omega - \omega^*)^T (\dot{\omega} - \dot{\omega}^*) \\
&= -q_e^T \Upsilon_1 q_e + (\omega - \omega^*)^T q_e + (\omega - \omega^*)^T (\dot{\omega} - \dot{\omega}^*) \\
&= -q_e^T \Upsilon_1 q_e + (\omega - \omega^*)^T (q_e + \dot{\omega} - \dot{\omega}^*) \\
&= -q_e^T \Upsilon_1 q_e - (\omega - \omega^*)^T \Upsilon_2 (\omega - \omega^*) + (\omega - \omega^*)^T \Upsilon_2 (\omega - \omega^*) \\
&\quad + (\omega - \omega^*)^T (q_e + \dot{\omega} - \dot{\omega}^*) \\
&= -q_e^T \Upsilon_1 q_e - (\omega - \omega^*)^T \Upsilon_2 (\omega - \omega^*) \\
&\quad + (\omega - \omega^*)^T [\Upsilon_2 (\omega - \omega^*) + q_e + \dot{\omega} - \dot{\omega}^*]
\end{aligned} \tag{5.72}$$

where $\Upsilon_2 = \begin{bmatrix} k_4 & 0 & 0 \\ 0 & k_5 & 0 \\ 0 & 0 & k_6 \end{bmatrix} > 0$ with the positive gains k_4, k_5, and k_6. To determine the final control law of the system, one has to make the following:

$$\Upsilon_2 (\omega - \omega^*) + q_e + \dot{\omega} - \dot{\omega}^* = 0 \tag{5.73}$$

According to the dynamic model from (4.11), we can now have the following:

$$\dot{\omega} = \begin{bmatrix} \dot{\omega}_x \\ \dot{\omega}_y \\ \dot{\omega}_z \end{bmatrix} = \begin{bmatrix} \frac{1}{I_x} (\tau_\phi + \omega_y \omega_z I_y - \omega_y \omega_z I_z - \omega_y J_r (\bar{\omega}_1 - \bar{\omega}_2 - \bar{\omega}_3 + \bar{\omega}_4)) \\ \frac{1}{I_y} (\tau_\theta - \omega_x \omega_z I_x + \omega_x \omega_z I_z + \omega_x J_r (\bar{\omega}_1 - \bar{\omega}_2 - \bar{\omega}_3 + \bar{\omega}_4)) \\ \frac{1}{I_z} (\tau_\psi + \omega_x \omega_y I_x - \omega_x \omega_y I_y) \end{bmatrix} \tag{5.74}$$

where (4.15) is used.

In order to yield the final format of the controller, we can now substitute the above equation into (5.73). The control law can then be derived as following:

$$\begin{aligned}
&\begin{bmatrix} \frac{1}{I_x} (\tau_\phi + \omega_y \omega_z I_y - \omega_y \omega_z I_z - \omega_y J_r (\bar{\omega}_1 - \bar{\omega}_2 - \bar{\omega}_3 + \bar{\omega}_4)) \\ \frac{1}{I_y} (\tau_\theta - \omega_x \omega_z I_x + \omega_x \omega_z I_z + \omega_x J_r (\bar{\omega}_1 - \bar{\omega}_2 - \bar{\omega}_3 + \bar{\omega}_4)) \\ \frac{1}{I_z} (\tau_\psi + \omega_x \omega_y I_x - \omega_x \omega_y I_y) \end{bmatrix} \\
= &- \begin{bmatrix} k_4 & 0 & 0 \\ 0 & k_5 & 0 \\ 0 & 0 & k_6 \end{bmatrix} \begin{bmatrix} (\omega_x - \omega_x^*) \\ (\omega_y - \omega_y^*) \\ (\omega_z - \omega_z^*) \end{bmatrix} - \begin{bmatrix} q_{1e} \\ q_{2e} \\ q_{3e} \end{bmatrix} + \begin{bmatrix} \dot{\omega}_x^* \\ \dot{\omega}_y^* \\ \dot{\omega}_z^* \end{bmatrix}
\end{aligned} \tag{5.75}$$

which can be rewritten as

$$\begin{aligned}
&\begin{bmatrix} \tau_\phi - \omega_y J_r (\bar{\omega}_1 - \bar{\omega}_2 - \bar{\omega}_3 + \bar{\omega}_4) \\ \tau_\theta + \omega_x J_r (\bar{\omega}_1 - \bar{\omega}_2 - \bar{\omega}_3 + \bar{\omega}_4) \\ \tau_\psi \end{bmatrix} \\
= &\begin{bmatrix} \frac{I_x}{l} (-k_4(\omega_x - \omega_x^*) - q_{1e} + \dot{\omega}_x^*) - \omega_y \omega_z I_y + \omega_y \omega_z I_z \\ \frac{I_y}{l} (-k_5(\omega_y - \omega_y^*) - q_{2e} + \dot{\omega}_y^*) + \omega_x \omega_z I_x - \omega_x \omega_z I_z \\ I_z (-k_6(\omega_z - \omega_z^*) - q_{3e} + \dot{\omega}_z^*) - \omega_x \omega_y I_x + \omega_x \omega_y I_y \end{bmatrix}
\end{aligned} \tag{5.76}$$

Hence, the control law can be expressed as:

$$\begin{bmatrix} \tau_\phi \\ \tau_\theta \\ \tau_\psi \end{bmatrix} = \begin{bmatrix} \frac{I_x}{l}\left(-k_4(\omega_x-\omega_x^*)-q_{1e}+\dot{\omega}_x^*\right)-\omega_y\omega_z I_y+\omega_y\omega_z I_z+\omega_y J_r\left(\bar{\omega}_1-\bar{\omega}_2-\bar{\omega}_3+\bar{\omega}_4\right) \\ \frac{I_y}{l}\left(-k_5(\omega_y-\omega_y^*)-q_{2e}+\dot{\omega}_y^*\right)+\omega_x\omega_z I_x-\omega_x\omega_z I_z-\omega_x J_r\left(\bar{\omega}_1-\bar{\omega}_2-\bar{\omega}_3+\bar{\omega}_4\right) \\ I_z\left(-k_6(\omega_z-\omega_z^*)-q_{3e}+\dot{\omega}_z^*\right)-\omega_x\omega_y I_x+\omega_x\omega_y I_y \end{bmatrix} \tag{5.77}$$

Substituting the aerodynamic equation (2.15) into (5.75)-(5.77), taking (2.15) into consideration, it follows that

$$\begin{bmatrix} bl(\bar{\omega}_1^2-\bar{\omega}_4^2)-\omega_y J_r\left(\bar{\omega}_1-\bar{\omega}_2-\bar{\omega}_3+\bar{\omega}_4\right) \\ bl(\bar{\omega}_2^2-\bar{\omega}_3^2)+\omega_x J_r\left(\bar{\omega}_1-\bar{\omega}_2-\bar{\omega}_3+\bar{\omega}_4\right) \\ d(\bar{\omega}_1^2+\bar{\omega}_4^2-\bar{\omega}_2^2-\bar{\omega}_3^2) \\ b(\bar{\omega}_1^2+\bar{\omega}_4^2+\bar{\omega}_2^2+\bar{\omega}_3^2) \end{bmatrix} = \begin{bmatrix} \frac{I_x}{l}\left(-k_4(\omega_x-\omega_x^*)-q_{1e}+\dot{\omega}_x^*\right)-\omega_y\omega_z I_y+\omega_y\omega_z I_z \\ \frac{I_y}{l}\left(-k_5(\omega_y-\omega_y^*)-q_{2e}+\dot{\omega}_y^*\right)+\omega_x\omega_z I_x-\omega_x\omega_z I_z \\ I_z\left(-k_6(\omega_z-\omega_z^*)-q_{3e}+\dot{\omega}_z^*\right)-\omega_x\omega_y I_x+\omega_x\omega_y I_y \\ U_1 \end{bmatrix} \tag{5.78}$$

where U_1 is the vertical lifting power given by the RC controller, later on, this lifting force will be generated by the backstepping altitude controller. Then, the desired rotational speeds of the propellers $\bar{\omega}_1, \bar{\omega}_2, \bar{\omega}_3, \bar{\omega}_4$ can then be calculated by utilizing the gradient decent method. The block diagram for the closed-loop system with the backstepping attitude control using the quaternion representation is shown in Fig. 5.9.

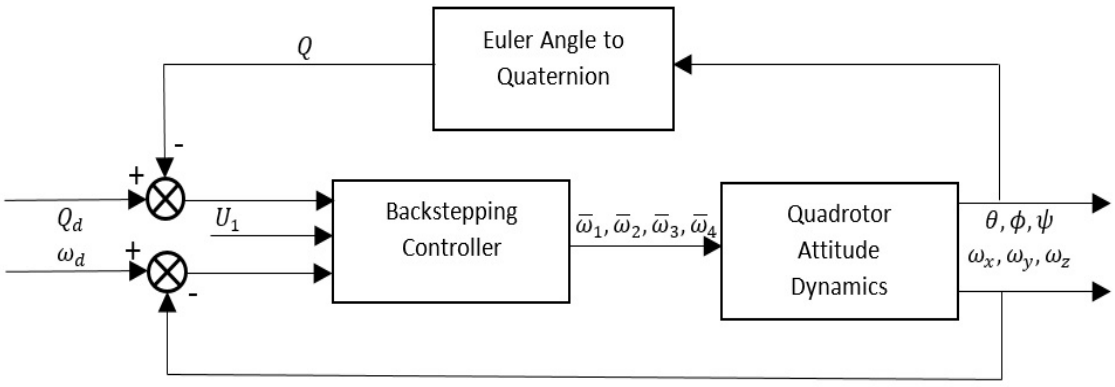

Figure 5.9: Block Diagram for Quaternion Backstepping Control

5.3.2 Experimental Results

The experimental results in Figs. 5.10-5.12 shows a promising outcome for the quaternion based backstepping control scheme. The flying behaviour is quite similar to the Euler angle based backstepping controller. The movements regarding to the pitch, roll and yaw directions are controlled within $\pm 10^{\circ}$, with relatively small angular velocity changes. The gain coefficients are, $k_1 = 140, k_2 = 300, k_3 = 0.5, k_4 = 2.0, k_5 = 2.2, k_6 = 190$. The selecting of these coefficients are based on try and error method.

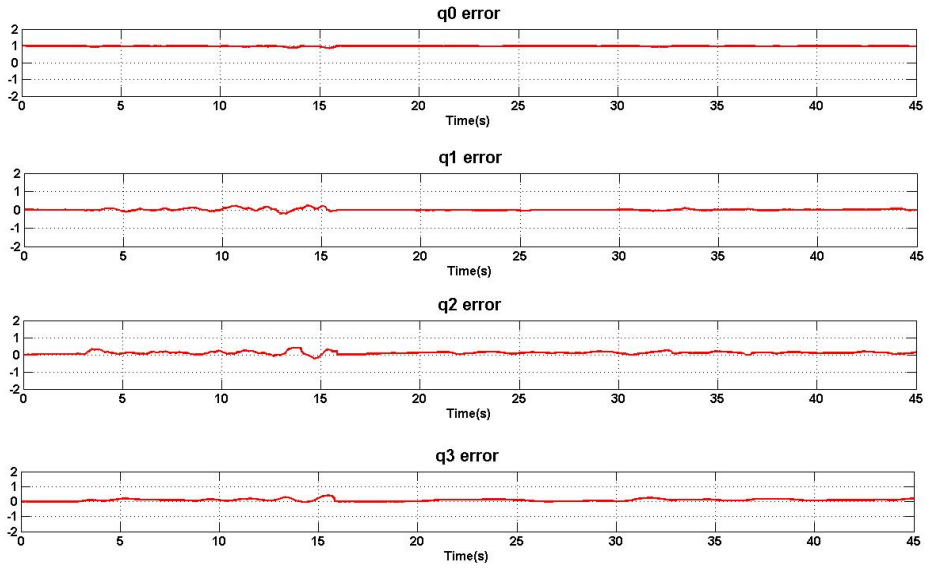

Figure 5.10: Quaternion Tracking Error

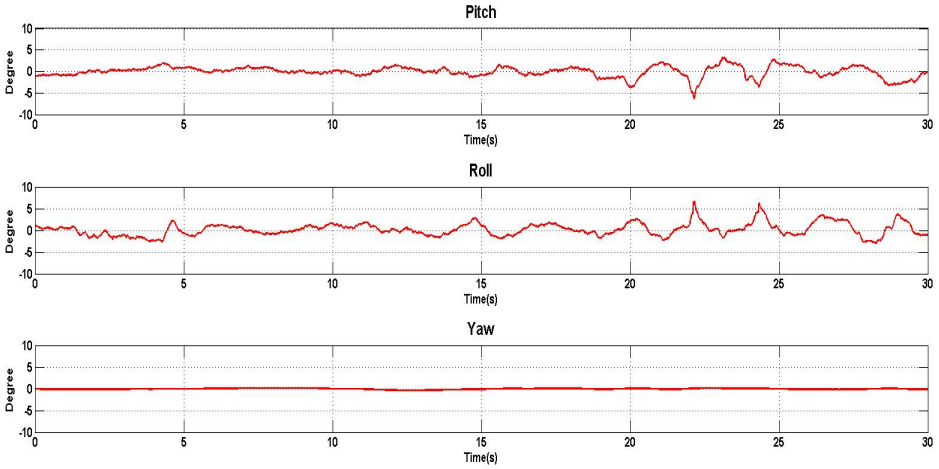

Figure 5.11: Euler Angle of the Quadrotor

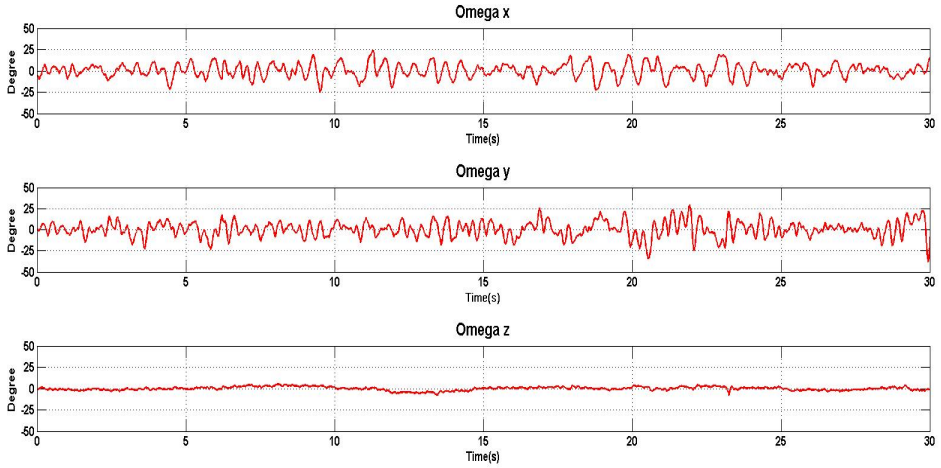

Figure 5.12: Angular Velocity of the Quadrotor

5.4 Integral Backstepping with Neural Network

5.4.1 Controller Design

Following by the integral backstepping derivation, an intelligent controller design method using the neural network is deployed as part of the controller design. A neural network imitates the function of a human brain, where the information is stored and processed in each neural cell. The information will then be passed onto different neural cells through various linkages. An unsupervised learning scheme is implemented into the controller design. Ideally, the designed adaptation rate $\hat{\varrho}$ will ultimately approach the desired ϱ. Such a property will be ensured by implementing the adaptation rate onto the Lyapunov function. Similar controller design approach can be found in [57–60].

Figs. 5.13-5.15 show a detailed working principle of the neural network, which consists of three different layers, input layer, hidden layer and output layer, respectively. The nonlinear term $f_\theta = \dot{\theta}\dot{\psi}\left(\frac{I_y - I_z}{I_x}\right)$, $f_\phi = \dot{\phi}\dot{\psi}(\frac{I_z - I_x}{I_y})$ and $f_\psi = \dot{\phi}\dot{\theta}(\frac{I_x - I_y}{I_z})$ are estimated with the neural network. Nine different neural cells are implemented as shown in Figs. 5.13-5.15. One of the key components for a well performing network is to select an appropriate embedded nonlinear function within each neural cell. In this thesis work, a triangular function is chosen for each neural cell.

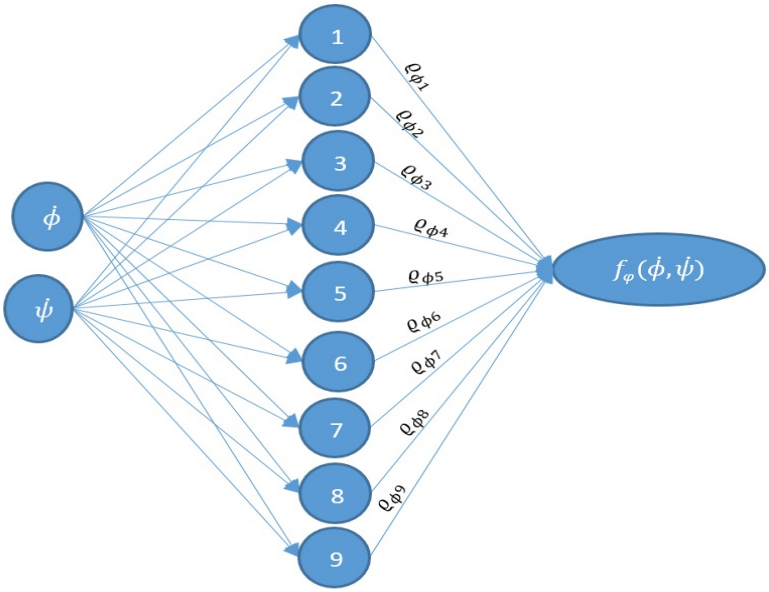

Figure 5.13: Neural Network in ϕ Direction

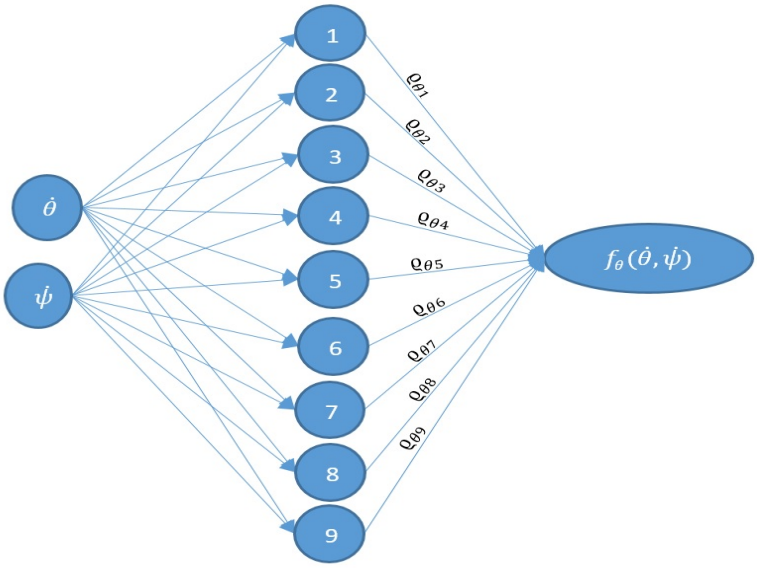

Figure 5.14: Neural Network in θ Direction

The theoretical development for the steps involving integral errors and tracking errors can be referred to Section 5.2.1. Starting from the equation (5.42), adding the estimation errors

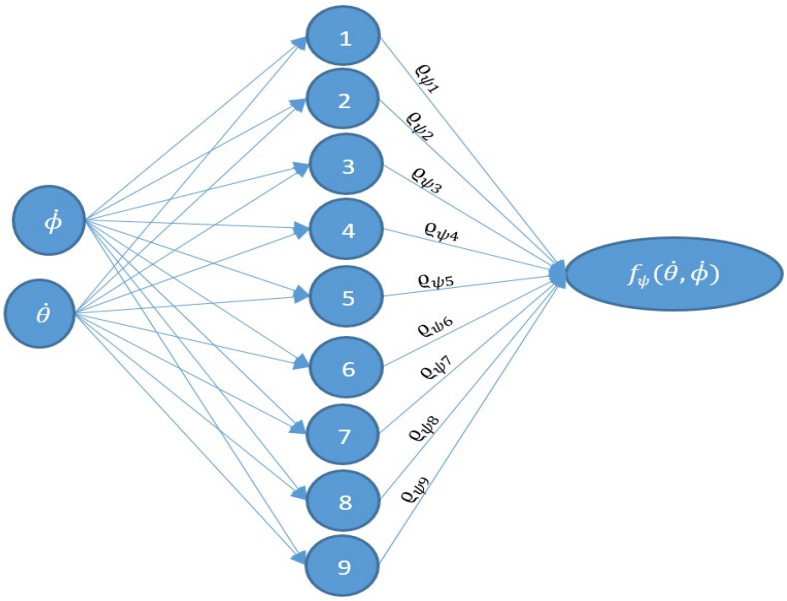

Figure 5.15: Neural Network in ψ Direction

to the Lyapunov function V_3 gives:

$$\begin{aligned} V_3 &= V_2 + \frac{1}{2}\bar{e}_2^2 + \frac{1}{2}\bar{e}_4^2 + \frac{1}{2}\bar{e}_6^2 \\ &+ \frac{1}{2}\left(\varrho_\theta - \hat{\varrho}_\theta\right)^T \Gamma_\theta \left(\varrho_\theta - \hat{\varrho}_\theta\right) \\ &+ \frac{1}{2}\left(\varrho_\phi - \hat{\varrho}_\phi\right)^T \Gamma_\phi \left(\varrho_\phi - \hat{\varrho}_\phi\right) \\ &+ \frac{1}{2}\left(\varrho_\psi - \hat{\varrho}_\psi\right)^T \Gamma_\psi \left(\varrho_\psi - \hat{\varrho}_\psi\right) \end{aligned} \tag{5.79}$$

where $\hat{\varrho}_\phi, \hat{\varrho}_\theta, \hat{\varrho}_\psi$ are the ideal estimations of the nonlinear terms and $\Gamma_\theta, \Gamma_\phi, \Gamma_\psi$ are positive definite symmetric matrices. Applying the time derivative onto (5.79), we then get the following:

$$
\begin{aligned}
\dot{V}_3 &= \dot{V}_2 + \bar{e}_2\dot{\bar{e}}_2 + \bar{e}_4\dot{\bar{e}}_4 + \bar{e}_6\dot{\bar{e}}_6 \\
&\quad + (\varrho_\theta - \hat{\varrho}_\theta)^T \Gamma_\theta \left(-\dot{\hat{\varrho}}_\theta\right) + (\varrho_\phi - \hat{\varrho}_\phi)^T \Gamma_\phi \left(-\dot{\hat{\varrho}}_\phi\right) + (\varrho_\psi - \hat{\varrho}_\psi)^T \Gamma_\psi \left(-\dot{\hat{\varrho}}_\psi\right) \\
&= -k_{i1}e_{i1}^2 - k_{i2}e_{i2}^2 - k_{i3}e_{i3}^2 - k_1\bar{e}_1^2 - k_3\bar{e}_3^2 - k_5\bar{e}_5^2 \\
&\quad + \bar{e}_1\bar{e}_2 + \bar{e}_3\bar{e}_4 + \bar{e}_5\bar{e}_6 + \bar{e}_2\dot{\bar{e}}_2 + \bar{e}_4\dot{\bar{e}}_4 + \bar{e}_6\dot{\bar{e}}_6 \\
&\quad + (\varrho_\theta - \hat{\varrho}_\theta)^T \Gamma_\theta \left(-\dot{\hat{\varrho}}_\theta\right) + (\varrho_\phi - \hat{\varrho}_\phi)^T \Gamma_\phi \left(-\dot{\hat{\varrho}}_\phi\right) + (\varrho_\psi - \hat{\varrho}_\psi)^T \Gamma_\psi \left(-\dot{\hat{\varrho}}_\psi\right) \\
&= -k_{i1}e_{i1}^2 - k_{i2}e_{i2}^2 - k_{i3}e_{i3}^2 - k_1\bar{e}_1^2 - k_3\bar{e}_3^2 - k_5\bar{e}_5^2 \\
&\quad + \bar{e}_2\left(\bar{e}_1 + k_1\dot{\bar{e}}_1 + \dot{\theta}\dot{\psi}\left(\frac{I_y - I_z}{I_x}\right) - \frac{J_r}{I_x}\dot{\theta}\bar{\omega} + \frac{l}{I_x}\tau_\phi - \ddot{\phi}_d + k_{i1}\dot{e}_1 + e_1\right) \\
&\quad + \bar{e}_4\left(\bar{e}_3 + k_3\dot{\bar{e}}_3 + \dot{\phi}\dot{\psi}\left(\frac{I_z - I_x}{I_y}\right) + \frac{J_r}{I_y}\dot{\phi}\bar{\omega} + \frac{l}{I_y}\tau_\theta - \ddot{\theta}_d + k_{i2}\dot{e}_3 + e_3\right) \\
&\quad + \bar{e}_6\left(\bar{e}_5 + k_5\dot{\bar{e}}_5 + \dot{\phi}\dot{\theta}\left(\frac{I_x - I_y}{I_z}\right) + \frac{1}{I_z}\tau_\psi - \ddot{\psi}_d + k_{i3}\dot{e}_5 + e_5\right) \\
&\quad + (\varrho_\theta - \hat{\varrho}_\theta)^T \Gamma_\theta \left(-\dot{\hat{\varrho}}_\theta\right) + (\varrho_\phi - \hat{\varrho}_\phi)^T \Gamma_\phi \left(-\dot{\hat{\varrho}}_\phi\right) + (\varrho_\psi - \hat{\varrho}_\psi)^T \Gamma_\psi \left(-\dot{\hat{\varrho}}_\psi\right) \qquad (5.80)
\end{aligned}
$$

The nonlinear terms can then be estimated by the following neural networks

$$f_\theta = \dot{\theta}\dot{\psi}\left(\frac{I_y - I_z}{I_x}\right) = \varrho_\theta\xi_\theta + \varepsilon_\theta \qquad (5.81)$$

$$f_\phi = \dot{\phi}\dot{\psi}\left(\frac{I_z - I_x}{I_y}\right) = \varrho_\phi\xi_\phi + \varepsilon_\phi \qquad (5.82)$$

$$f_\psi = \dot{\phi}\dot{\theta}\left(\frac{I_x - I_y}{I_z}\right) = \varrho_\psi\xi_\psi + \varepsilon_\psi \qquad (5.83)$$

According to the universal approximation theorem, the absolute values of the approximation error ε_θ, ε_ϕ, ε_ψ can be made arbitrarily small, which is considered to be bounded [61]. Substituting (5.81), (5.82), (5.83) into (5.80), it follows that

$$
\begin{aligned}
\dot{V}_3 &= -k_{i1}e_{i1}^2 - k_{i2}e_{i2}^2 - k_{i3}e_{i3}^2 - k_1\bar{e}_1^2 - k_3\bar{e}_3^2 - k_5\bar{e}_5^2 \\
&\quad + \bar{e}_2\left(\bar{e}_1 + k_1\dot{\bar{e}}_1 + \varrho_\theta\xi_\theta + \varepsilon_\theta - \frac{J_r}{I_x}\dot{\theta}\bar{\omega} + \frac{l}{I_x}\tau_\phi - \ddot{\phi}_d + k_{i1}\dot{e}_1 + e_1\right) \\
&\quad + \bar{e}_4\left(\bar{e}_3 + k_3\dot{\bar{e}}_3 + \varrho_\phi\xi_\phi + \varepsilon_\phi + \frac{J_r}{I_y}\dot{\phi}\bar{\omega} + \frac{l}{I_y}\tau_\theta - \ddot{\theta}_d + k_{i2}\dot{e}_3 + e_3\right) \\
&\quad + \bar{e}_6\left(\bar{e}_5 + k_5\dot{\bar{e}}_5 + \varrho_\psi\xi_\psi + \varepsilon_\psi + \frac{1}{I_z}\tau_\psi - \ddot{\psi}_d + k_{i3}\dot{e}_5 + e_5\right) \\
&\quad + (\varrho_\theta - \hat{\varrho}_\theta)^T \Gamma_\theta \left(-\dot{\hat{\varrho}}_\theta\right) + (\varrho_\phi - \hat{\varrho}_\phi)^T \Gamma_\phi \left(-\dot{\hat{\varrho}}_\phi\right) + (\varrho_\psi - \hat{\varrho}_\psi)^T \Gamma_\psi \left(-\dot{\hat{\varrho}}_\psi\right)
\end{aligned} \qquad (5.84)
$$

$$\begin{aligned}\dot{V}_3 &= -k_{i1}e_{i1}^2 - k_{i2}e_{i2}^2 - k_{i3}e_{i3}^2 - k_1\bar{e}_1^2 - k_3\bar{e}_3^2 - k_5\bar{e}_5^2 \\ &+\bar{e}_2\left(\bar{e}_1 + k_1\dot{\bar{e}}_1 + \hat{\varrho}_\theta\xi_\theta + \varepsilon_\theta - \frac{J_r}{I_x}\dot{\theta}\bar{\omega} + \frac{l}{I_x}\tau_\phi - \ddot{\phi}_d + k_{i1}\dot{e}_1 + e_1\right) \\ &+\bar{e}_4\left(\bar{e}_3 + k_3\dot{\bar{e}}_3 + \hat{\varrho}_\phi\xi_\phi + \varepsilon_{_\phi} + \frac{J_r}{I_y}\dot{\phi}\bar{\omega} + \frac{l}{I_y}\tau_\theta - \ddot{\theta}_d + k_{i2}\dot{e}_3 + e_3\right) \\ &+\bar{e}_6\left(\bar{e}_5 + k_5\dot{\bar{e}}_5 + \hat{\varrho}_\psi\xi_\psi + \varepsilon_{_\psi} + \frac{1}{I_z}\tau_\psi - \ddot{\psi}_d + k_{i3}\dot{e}_5 + e_5\right) \\ &+\left(\varrho_\theta - \hat{\varrho}_\theta\right)^T\Gamma_\theta\left(\Gamma_\theta^{-1}\bar{e}_2\xi_\theta - \dot{\hat{\varrho}}_\theta\right) + \left(\varrho_\phi - \hat{\varrho}_\phi\right)^T\Gamma_\phi\left(\Gamma_\phi^{-1}\bar{e}_4\xi_\phi - \dot{\hat{\varrho}}_\phi\right) \\ &+\left(\varrho_\psi - \hat{\varrho}_\psi\right)^T\Gamma_\psi\left(\Gamma_\psi^{-1}\bar{e}_6\xi_\psi - \dot{\hat{\varrho}}_\psi\right) \end{aligned} \tag{5.85}$$

Introduce the following adaptation laws for $\hat{\varrho}_\phi, \hat{\varrho}_\theta, \hat{\varrho}_\psi$

$$\begin{aligned}\dot{\hat{\varrho}}_\theta &= \Gamma_\theta^{-1}\bar{e}_2\xi_\theta - \sigma_\theta\hat{\varrho}_\theta \\ \dot{\hat{\varrho}}_\phi &= \Gamma_\phi^{-1}\bar{e}_4\xi_\phi - \sigma_\phi\hat{\varrho}_\phi \\ \dot{\hat{\varrho}}_\psi &= \Gamma_\psi^{-1}\bar{e}_6\xi_\psi - \sigma_\psi\hat{\varrho}_\psi\end{aligned} \tag{5.86}$$

Then, $\dot{V}_3$ becomes

$$\begin{aligned}\dot{V}_3 &= -k_{i1}e_{i1}^2 - k_{i2}e_{i2}^2 - k_{i3}e_{i3}^2 - k_1\bar{e}_1^2 - k_3\bar{e}_3^2 - k_5\bar{e}_5^2 \\ &+\bar{e}_2\left(\bar{e}_1 + k_1\dot{\bar{e}}_1 + \hat{\varrho}_\theta\xi_\theta - \frac{J_r}{I_x}\dot{\theta}\bar{\omega} + \frac{l}{I_x}\tau_\phi - \ddot{\phi}_d + k_{i1}\dot{e}_1 + e_1\right) \\ &+\bar{e}_4\left(\bar{e}_3 + k_3\dot{\bar{e}}_3 + \hat{\varrho}_\phi\xi_\phi + \frac{J_r}{I_y}\dot{\phi}\bar{\omega} + \frac{l}{I_y}\tau_\theta - \ddot{\theta}_d + k_{i2}\dot{e}_3 + e_3\right) \\ &+\bar{e}_6\left(\bar{e}_5 + k_5\dot{\bar{e}}_5 + \hat{\varrho}_\psi\xi_\psi + \frac{1}{I_z}\tau_\psi - \ddot{\psi}_d + k_{i3}\dot{e}_5 + e_5\right) \\ &+\bar{e}_2\varepsilon_\theta + \bar{e}_4\varepsilon_{_\phi} + \bar{e}_6\varepsilon_{_\psi} \\ &+\sigma_\theta\left(\varrho_\theta - \hat{\varrho}_\theta\right)^T\Gamma_\theta\hat{\varrho}_\theta + \sigma_\phi\left(\varrho_\phi - \hat{\varrho}_\phi\right)^T\Gamma_\phi\hat{\varrho}_\phi + \sigma_\psi\left(\varrho_\psi - \hat{\varrho}_\psi\right)^T\Gamma_\psi\hat{\varrho}_\psi \end{aligned} \tag{5.87}$$

By using Young's inequality $xy \leq \frac{1}{2}x^2 + \frac{1}{2}y^2$, it follows that $\bar{e}_2\varepsilon_\theta \leq \frac{1}{2}\bar{e}_2^2 + \frac{1}{2}\varepsilon_\theta^2$, $\bar{e}_4\varepsilon_{_\phi} \leq \frac{1}{2}\bar{e}_4^2 + \frac{1}{2}\varepsilon_{_\phi}^2$, $\bar{e}_6\varepsilon_{_\psi} \leq \frac{1}{2}\bar{e}_6^2 + \frac{1}{2}\varepsilon_{_\psi}^2$. Therefore, (5.87) can be expressed as:

$$
\begin{aligned}
\dot{V}_3 \leq\ & -k_{i1}e_{i1}^2 - k_{i2}e_{i2}^2 - k_{i3}e_{i3}^2 - k_1\bar{e}_1^2 - k_3\bar{e}_3^2 - k_5\bar{e}_5^2 \\
& +\bar{e}_2\left(\bar{e}_1 + k_1\dot{\bar{e}}_1 + \hat{\varrho}_\theta\xi_\theta - \frac{J_r}{I_x}\dot{\theta}\bar{\omega} + \frac{l}{I_x}\tau_\phi - \ddot{\phi}_d + k_{i1}\dot{e}_1 + e_1\right) \\
& +\bar{e}_4\left(\bar{e}_3 + k_3\dot{\bar{e}}_3 + \hat{\varrho}_\phi\xi_\phi + \frac{J_r}{I_y}\dot{\phi}\bar{\omega} + \frac{l}{I_y}\tau_\theta - \ddot{\theta}_d + k_{i2}\dot{e}_3 + e_3\right) \\
& +\bar{e}_6\left(\bar{e}_5 + k_5\dot{\bar{e}}_5 + \hat{\varrho}_\psi\xi_\psi + \frac{1}{I_z}\tau_\psi - \ddot{\psi}_d + k_{i3}\dot{e}_5 + e_5\right) \\
& +\frac{1}{2}\bar{e}_2^2 + \frac{1}{2}\varepsilon_\theta^2 + \frac{1}{2}\bar{e}_4^2 + \frac{1}{2}\varepsilon_\phi^2 + \frac{1}{2}\bar{e}_6^2 + \frac{1}{2}\varepsilon_\psi^2 \\
& +\sigma_\theta\left(\varrho_\theta - \hat{\varrho}_\theta\right)^T\Gamma_\theta\varrho_\theta + \sigma_\phi\left(\varrho_\phi - \hat{\varrho}_\phi\right)^T\Gamma_\phi\varrho_\phi + \sigma_\psi\left(\varrho_\psi - \hat{\varrho}_\psi\right)^T\Gamma_\psi\varrho_\psi \\
& -\sigma_\theta\left(\varrho_\theta - \hat{\varrho}_\theta\right)^T\Gamma_\theta\left(\varrho_\theta - \hat{\varrho}_\theta\right) - \sigma_\phi\left(\varrho_\phi - \hat{\varrho}_\phi\right)^T\Gamma_\phi\left(\varrho_\phi - \hat{\varrho}_\phi\right) \\
& -\sigma_\psi\left(\varrho_\psi - \hat{\varrho}_\psi\right)^T\Gamma_\psi\left(\varrho_\psi - \hat{\varrho}_\psi\right)
\end{aligned} \tag{5.88}
$$

By using Young's inequality $x^T\Gamma y \leq \frac{1}{2}x^T\Gamma x + \frac{1}{2}y^T\Gamma y$, it can be verified that

$$
\begin{aligned}
\left(\varrho_\theta - \hat{\varrho}_\theta\right)^T\Gamma_\theta\varrho_\theta &\leq \frac{1}{2}\left(\varrho_\theta - \hat{\varrho}_\theta\right)^T\Gamma_\theta\left(\varrho_\theta - \hat{\varrho}_\theta\right) + \frac{1}{2}\varrho_\theta^T\Gamma_\theta\varrho_\theta \\
\left(\varrho_\phi - \hat{\varrho}_\phi\right)^T\Gamma_\phi\varrho_\phi &\leq \frac{1}{2}\left(\varrho_\phi - \hat{\varrho}_\phi\right)^T\Gamma_\phi\left(\varrho_\phi - \hat{\varrho}_\phi\right) + \frac{1}{2}\varrho_\phi^T\Gamma_\phi\varrho_\phi \\
\left(\varrho_\psi - \hat{\varrho}_\psi\right)^T\Gamma_\psi\varrho_\psi &\leq \frac{1}{2}\left(\varrho_\psi - \hat{\varrho}_\psi\right)^T\Gamma_\psi\left(\varrho_\psi - \hat{\varrho}_\psi\right) + \frac{1}{2}\varrho_\psi^T\Gamma_\psi\varrho_\psi
\end{aligned} \tag{5.89}
$$

With (5.89), (5.88) can be rewritten as:

$$
\begin{aligned}
\dot{V}_3 \leq\ & -k_{i1}e_{i1}^2 - k_{i2}e_{i2}^2 - k_{i3}e_{i3}^2 - k_1\bar{e}_1^2 - k_3\bar{e}_3^2 - k_5\bar{e}_5^2 \\
& +\bar{e}_2\left(\frac{1}{2}\bar{e}_2 + \bar{e}_1 + k_1\dot{\bar{e}}_1 + \hat{\varrho}_\theta\xi_\theta - \frac{J_r}{I_x}\dot{\theta}\bar{\omega} + \frac{l}{I_x}\tau_\phi - \ddot{\phi}_d + k_{i1}\dot{e}_1 + e_1\right) \\
& +\bar{e}_4\left(\frac{1}{2}\bar{e}_4 + \bar{e}_3 + k_3\dot{\bar{e}}_3 + \hat{\varrho}_\phi\xi_\phi + \frac{J_r}{I_y}\dot{\phi}\bar{\omega} + \frac{l}{I_y}\tau_\theta - \ddot{\theta}_d + k_{i2}\dot{e}_3 + e_3\right) \\
& +\bar{e}_6\left(\frac{1}{2}\bar{e}_6 + \bar{e}_5 + k_5\dot{\bar{e}}_5 + \hat{\varrho}_\psi\xi_\psi + \frac{1}{I_z}\tau_\psi - \ddot{\psi}_d + k_{i3}\dot{e}_5 + e_5\right) \\
& -\frac{1}{2}\sigma_\theta\left(\varrho_\theta - \hat{\varrho}_\theta\right)^T\Gamma_\theta\left(\varrho_\theta - \hat{\varrho}_\theta\right) - \frac{1}{2}\sigma_\phi\left(\varrho_\phi - \hat{\varrho}_\phi\right)^T\Gamma_\phi\left(\varrho_\phi - \hat{\varrho}_\phi\right) \\
& -\frac{1}{2}\sigma_\psi\left(\varrho_\psi - \hat{\varrho}_\psi\right)^T\Gamma_\psi\left(\varrho_\psi - \hat{\varrho}_\psi\right) \\
& +\frac{1}{2}\varepsilon_\theta^2 + \frac{1}{2}\varepsilon_\phi^2 + \frac{1}{2}\varepsilon_\psi^2 + \frac{1}{2}\varrho_\theta^T\Gamma_\theta\varrho_\theta + \frac{1}{2}\varrho_\phi^T\Gamma_\phi\varrho_\phi + \frac{1}{2}\varrho_\psi^T\Gamma_\psi\varrho_\psi
\end{aligned} \tag{5.90}
$$

Set the following to yield the control law in (5.92).

$$\begin{bmatrix} -k_2\bar{e}_2 \\ -k_4\bar{e}_4 \\ -k_6\bar{e}_6 \end{bmatrix} = \begin{bmatrix} \frac{1}{2}\bar{e}_2 + \bar{e}_1 + k_1\dot{\bar{e}}_1 + \hat{\varrho}_\theta\xi_\theta - \frac{J_r}{I_x}\dot{\theta}\bar{\omega} + \frac{l}{I_x}\tau_\phi - \ddot{\phi}_d + k_{i1}\dot{e}_1 + e_1 \\ \frac{1}{2}\bar{e}_4 + \bar{e}_3 + k_3\dot{\bar{e}}_3 + \hat{\varrho}_\phi\xi_\phi + \frac{J_r}{I_y}\dot{\phi}\bar{\omega} + \frac{l}{I_y}\tau_\theta - \ddot{\theta}_d + k_{i2}\dot{e}_3 + e_3 \\ \frac{1}{2}\bar{e}_6 + \bar{e}_5 + k_5\dot{\bar{e}}_5 + \hat{\varrho}_\psi\xi_\psi + \frac{1}{I_z}\tau_\psi - \ddot{\psi}_d + k_{i3}\dot{e}_5 + e_5 \end{bmatrix} \tag{5.91}$$

$$\begin{bmatrix} \tau_\phi \\ \tau_\theta \\ \tau_\psi \end{bmatrix} = \begin{bmatrix} \frac{I_x}{l}\left(-k_2\bar{e}_2 - \frac{1}{2}\bar{e}_2 - \bar{e}_1 - k_1\dot{\bar{e}}_1 - \hat{\varrho}_\theta\xi_\theta + \frac{J_r}{I_x}\dot{\theta}\bar{\omega} + \ddot{\phi}_d - k_{i1}\dot{e}_1 - e_1\right) \\ \frac{I_y}{l}\left(-k_4\bar{e}_4 - \frac{1}{2}\bar{e}_4 - \bar{e}_3 - k_3\dot{\bar{e}}_3 - \hat{\varrho}_\phi\xi_\phi - \frac{J_r}{I_y}\dot{\phi}\bar{\omega} + \ddot{\theta}_d - k_{i2}\dot{e}_3 - e_3\right) \\ I_z\left(-k_6\bar{e}_6 - \frac{1}{2}\bar{e}_6 - \bar{e}_5 - k_5\dot{\bar{e}}_5 - \hat{\varrho}_\psi\xi_\psi + \ddot{\psi}_d - k_{i3}\dot{e}_5 - e_5\right) \end{bmatrix} \tag{5.92}$$

With (5.92), (5.90) can be rewritten as follows:

$$\begin{aligned} \dot{V}_3 \leq\ & -k_{i1}e_{i1}^2 - k_{i2}e_{i2}^2 - k_{i3}e_{i3}^2 - k_1\bar{e}_1^2 - k_3\bar{e}_3^2 - k_5\bar{e}_5^2 - k_2\bar{e}_2^2 - k_4\bar{e}_4^2 - k_6\bar{e}_6^2 \\ & -\frac{1}{2}\sigma_\theta\left(\varrho_\theta - \hat{\varrho}_\theta\right)^T\Gamma_\theta\left(\varrho_\theta - \hat{\varrho}_\theta\right) - \frac{1}{2}\sigma_\phi\left(\varrho_\phi - \hat{\varrho}_\phi\right)^T\Gamma_\phi\left(\varrho_\phi - \hat{\varrho}_\phi\right) - \frac{1}{2}\sigma_\psi\left(\varrho_\psi - \hat{\varrho}_\psi\right)^T\Gamma_\psi\left(\varrho_\psi - \hat{\varrho}_\psi\right) \\ & +\frac{1}{2}\varepsilon_\theta^2 + \frac{1}{2}\varepsilon_\phi^2 + \frac{1}{2}\varepsilon_\psi^2 + \frac{1}{2}\varrho_\theta^T\Gamma_\theta\varrho_\theta + \frac{1}{2}\varrho_\phi^T\Gamma_\phi\varrho_\phi + \frac{1}{2}\varrho_\psi^T\Gamma_\psi\varrho_\psi \\ \leq\ & -aV_3 + b \end{aligned} \tag{5.93}$$

where $a = 2\min\{k_{i1}, k_{i2}, k_{i3}, k_1, k_3, k_5, k_2, k_4, k_6, \frac{1}{2}\sigma_\theta, \frac{1}{2}\sigma_\phi, \frac{1}{2}\sigma_\psi\}$ and $b = \frac{1}{2}\varepsilon_\theta^2 + \frac{1}{2}\varepsilon_\phi^2 + \frac{1}{2}\varepsilon_\psi^2 + \frac{1}{2}\varrho_\theta^T\Gamma_\theta\varrho_\theta + \frac{1}{2}\varrho_\phi^T\Gamma_\phi\varrho_\phi + \frac{1}{2}\varrho_\psi^T\Gamma_\psi\varrho_\psi$. It can be verified that b is bounded, because the absolute values of ε_ϕ, ε_θ, ε_ψ are arbitrarily small, and the last three terms in b are constant. It follows from Halanay inequality [62] that all the error terms in V_3 are bounded.

Again, using the aerodynamic equations in (2.15) and (2.16), the angular velocities of the motors can be calculated by solving

$$\begin{bmatrix} b(\bar{\omega}_1^2 + \bar{\omega}_4^2 + \bar{\omega}_2^2 + \bar{\omega}_3^2) \\ bl(\bar{\omega}_1^2 - \bar{\omega}_4^2) - \frac{J_r}{l}\dot{\theta}\bar{\omega} \\ bl(\bar{\omega}_2^2 - \bar{\omega}_3^2) + \frac{J_r}{l}\dot{\phi}\bar{\omega} \\ d(\bar{\omega}_1^2 + \bar{\omega}_4^2 - \bar{\omega}_2^2 - \bar{\omega}_3^2) \end{bmatrix} = \begin{bmatrix} U_1 \\ \frac{I_x}{l}\left(-k_2\bar{e}_2 - \frac{1}{2}\bar{e}_2 - \bar{e}_1 - k_1\dot{\bar{e}}_1 - \hat{\varrho}_\theta\xi_\theta + \ddot{\phi}_d - k_{i1}\dot{e}_1 - e_1\right) \\ \frac{I_y}{l}\left(-k_4\bar{e}_4 - \frac{1}{2}\bar{e}_4 - \bar{e}_3 - k_3\dot{\bar{e}}_3 - \hat{\varrho}_\phi\xi_\phi + \ddot{\theta}_d - k_{i2}\dot{e}_3 - e_3\right) \\ I_z\left(-k_6\bar{e}_6 - \frac{1}{2}\bar{e}_6 - \bar{e}_5 - k_5\dot{\bar{e}}_5 - \hat{\varrho}_\psi\xi_\psi + \ddot{\psi}_d - k_{i3}\dot{e}_5 - e_5\right) \end{bmatrix} \tag{5.94}$$

with the gradient decent method, where U_1 is the vertical lifting power given by the RC controller, later on, this lifting force will be generated by the backstepping altitude controller. Fig. 5.16 shows the block diagram for the closed-loop system using the integral backstepping controller.

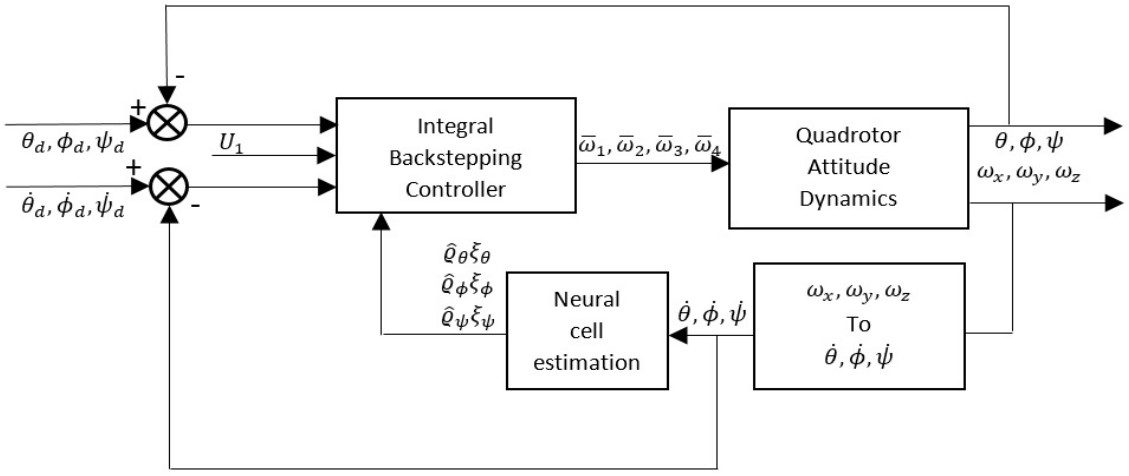

Figure 5.16: Block Diagram for Integral Backstepping with Neural Network Control

5.4.2 Experimental Results

A neural network mechanism is implemented into the controller design, where all the possible outputs from each neural cells are displayed in Fig. 5.17. By observing the actual experiment results for the pitch, roll and yaw movements in Figs. (5.18)-(5.20), the fluctuation is within the $\pm 10^\circ$ range, with acceptable amount of changes in the angular velocity. The gain coefficients are $k_{i1} = 1, k_1 = 11, k_2 = 2, k_{i2} = 1, k_3 = 17, k_4 = 2, k_{i3} = 0.7, k_4 = 1.0, k_5 = 300$. Notice the gain factors are slightly different in comparison with the integral backstepping controller. This is due to the introducing of the nonlinear estimations terms from neural network, hence the controller responses varies in order to cancel out the estimation terms.

For the demonstration purposes, the neural cells output shown in Fig. 5.17 only describes the estimation nonlinear term of $f_\theta(\dot{\theta}, \dot{\psi})$. However, in the practical implementation, $f_\phi(\dot{\phi}, \dot{\psi})$ and $f_\psi(\dot{\theta}, \dot{\phi})$ are also involved in the calculations.

5.5 Altitude Control

5.5.1 Controller Design

The altitude controller design is strictly followed by the backstepping method. Define the errors by

$$e_9 = z - z_d \tag{5.95}$$
$$e_{10} = \dot{z} - \dot{z}_d \tag{5.96}$$

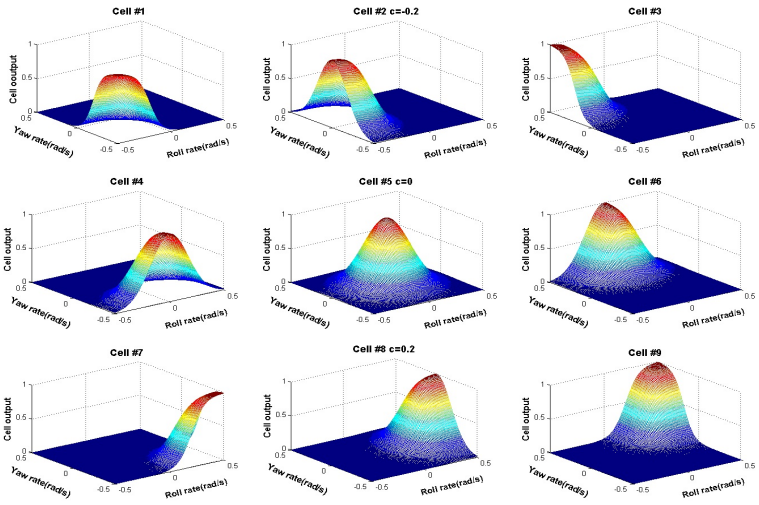

Figure 5.17: Neural Cells Outputs for $\dot{\phi}$ input and $\dot{\psi}$ input

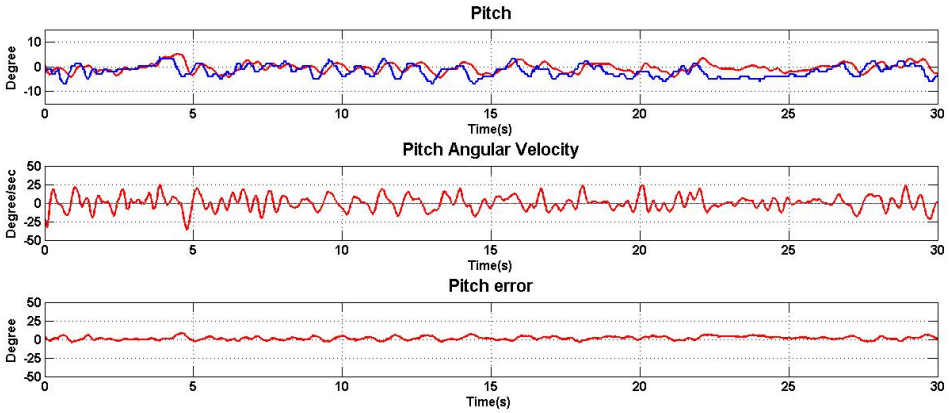

Figure 5.18: Integral Backstepping with Neural Network in ϕ Direction

The Lyapunov function can then be chosen as follows:

$$V_1 = \frac{1}{2}e_9^2 \tag{5.97}$$

By differentiating (5.97), one can yield the equation below:

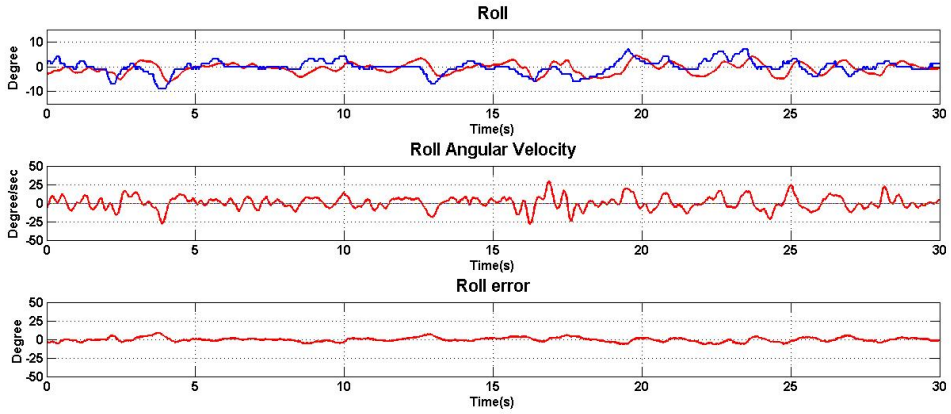

Figure 5.19: Integral Backstepping with Neural Network in θ Direction

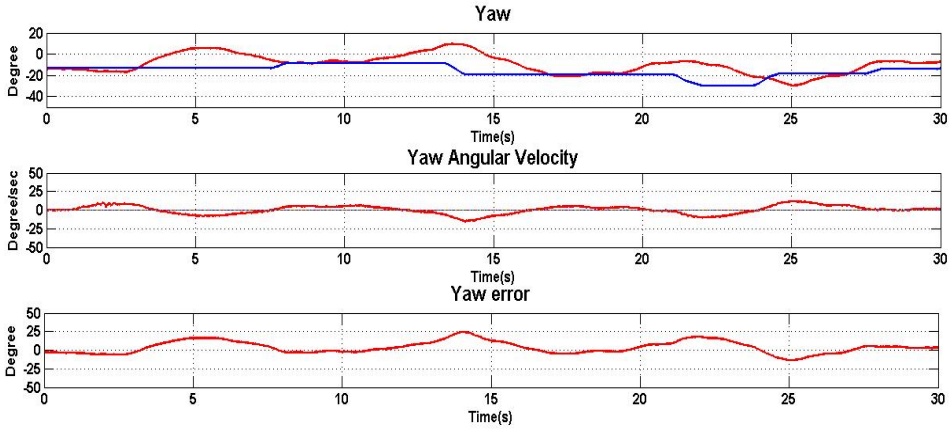

Figure 5.20: Integral Backstepping with Neural Network in ψ Direction

$$\begin{aligned}
\dot{V}_1 &= e_9\dot{e}_9 \\
&= e_9 e_{10} \\
&= -k_9 e_9^2 + k_9 e_9^2 + e_9 e_{10} \\
&= -k_9 e_9^2 + e_9\left(k_9 e_9 + e_{10}\right) \\
&= -k_9 e_9^2 + e_9 \bar{e}_{10}
\end{aligned} \tag{5.98}$$

where k_9 is a positive gain and

$$\bar{e}_{10} = k_9 e_9 + e_{10} \tag{5.99}$$

The time derivative of (5.99) can be expressed as:

$$\begin{aligned}\dot{\bar{e}}_{10} &= k_9\dot{e}_9 + \dot{e}_{10} \\ &= k_9 e_{10} + \dot{e}_{10}\end{aligned} \tag{5.100}$$

The Lyapunov function V_2 can then be defined as:

$$V_2 = V_1 + \frac{1}{2}\bar{e}_{10}^2 \tag{5.101}$$

Again, applying the time derivative onto (5.101), one can have the following:

$$\begin{aligned}\dot{V}_2 &= \dot{V}_1 + \bar{e}_{10}\dot{\bar{e}}_{10} \\ &= -k_9 e_9^2 + e_9\bar{e}_{10} + \bar{e}_{10}\left(k_9 e_{10} + \dot{e}_{10}\right) \\ &= -k_9 e_9^2 + \bar{e}_{10}\left(e_9 + k_9 e_{10} + \dot{e}_{10}\right)\end{aligned} \tag{5.102}$$

Set the following:

$$\begin{aligned}-k_{10}\bar{e}_{10} &= e_9 + k_9 e_{10} + \dot{e}_{10} \\ &= e_9 + k_9 e_{10} + \ddot{z} - \ddot{z}_d\end{aligned} \tag{5.103}$$

where k_{10} is a positive gain.

Then, one can introduce the dynamic model (4.5) into (5.103), which results in the following equation.

$$-k_{10}\bar{e}_{10} = e_9 + k_9 e_{10} + \cos\phi\cos\theta\frac{U_1}{m} - g - \ddot{z}_d \tag{5.104}$$

Solving it for U_1 produces

$$\begin{aligned}U_1 &= m\left(\frac{-k_{10}\bar{e}_{10} - e_9 - k_9 e_{10} + g + \ddot{z}_d}{\cos\phi\cos\theta}\right) \\ &= m\left(\frac{-\left(k_9 k_{10} + 1\right)e_9 - \left(k_9 + k_{10}\right)e_{10} + g + \ddot{z}_d}{\cos\phi\cos\theta}\right)\end{aligned} \tag{5.105}$$

which makes $\dot{V}_2 = -k_9 e_9^2 - k_{10}\bar{e}_{10}^2$, a negative definite function.

(5.105), together with the attitude controllers discussed in Section 5.1.1, Section 5.2.1, and Section 5.4.1, is able to achieve the altitude control while maintaining the attitude stabilization. The structure of the controller can be clearly seen from the block diagram shown in Fig. 5.21.

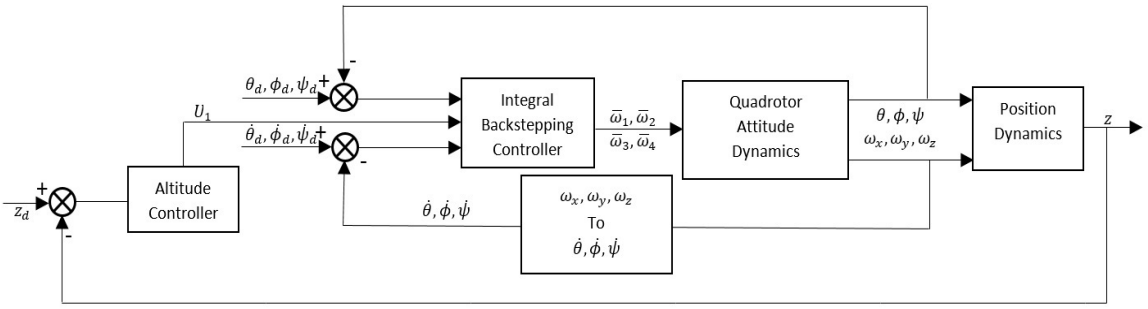

Figure 5.21: Block Diagram for Altitude Control with Integral Backstepping Controller

5.5.2 Experimental Results

The altitude control experiment results are shown in Fig. 5.22, where a step function jumping from 0.7 meters to 1.2 meters is given to the system. While maintaining a stable attitude control of the quadrotor by a human operator, an increasing and later on a decreasing command is send out from a ground computer. Notice in (5.105), the controller outputs an infinite value when the Euler angle ϕ or θ reaches 90°. This can be avoided by using the quaternion representations, and it will be considered for the future work. The performance of the controller is quite stable with an overshoot of 8.3%.

The gain coefficients are $k_9 = 15.8, k_{10} = 3.8$. While performing the altitude tracking experiments, the integral backstepping controller is used for the attitude control of the quadrotor, hence the gain coefficients can be referred to Section 5.2.

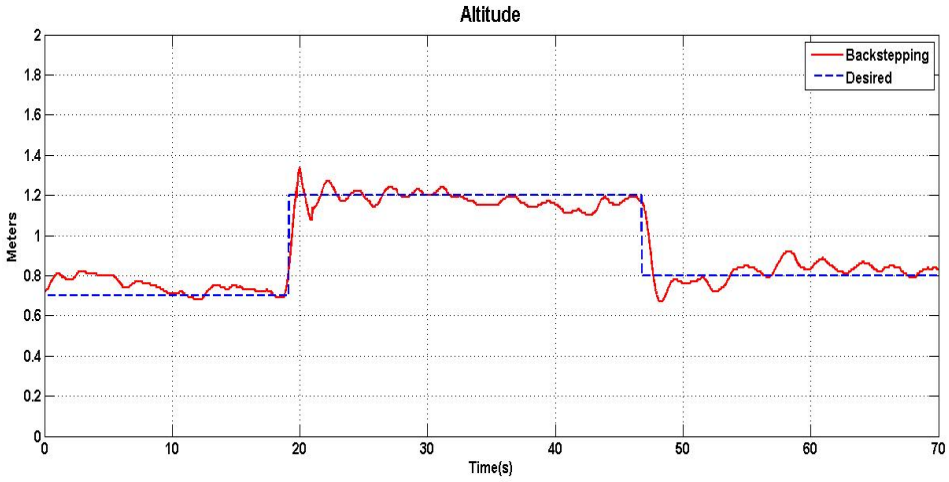

Figure 5.22: Altitude Tracking

Chapter 6

Conclusion

In this thesis work, various nonlinear controllers based on the backstepping technique have been discussed and implemented to stabilize a quadrotor. Prior to the design of the nonlinear controller, an attitude estimation method has been introduced. Later on, two different dynamic models based on the Euler Lagrangian and the Newton motion of equations have been discussed. The theory development for the backstepping nonlinear controller design has been provided and the experiments on the quadrotor have been successfully conducted to verify the backstepping nonlinear controller, which is followed by an integral backstepping controller design. The above two nonlinear controllers are based on the Euler angle as a way of representing the attitude of the quadrotor. The major drawback of such an attitude representation is the singularity problem, which is also known as the gimbal lock. In order to solve such a problem, the quaternion representation has been used for the backstepping controller. To cope with the environment changes and the model parameters uncertainties, a neural network mechanism has been adopted for the controller design. The neural network used in this thesis work consists of three layers, the input layer, the output layer and the hidden layer. To reach the better estimation outcomes and reduce the computation stress, nine neural cells have been embedded into the hidden layer. Within each neural cell, a triangular function is applied to imitate the nonlinear characteristics.

The theory development for the altitude control scheme strictly follows the backstepping technique. The Euler angle representation exhibits its disadvantage when observing the final control law in (5.105), at the instantaneous time when the Euler angle reaches 90°, U_1 becomes infinity.

The future work is quite extensive for this thesis work. Based on the theory development and the experimental try outs, it is concluded that many different improvements need to be made for a better performance of the quadrotor.

Firstly, the quaternion representation should be implemented for all the proposed controller designs. At this point of the research, only the backstepping controller was tested with the unit quaternion representation. In comparison with the rotational matrix representation, the quaternion representation has its unique mathematical characteristics, no singularity

problem, and is less complex in comparison with the rotational matrix.

Secondly, the PWM output is directly fed into the ESC module to generate a final mechanical rotation on the motors. A nonlinear relationship may exist in between the PWM signal and the RPM output. To find such a relationship, one should collect different testing points of PWM values under different motor speeds. By using these experimental data, a polynomial function can be constructed to model the nonlinear relationship between the PWM and RPM. The final mechanical RPM can then be compensated with this computed nonlinear characteristics.

Thirdly, one should consider to embed a more complex and extensive nonlinear function into each neural cell. Due to the limitation of the computational power, a triangular function is used at this point of the research. To improve the accuracy of the estimations, more neural cells can also be added, and a possible fuzzy set can be implemented.

The altitude control uses a sonar sensor to give the feedback signals. Though it is only effective at a lower altitude. A barometric pressure sensor may be used for a higher altitude applications. If a pressure sensor is employed, a possible sensor approximation algorithm might be used, since the sensor readings are drastically affected by the air pressure, humidity, and the vibrations.

Appendix A

C Language Flow Chart

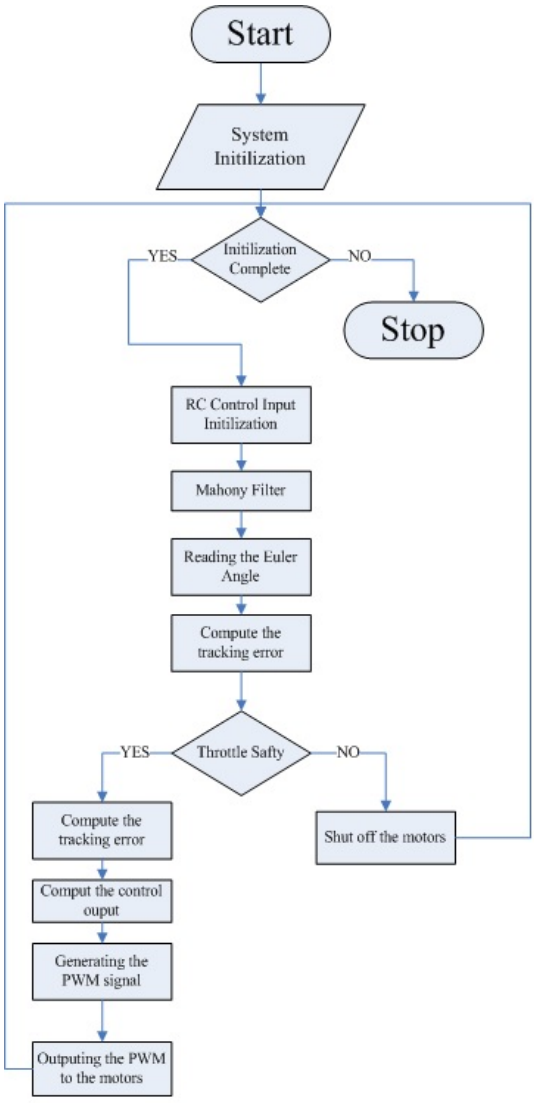

Appendix B

Digital Compass Calibration

The digital compass is affected by different sources of errors. The error properties are discussed in details [41] [51] for their physical meanings and electrical characteristics. This appendix is to further clarify the procedure for calibrating the digital compass. The digital compass used in this thesis work is HMC5883L. For more detailed technical specifications, one can refer to Section 2.1.2.

For an ideal magnetic field without any interferences, the measured data taken from rotating the sensor in all directions in the three dimensional space should show a perfect sphere. Depending on the geographic location, the following equation should be true.

$$B_{x-b}^2 + B_{y-b}^2 + B_{z-b}^2 = B_H^2 \tag{B.1}$$

where $B_{x-b}, B_{y-b}, B_{z-b}$ are the magnetic field without any errors in the body frame. In Section 3.2, the following relationships are provided:

$$\hat{B}_{x-b} = aB_{x-b} + x_o \tag{B.2}$$
$$\hat{B}_{y-b} = b(B_{y-b}\cos(\rho) + B_{x-b}\sin(\rho)) + y_0 \tag{B.3}$$
$$\hat{B}_{z-b} = c(B_{z-b}\cos(\phi)\cos(\theta) + B_{b-x}\sin(\phi)\cos(\theta) + B_{b-y}\sin(\theta)) + z_0 \tag{B.4}$$

As mentioned earlier in Section 3.2, $x_0, y_0, z_0, a, b, c, \rho, \phi, \theta.$ are the unknown sources of errors. $\hat{B}_{x-b}, \hat{B}_{y-b}, \hat{B}_{z-b}$ are the actual measurements from the digital compass in the body frame. $B_{x-b}, B_{y-b}, B_{z-b}$ are the real magnetic field strength without any errors. By rewriting ($B.2$),($B.3$),($B.4$), one can derive the following:

$$B_{x-b} = \frac{1}{a}\left(\hat{B}_{x-b} - x_o\right) \tag{B.5}$$
$$B_{y-b} = \frac{1}{\cos(\rho)}\left(\frac{1}{b}\left(\hat{B}_{y-b} - y_0\right) - \frac{1}{a}\left(\hat{B}_{x-b} - x_o\right)\sin(\rho)\right) \tag{B.6}$$
$$B_{z-b} = \frac{1}{\cos(\phi)\cos(\theta)}\left(\frac{1}{c}\left(\hat{B}_{z-b} - z_0\right) - B_{b-x}\sin(\phi)\cos(\theta) - B_{b-y}\sin(\theta)\right) \tag{B.7}$$

Substituting (B.5),(B.6),(B.7) into (B.1) produces

$$\begin{aligned} B_H^2 &= \left(\frac{1}{a}\left(\hat{B}_{x-b}-x_o\right)\right)^2+\left(\frac{1}{\cos(\rho)}\left(\frac{1}{b}\left(\hat{B}_{y-b}-y_0\right)-\frac{1}{a}\left(\hat{B}_{x-b}-x_o\right)\sin(\rho)\right)\right)^2 \\ &+\left(\frac{\frac{1}{c}\left(\hat{B}_{z-b}-z_0\right)-\frac{1}{a}\left(\hat{B}_{x-b}-x_o\right)\sin(\phi)\cos(\theta)}{\cos(\phi)\cos(\theta)}\right. \\ &\left.-\frac{\sin(\theta)\left(\frac{1}{b}\left(\hat{B}_{y-b}-y_0\right)-\frac{1}{a}\left(\hat{B}_{x-b}-x_o\right)\sin(\rho)\right)}{\cos(\rho)\cos(\phi)\cos(\theta)}\right)^2 \end{aligned} \tag{B.8}$$

which can then be rewritten as

$$\begin{aligned} &A\hat{B}_{x-b}^2+B\hat{B}_{x-b}\hat{B}_{y-b}+C\hat{B}_{x-b}\hat{B}_{z-b}+D\hat{B}_{y-b}^2 \\ &+E\hat{B}_{y-b}\hat{B}_{z-b}+F\hat{B}_{z-b}^2F+G\hat{B}_{x-b}+H\hat{B}_{y-b}+I\hat{B}_{z-b}+J=0 \end{aligned} \tag{B.9}$$

where $A, B, C, D, E, F, G, H, I, J$ are the functions containing the $x_0, y_0, z_0, a, b, c, \rho, \phi, \theta$. (B.9) can then be further elaborated into:

$$\begin{aligned} &-\frac{H}{D}\frac{1}{\hat{B}_{y-b}}-\frac{J}{D}\frac{1}{\hat{B}_{y-b}^2}-\frac{F}{D}\frac{\hat{B}_{z-b}^2}{\hat{B}_{y-b}^2}-\frac{A}{D}\frac{\hat{B}_{x-b}}{\hat{B}_{y-b}^2}-\frac{B}{D}\frac{\hat{B}_{x-b}}{\hat{B}_{y-b}} \\ &-\frac{G}{D}\frac{\hat{B}_{x-b}}{\hat{B}_{y-b}^2}-\frac{E}{D}\frac{\hat{B}_{z-b}}{\hat{B}_{y-b}}-\frac{I}{D}\frac{\hat{B}_{z-b}}{\hat{B}_{y-b}^2}-\frac{C}{D}\frac{\hat{B}_{x-b}\hat{B}_{z-b}}{\hat{B}_{y-b}^2}=1 \end{aligned} \tag{B.10}$$

which can then be put into the matrix form as follows:

$$\begin{bmatrix} \frac{\hat{B}_{x-b}}{\hat{B}_{y-b}^2} \\ \frac{\hat{B}_{x-b}}{\hat{B}_{y-b}} \\ \frac{\hat{B}_{x-b}\hat{B}_{z-b}}{\hat{B}_{y-b}^2} \\ \frac{\hat{B}_{z-b}}{\hat{B}_{y-b}} \\ \frac{\hat{B}_{z-b}^2}{\hat{B}_{y-b}^2} \\ \frac{\hat{B}_{x-b}}{\hat{B}_{y-b}^2} \\ \frac{1}{\hat{B}_{y-b}} \\ \frac{\hat{B}_{z-b}}{\hat{B}_{y-b}^2} \\ \frac{1}{\hat{B}_{y-b}^2} \end{bmatrix}^T \begin{bmatrix} -\frac{A}{D} \\ -\frac{B}{D} \\ -\frac{C}{D} \\ -\frac{E}{D} \\ -\frac{F}{D} \\ -\frac{G}{D} \\ -\frac{H}{D} \\ -\frac{I}{D} \\ -\frac{J}{D} \end{bmatrix} = 1 \tag{B.11}$$

where $A, B, C, D, E, F, G, H, I, J$ are determined by

$$A = \frac{1}{a^2} + \frac{\sin^2(\rho)}{a^2\cos^2(\rho)} + \frac{\sin^2(\phi)}{a^2\cos^2(\phi)} - \frac{2\sin(\rho)\sin(\theta)\sin(\phi)\cos(\theta)}{a^2\cos(\rho)\cos^2(\phi)\cos^2(\theta)} \tag{B.12}$$

$$B = \frac{2\sin(\theta)\sin(\phi)\cos(\theta)}{ab\cos(\rho)\cos^2(\phi)\cos^2(\theta)} - \frac{2\sin(\rho)}{ab\cos^2(\rho)} - \frac{2\sin(\rho)\sin^2(\theta)}{ab\cos^2(\phi)\cos^2(\theta)\cos^2(\rho)} \tag{B.13}$$

$$C = \frac{2\sin(\rho)\sin(\theta)}{ac\cos(\rho)\cos^2(\phi)\cos^2(\theta)} - \frac{2\sin(\phi)\cos(\theta)}{ac\cos^2(\phi)\cos^2(\theta)} \tag{B.14}$$

$$D = \frac{1}{\cos^2(\rho)b^2} + \frac{\sin^2(\theta)}{\cos^2(\rho)\cos^2(\phi)\cos^2(\theta)b^2} \tag{B.15}$$

$$E = -\frac{2\sin(\theta)}{bc\cos(\rho)\cos^2(\phi)\cos^2(\theta)} \tag{B.16}$$

$$F = \frac{1}{c^2\cos^2(\phi)\cos^2(\theta)} \tag{B.17}$$

(B.18)

$$\begin{aligned} G = {} & \frac{2y_0\sin(\rho)}{ab\cos^2(\rho)} - \frac{2x_o}{a^2} - \frac{2x_o\sin^2(\rho)}{a^2\cos^2(\rho)} - \frac{2x_o\sin^2(\phi)}{a^2\cos^2(\phi)} + \\ & \frac{2\sin(\rho)\sin^2(\theta)y_0}{ab\cos^2(\phi)\cos^2(\theta)\cos^2(\rho)} - \frac{2x_o\sin^2(\theta)\sin^2(\rho)}{a^2\cos^2(\phi)\cos^2(\theta)\cos^2(\rho)} \\ & + \frac{2z_0\sin(\phi)\cos(\theta)}{ac\cos^2(\phi)\cos^2(\theta)} - \frac{2y_0\sin(\theta)\sin(\phi)\cos(\theta)}{ab\cos(\rho)\cos^2(\phi)\cos^2(\theta)} \\ & - \frac{2\sin(\rho)\sin(\theta)z_0}{ac\cos(\rho)\cos^2(\phi)\cos^2(\theta)} + \frac{2x_o\sin(\rho)\sin(\theta)\sin(\phi)\cos(\theta)}{a^2\cos(\rho)\cos^2(\phi)\cos^2(\theta)} \end{aligned} \tag{B.19}$$

$$\begin{aligned} H = {} & -\frac{2y_0}{\cos^2(\rho)b^2} + \frac{2x_o\sin(\rho)}{ab\cos^2(\rho)} \\ & - \frac{2\sin^2(\theta)y_0}{\cos^2(\rho)\cos^2(\phi)\cos^2(\theta)b^2} + \frac{2\sin(\rho)\sin^2(\theta)x_o}{ab\cos^2(\phi)\cos^2(\theta)\cos^2(\rho)} \\ & - \frac{2x_o\sin(\theta)\sin(\phi)\cos(\theta)}{ab\cos(\rho)\cos^2(\phi)\cos^2(\theta)} - \frac{2\sin(\theta)z_0}{bc\cos(\rho)\cos^2(\phi)\cos^2(\theta)} \end{aligned} \tag{B.20}$$

$$\begin{aligned} I = {} & -\frac{2z_0}{c^2\cos^2(\phi)\cos^2(\theta)} + \frac{2x_o\sin(\phi)\cos(\theta)}{ac\cos^2(\phi)\cos^2(\theta)} \\ & + \frac{2y_0\sin(\theta)}{bc\cos(\rho)\cos^2(\phi)\cos^2(\theta)} - \frac{2\sin(\rho)x_o\sin(\theta)}{ac\cos(\rho)\cos^2(\phi)\cos^2(\theta)} \end{aligned} \tag{B.21}$$

(B.22)

$$
\begin{aligned}
J \;=\; & \frac{z_0^2}{c^2\cos^2(\phi)\cos^2(\theta)} + \frac{x_o^2\sin^2(\phi)}{a^2\cos^2(\phi)} + \frac{y_0^2\sin^2(\theta)}{\cos^2(\rho)\cos^2(\phi)\cos^2(\theta)b^2} \\
& - \frac{2\sin(\rho)\sin^2(\theta)x_o y_0}{ab\cos^2(\phi)\cos^2(\theta)\cos^2(\rho)} + \frac{x_o^2\sin^2(\theta)\sin^2(\rho)}{a^2\cos^2(\phi)\cos^2(\theta)\cos^2(\rho)} \\
& - \frac{2x_o z_0\sin(\phi)\cos(\theta)}{ac\cos^2(\phi)\cos^2(\theta)} + \frac{2x_o y_0\sin(\theta)\sin(\phi)\cos(\theta)}{ab\cos(\rho)\cos^2(\phi)\cos^2(\theta)} \\
& - \frac{2x_o^2\sin(\rho)\sin(\theta)\sin(\phi)\cos(\theta)}{a^2\cos(\rho)\cos^2(\phi)\cos^2(\theta)} - \frac{2y_0\sin(\theta)z_0}{bc\cos(\rho)\cos^2(\phi)\cos^2(\theta)} \\
& - \frac{2\sin(\rho)x_o\sin(\theta)z_0}{ac\cos(\rho)\cos^2(\phi)\cos^2(\theta)} + B_H^2
\end{aligned} \tag{B.23}
$$

where B_H is the earth magnetic field, which is 0.5648 Guass. Define the following matrices

$$
P = \begin{bmatrix} -\frac{A}{D} \\ -\frac{B}{D} \\ -\frac{C}{D} \\ -\frac{E}{D} \\ -\frac{F}{D} \\ -\frac{G}{D} \\ -\frac{H}{D} \\ -\frac{I}{D} \\ -\frac{J}{D} \end{bmatrix}^T \qquad W = \begin{bmatrix} 1 \\ 1 \\ 1 \\ 1 \\ . \\ . \\ . \\ . \\ 1_k \end{bmatrix} \tag{B.24}
$$

$$
\aleph = \begin{bmatrix}
\frac{\hat{B}_{x1-b}}{\hat{B}^2_{y1-b}} & \frac{\hat{B}_{x1-b}\hat{B}_{y1-b}}{\hat{B}^2_{y1-b}} & \frac{\hat{B}_{x1-b}\hat{B}_{z1-b}}{\hat{B}^2_{y1-b}} & \frac{\hat{B}_{y1-b}\hat{B}_{z1-b}}{\hat{B}^2_{y1-b}} & \frac{\hat{B}^2_{z1-b}}{\hat{B}^2_{y1-b}} & \frac{\hat{B}_{x1-b}}{\hat{B}^2_{y1-b}} & \frac{\hat{B}_{y1-b}}{\hat{B}^2_{y1-b}} & \frac{\hat{B}_{z1-b}}{\hat{B}^2_{y1-b}} & \frac{1}{\hat{B}^2_{y1-b}} \\
\frac{\hat{B}_{x2-b}}{\hat{B}^2_{y2-b}} & \frac{\hat{B}_{x2-b}\hat{B}_{y2-b}}{\hat{B}^2_{y2-b}} & \frac{\hat{B}_{x2-b}\hat{B}_{z2-b}}{\hat{B}^2_{y2-b}} & \frac{\hat{B}_{y2-b}\hat{B}_{z2-b}}{\hat{B}^2_{y2-b}} & \frac{\hat{B}^2_{z2-b}}{\hat{B}^2_{y2-b}} & \frac{\hat{B}_{x2-b}}{\hat{B}^2_{y2-b}} & \frac{\hat{B}_{y2-b}}{\hat{B}^2_{y2-b}} & \frac{\hat{B}_{z2-b}}{\hat{B}^2_{y2-b}} & \frac{1}{\hat{B}^2_{y2-b}} \\
\frac{\hat{B}_{x3-b}}{\hat{B}^2_{y3-b}} & \frac{\hat{B}_{x3-b}\hat{B}_{y3-b}}{\hat{B}^2_{y3-b}} & \frac{\hat{B}_{x3-b}\hat{B}_{z3-b}}{\hat{B}^2_{y3-b}} & \frac{\hat{B}_{y3-b}\hat{B}_{z3-b}}{\hat{B}^2_{y3-b}} & \frac{\hat{B}^2_{z3-b}}{\hat{B}^2_{y3-b}} & \frac{\hat{B}_{x3-b}}{\hat{B}^2_{y3-b}} & \frac{\hat{B}_{y3-b}}{\hat{B}^2_{y3-b}} & \frac{\hat{B}_{z3-b}}{\hat{B}^2_{y3-b}} & \frac{1}{\hat{B}^2_{y3-b}} \\
. & . & . & . & . & . & . & . & . \\
. & . & . & . & . & . & . & . & . \\
. & . & . & . & . & . & . & . & . \\
. & . & . & . & . & . & . & . & . \\
. & . & . & . & . & . & . & . & . \\
\frac{\hat{B}_{xk-b}}{\hat{B}^2_{yk-b}} & \frac{\hat{B}_{xk-b}\hat{B}_{yk-b}}{\hat{B}^2_{yk-b}} & \frac{\hat{B}_{xk-b}\hat{B}_{zk-b}}{\hat{B}^2_{yk-b}} & \frac{\hat{B}_{yk-b}\hat{B}_{zk-b}}{\hat{B}^2_{yk-b}} & \frac{\hat{B}^2_{zk-b}}{\hat{B}^2_{yk-b}} & \frac{\hat{B}_{xk-b}}{\hat{B}^2_{yk-b}} & \frac{\hat{B}_{yk-b}}{\hat{B}^2_{yk-b}} & \frac{\hat{B}_{zk-b}}{\hat{B}^2_{yk-b}} & \frac{1}{\hat{B}^2_{yk-b}}
\end{bmatrix} \tag{B.25}
$$

Taking k numbers of data points to construct the matrix $\aleph$, one can then apply the linear regreassion method to estimate P.

$$
P = (\aleph^T\aleph)^{-1}\aleph \tag{B.26}
$$

With P determined, all the sources of errors $x_0, y_0, z_0, a, b, c, \rho, \phi, \theta$ can be then computed by using the result of the P matrix, along with (B.12-B.23). This can be done in the matlab, using the gradient decent method.

Bibliography

[1] L. Kendra and L. B. Cook, "The silent force multiplier: The history and role of uavs in warfare," *Aerospace Conference, IEEE*, 2007.

[2] P. N. Patel, M. A. Patel, R. M. Faldu, and Y. R. Dave, "Quadcopter for agricultural surveillance," *Advance in Electronic and Electric Engineering.*, vol. 3, no. 4, pp. 427–432, 2013.

[3] K. Agrawal and P. Shrivastav, "Multi-rotors: A revolution in unmanned aerial vehicle," *International Journal of Science and Research*, pp. 2319–7064, 2013.

[4] M. D. Shuster, "A survey of attitude representations," *The journal of the astronautical science*, vol. 41, no. 4, pp. 439–517, 1993.

[5] M. D. Hua, G. Ducard, T. Hamel, R. Mahony, and K. Rudin, "Implementation of a nonlinear attitude estimator for aerial robotic vehicles," *IEEE transactions on control systems technology*, vol. 22, no. 1, 2014.

[6] T. Hamel and R. Mahony, "Attitude estimation on SO(3) based on direct inertial measurements," *Proceedings IEEE international conference on robotics and automation*, pp. 2170–2175, 2006.

[7] S. F. Schmidt, "The Kalman filter - its recognition and development for aerospace applications," *Journal of guidance, Control and dynamics*, vol. 4, no. 1, pp. 4–7, 1981.

[8] E. J. Lefferts, F. L. Markley, and M. D. Shuster, "Kalman filtering for spacecraft attitude estimation," *Journal of guidance, Control and dynamics*, vol. 4, no. 1, pp. 4–7, 1982.

[9] M. D. Shuster, "Attitude determination from vector observations: quaternion estimation," *IEEE transactions on aerospace and electronic systems*, vol. 321, no. 1, pp. 128–136, 1985.

[10] Y. C. Choi and H. S. Ahn, "Nonlinear control of quadrotor for point tracking: actual implementation and experimental tests," *IEEE/ASME transactions on mechatronics*, vol. 20, no. 3, pp. 1179–1192, 2015.

[11] S. Bouabdallah and Roland, "Full control of a quadrotor," *IEEE/RSJ international conference on intelligent robots and systems*, 2007.

[12] A. Tayebi, "Unit quaternion-based output feedback for the attitude tracking problem," *IEEE transactions on automatic control*, vol. 53, no. 6, July 2008.

[13] T. Madani and A. Benallegue, "Backstepping control for a quadrotor helicopter," *IEEE/RSJ international conference on intelligent robots and systems*, 2006.

[14] S. Bouabdallah, A. Noth, and R. Siegwart, "PID vs LQR control techniques applied to an indoor micro quadrotor," *Proceedings IEEE/RSJ international conference on intelligent robots and systems*, vol. 3, pp. 2451–2456, 2004.

[15] J. Li and Y. Li, "Dynamic analysis and pid control for a quadrotor," *International conference on mechatronics and automation (ICMA)*, pp. 573–578, 2011.

[16] A. Benallegue, A. Mokhtari, and L. Fridman, "Feedback linearization and high order sliding mode observer for a quadrotor UAV," *International workshop on Variable structure systems(VSS)*, pp. 365–372, 2006.

[17] I. Voos, "Nonlinear control of a quadrotor micro-uav using feedback-linearization," pp. 1–4, January 2009.

[18] K. Torabi and A. G. Kashani, "Robust control of a quadrotor," *Artificial intelligence in electrical engineering*, vol. 3, no. 15, December 2015.

[19] S. M. Joshi, A. G. Kelkar, and J. T. Y. Wen, "Robust attitude stabilization of spacecraft using nonlinear quaternion feedback," *IEEE transactions on automatic control*, vol. 40, no. 10, pp. 1800–1803, Oct. 1995.

[20] J. T. Y. Wen and K. Kreutz-Delgado, "The attitude control problem," *IEEE transactions on automatic control*, vol. 36, no. 10, pp. 1148–1162, Oct. 1991.

[21] A. Tayebi and S. McGilvray, "Attitude stabilization of a VTOL quadrotor aircraft," *IEEE transactions on control systems technology*, vol. 14, no. 3, May. 2006.

[22] T. Lee, M. Leok, and N. H. McClamroch, "Nonlinear robust tracking control of a quadrotor UAV on SO(3)," *Asian journal of control*, vol. 15, pp. 391–408, July, 2012.

[23] D. Cabecinhas, R. Cunha, and C. Silvestre, "A nonlinear quadrotor trajectory tracking controller with disturbance rejection," *Control engineering practice*, vol. 26, pp. 1–10, May 2014.

[24] D. Jose, R. Noriega, and D. H. Wang, "A direct adaptive neural network control for unknown nonlinear systems and its application," *IEEE transactions on neural networks*, vol. 9, no. 1, Jan,1998.

[25] R. Hercus, H. S. Kong, K. F. Ho, and N. S. Bhd, "Control of an unmanned aerial vehicle using a neuronal network," *Procedings conference on computational intelligence,cognitive algorithms mind and brain(CCMB)*, pp. 16–19, April 2013.

[26] M. Lower and W. Tarnawski, "Theory and engineering of complex systems and dependability," vol. 365, pp. 265–274, 2015.

[27] C. Zhang, H. Hu, and J. Wang, "An adaptive neural network approach to the tracking control of micro aerial vehicles in constrained space," *International journal of systems science*, vol. 48, pp. 84–94, May,2016.

[28] M. O. Efe, "Neural network assisted computationally simple $PI^{\lambda}D^{\mu}$ control of a quadrotor uav," *International journal of systems science*, vol. 7, no. 2, May,2011.

[29] M. Muller, S. Lupashin, and R. D'Andrea, "Quadrocopter ball juggling," *IEEE/RSJ international conference on intelligent robots and systems*, pp. 5113–5120, Sept,2011.

[30] D. Mellinger, N. Michael, and V. Kumar, "Trajectory generation and control for precise aggressive maneuvers with quadrotors," *International conference on experimental robotics*, pp. 5113–5120, Dec. 2010.

[31] M. Hehn and R. D'Andrea, "A flying inverted pendulum," *IEEE international conference on robotics and automation (ICRA)*, pp. 763–770, May. 2011.

[32] Q. Lindsey, D. Mellinger, and V. Kumar, "Construction of cubic structures with quadrotor teams," *Proccedings. on robotics science and systems*, June. 2011.

[33] P. E. I. pounds, "Design construction and control of a large quadrotor micro air vehicle," June.2007.

[34] http://www.hobbyking.com/.

[35] http://www.ti.com/lsds/ti/microcontrollers_16-bit_32-bit/c2000_performance/real-time_control/overview.page?DCMP=dsp_C2000&HQS=c2000.

[36] http://myfirstdrone.com/build-your-first-quad/.

[37] http://www.instructables.com/id/Sturdy-Quadcopter-Build/.

[38] http://www.instructables.com/id/The-Ultimate-DIY-Guide-to-Quadcopters/step5/BUILDING-Assembling-the-Frame/.

[39] https://oscarliang.com/build-a-quadcopter-beginners-tutorial-1/.

[40] http://m-selig.ae.illinois.edu/props/volume-1/propDB-volume-1.html.

[41] M. Wang, "Attitude control of a quadrotor UAV," *Master thesis, Lakehead University, Ontario, Canada*, 2015.

[42] M. R. Jardin and E. R. Mueller, "Optimized measurements of uav mass moment of inertia with a bifilar pendulum," *AIAA Guidance, Navigation and Control Conference and Exhibit, Hilton Head, SC, USA*, 2007.

[43] R. W. Prouty, "Helicopter performance, stability and control," *Melbourne, FL:Krieger, USA*, 1995.

[44] J. G. Leishman, "Principles of helicopter aerodynamics," *Cambridge University Press, Cambridge, U.K.*, 2006.

[45] "Apc propellers, props for model airplanes. [online]," http://www.apcprop.com/v/index.html.

[46] "[online].," http://m-selig.ae.illinois.edu/props/volume-1/propDB-volume-1.html.

[47] D. Choukroun, "Novel methods for attitude determination using vector observations," *Ph.D. dissertation, Israel institute of technology, Haifa, Israel*, Jan,2003.

[48] J. L. Crassidis, F. L. Markley, and Y. Cheng, "Survey of nonlinear attitude estimation methods," *Journal of guidance, control and dynamics*, vol. 30, no. 1, pp. 12–28, 2007.

[49] M. D. Hua, "Contributions to the automatic control of aerial vehicles," *PhD. dissertation, University of Nice Sophia Antipolis, Nice, France*, 2009.

[50] R. Mahony, T. Hamel, and J. M. Pflimlin, "Nonlinear complementary filters on the special orthogonal group," *IEEE transactions on automatic control*, vol. 53, no. 5, pp. 1203–1218, 2008.

[51] C. C. Foster and G. H. Elkaim, "Extension of a two-step calibration methodology to include nonorthogonal sensor axes," *IEEE transactions on aerospace and electronic systems*, vol. 44, no. 3, pp. 1070–1078, 2008.

[52] M. Barczyk, "Nonlinear state estimation and modeling of a helicopter uav," *PhD thesis, University of Alberta, Ontario, Canada*, 2012.

[53] C. Finlay, S. Maus, C. Beggan, T. Bondar, A. Chambodut, T. Chernova, A. Chulliat, V. Golovkov, B. Hamilton, and M. Hamoudi, "International geomagnetic reference field: the eleventh generation," *Geophysical journal international*, vol. 183, no. 3, pp. 1216–1230, 2010.

[54] S. Maus, S. Macmillan, S. McLean, B. Hamilton, A. Thomson, M. Nair, and C. Rollin, "The us/uk world magnetic model for 2010-2015," *NOAA technical report NESDIS/NGDC*, 2010.

[55] T. Hamel, R. Mahony, R. Lozano, and J. Ostrowski, "Dynamic modeling and configuration stabilization for an x4-flyer," *Proccedings of IFAC world congress, Barcelona, Spain*, 2002.

[56] S. P. Bhat and D. S. Bernstein, "A topological obstruction to continuous global stabilization of rotational motion and the unwinding phenomenon," *Systems and Control Letters*, vol. 39, no. 1, pp. 63–70, 2000.

[57] B. S. Kim and A. J. Calise, "Nonlinear flight control using neural networks," *Journal of guidance, control and dynamics*, vol. 20, no. 1, 1997.

[58] C. Nicol, C. J. B. Macnab, and A. Ramirez-Serrano, "Robust adaptive control of a quadrotor helicopter," *Mechatronics*, vol. 21, no. 6, pp. 927–938, 2011.

[59] T. Madani and A. Benallegue, "Adaptive control via backstepping technique and neural networks of a quadrotor helicopter," *Proceedings of IFAC world congress*, vol. 41, no. 2, pp. 6513–6518, 2008.

[60] H. Voos, "Nonlinear and neural network-based control of a small four rotor aerial robot," *IEEE/ASME international conference on advanced intelligent mechatronics*, pp. 4–7, 2007.

[61] K. Hornik, M. Stinchcombe, and H. White, "Multilayer feedforward networks are universal approximators," *Nueral Networks*, vol. 2, no. 5, pp. 359–366, 1989.

[62] K. Gopalsamy, "*Stability and oscillations in delay differential equations of population dynamic*," *Kluwer Academic, Dordrecht*, 1992.